Mechanical and Fatigue Testing of Rapid Prototyped Aerospace Titanium Component by Electron Beam Melting Process

Arrian B. Forbush

A thesis

submitted in partial fulfillment of the

requirements for the degree of

Master of Science in Mechanical Engineering

University of Washington

2014

Committee:

Ramulu Mamidala

Paul Edwards

John Kramlich

Program Authorized to Offer Degree:

Department of Mechanical Engineering

University of Washington

Abstract

Fatigue Testing and Evaluation of Rapid Prototyped Aerospace Titanium Component by Electron Beam Melting Process

Arrian Bryce Forbush

Chair of Supervisory Committee:

Professor M. Ramulu

Mechanical Engineering

The mechanical and fatigue behavior of a Ti-6Al-4V structural component that was manufactured by electron beam melting (EBM) was studied. Ti-6Al-4V EBM components were subjected to cyclic loading and monotonic loading tests. The results indicated that the EBM component did not fail before the fasteners in both tests. This was a preliminary study regarding an attempt to model an EBM component to validate the physical tests. An attempt was made to model the monotonic and cyclic testing in the linear elastic region using finite elements with the assumed loading conditions to investigate the stress distributions at each loading condition. Additionally, an attempt was made to use finite element modeling to validate the experimental results within the elastic range.

Table of Contents

Table of Figures

List of Tables

Acknowledgements

The author expresses sincere appreciation to Professor Dr. Ramulu Mamidala for his knowledge and assistance to complete this project. Fellow graduate student, Alex O'Connor, provided invaluable assistance with the physical testing and interpretation of results.

I am grateful to the members of my committee including Dr. Mamidala, Dr. Kramlich, and Dr. Edwards for their support and reviews of this document.

This research was made possible by the financial support of the Boeing Company.

Dedication

To my wife, Rachel, and my children.

Chapter 1: Introduction

1.1 Overview

The scope of manufacturing metal-alloy components from powder via additive manufacturing or rapid prototyping, selective laser sintering (SLS or SLM), electron beam melting (EBM), and other various methods that combine metallic powders is relatively limited to size and use. The limitation regarding size is related to the size of the machine and capabilities. The limitation regarding industry implementation is related to the mechanical and fatigue properties required by its intended design usage. Fatigue and mechanical properties of components as built (without post processing) manufactured from titanium or other metallic powders by electron beam sintering and melting, for example, differ from those manufactured or machined from wrought solid titanium or other metals. However, there are numerous benefits that are derived from additive manufacturing. For example, titanium is extremely expensive to process and form into components. The traditional method of machining titanium from bar stock is quite expensive and time consuming which involves special tooling and waste material such as metal shavings. Additionally, only geometries that are physically able to be constructed using the traditional machining method may be used. As a result of additive manufacturing, components are able to be constructed according to optimum design to carry the loads of the structure while using less material which results in less weight. Less weight is an obvious benefit in aerospace and in other industrial areas [1]. The desired outcome of additive manufacturing is to ultimately save money in manufacturing costs by using less energy and material (less carbon footprint). Furthermore, lighter material will have an effect on fuel savings in transportation

such as in automotive, locomotive, and aerospace etc. which will ultimately reduce the carbon footprint during the lifespan of the product from conception through implementation.

Additive manufacturing that forms components using powdered metals is similar to three-dimensional printing for plastics. The process takes a 3D CAD model and constructs a part using a layer-by-layer approach [2]. The economical reasoning governing the use of powder titanium or other metals via additive manufacturing guarantees the limitation of material waste due to shavings from wrought metal using conventional manufacturing processes e.g. machining. The AM processes requires metallic powders or feed wire and a heat source such as from a laser or electron beam to fuse or melt the powders or wire together. This process enables manufacturers to produce components to net or near net shape. The desired outcome of additive manufacturing is to limit the amount of post-manufacturing processes that would negate the cost and energy savings that were intended first handedly. In essence, any post-manufacturing processes would increase the total cost and the environmental carbon footprint.

This research examined electron beam melting (EBM), an additive manufacturing process, using titanium powder to manufacture components that were presently used in the industry that were manufactured by conventional methods. Titanium is a beneficial material that is used in many types of industries, and titanium is beneficial to the health industry and aerospace due to its biocompatibility and high strength to weight ratio [3,4]. As a result, titanium is being used in the health industry for implants. Since each individual patient is different (size and shape), an additive manufacturing process would make it more affordable to construct a custom part which would be more comfortable for the patient. The additive manufacturing process takes

information from three dimensional computer aided drawing models or other images or models derived from MRI or CAT scans [5,6,7]. The simplicity of additive manufacturing of titanium increases the viability of the EBM manufacturing process due to economics and resources. The question is whether mechanical and fatigue properties of components manufactured from the AM process are competent for heavy cyclic loading that which their wrought material counterparts perform.

The purpose of this research was to determine the viability of using EBM technology with titanium powder without heavily relying on difficult or cost cumbersome post processing methods. The mechanical and fatigue properties of additive manufacturing using titanium powders were examined. Additionally, the physical testing of the aerospace component used in this research was compared to finite element modeling.

Coupon samples that were manufactured by using Electron Beam Melting (EBM) technology were previously tested by the sponsor. The testing included static tensile, fracture toughness, and fatigue tests. The material data obtained from the coupon samples were used in comparison and validation of the structural component tested in this research. In this research, there were two different types of manufactured structural specimens that underwent cyclic loading and tensile testing. The two different types of specimens that were included were four samples manufactured by electron beam melting (EBM) and another four were manufactured by EBM and were subjected to post process machining to decrease the surface roughness. In this research, a test fixture was manufactured that was required to securely fasten the specimen to the cyclic loading testing machine and the static tensile testing machine. The

sponsor provided fasteners that were industry specific to secure the specimen to the testing fixture. The cyclic loading applied to the structural member that was attached to the test fixture which simulated design loading. The testing provided information how the component would perform under real loading conditions. Additionally, the cyclic testing would determine whether the electron beam melting process would be viable for this specific design and implementation without any post-processing methods.

During fatigue testing, each component underwent normal loading conditions at double the intended life cycles. Three components (one component as built and two components with post-process machining), additionally experienced double the design load until fracture. It was predicted that the fasteners would fail before the component. Additionally, static loading was used on four components (two as built and two with post-process machining) until failure. Finite element models were provided using the material data generated by the sponsor [1] and ARCAM manufacturer to compare and validate the testing results [8].

1.2 Objectives

The objectives of this research are:

- Experimental testing of both monotonic and cyclic testing of electron beam melted components.
- Numerical modeling of the component behavior both loading conditions to deduce the stress distribution and failure analysis.

Chapter 2: Background and Literature Review

2.1 Additive Manufacturing

Additive manufacturing uses a layer-by-layer type technique to form a net-shape component from a three-dimensional model. The solid component is fabricated gradually by an additive process to a shape derived from CAD, CT scans, MRI etc. [5]. In additive manufacturing, the method by which the material is fused together differs by the heat source, for an example, such as an electron beam or laser and raw materials in powdered material or wire form etc. [7, 9]. Additive Manufacturing (AM) traditionally has been used on plastics, and it is now a feasible option for metal alloys, including Ti-6Al-4V [10]. Additionally, AM is applicable to many different materials including metals, ceramics, polymers, composites and biological arrangements [11]. Additive manufacturing is a relatively new innovative process that could potentially transform current or future manufacturing methodology. Traditionally, manufacturing is either a formative (casting or molding) or a subtractive process (machining) [12]. For instance, machining titanium is very time consuming and cumbersome which requires expensive tools and high cutting forces. Traditional machining results in material waste such as shavings which are scrapped that add to the total cost of manufacturing. Additionally, high temperature is an issue while machining titanium which ultimately limits tool life and cutting speed [13]. Titanium is expensive and it is a desirable material in industries such as aerospace and biological application due to its superior mechanical properties e.g. high strength to weight ratio, corrosive resistance, and superior biocompatibility for biological applications [5, 3, 14]. Since the cost of titanium is more than steel and aluminum the benefit of material utilization increases with AM of titanium. Conventional machining of titanium includes poor material

utilization and high machining time. Additionally, titanium has low machinability due to its poor thermal properties which results in high costs and high lead time. As a result, additive manufacturing (AM) is an alternative viable option that industries could utilize to save material and ultimately ease the process of forming complex titanium components. Additionally, AM eliminates the necessity for dies and machining, which ultimately reduces the long lead times and associated expenses.

2.1.1 Benefits of Additive Manufacturing

Additive manufacturing potentially reduces energy usage compared to conventional manufacturing processes that result less of a carbon footprint. With respect to the aviation industry any decrease in aircraft weight reduces fuel consumption in flight. Additive manufacturing enables the flexibility to design components according to the load transfer requirements in a fashion that is otherwise impossible using conventional methods such as machining. AM allows the processing of structural components that optimizes the geometry necessary to carry the design loads which has a potential of approximately 50 percentage weight reduction [15]. AM provides the capability to fabricate hollow structures which lowers the weight and reduces total energy and cost savings during implementation. For example, in the aerospace industry, 1 kilogram reduction of weight of the aircraft could potentially save approximately 3,000 USD per year in fuel consumption. Additionally, in the automotive industry, a 10 percent weight reduction correlates with approximately 6 to 8 percentage reduction of fuel consumption. AM also is a beneficial manufacturing tool in the medical industry which specimens could imitate bone structures [12], and AM produced titanium components could be formed as a cellular structure to match bone material properties such as

Young's modulus to limit stress shielding phenomena which leads to the eventual loosening of implants [16]. Additionally, components for aerospace or in the automotive industry could be manufactured with AM technology on site such as a dealership according to need and demand [11, 12].

The rising demand of material and its associated costs suggests that additional manufacturers would possibly adopt additive manufacturing processes to save money as a result of rising costs of fuel and material. Additive manufacturing techniques would possibly reduce costs by reducing labor requirements, worn out tools, and increased material utilization (less material waste). The automated nature of additive manufacturing would possibly increase manufacturing opportunities domestically and decrease the reliance on importing from overseas [12]. Additionally, AM is a viable process that could replace conventional manufacturing practices, especially for complicated specimens with specific geometry such as biomedical implants for an example. The biocompatibility of titanium and the ability of AM processing to produce precise geometric shapes would be beneficial in the medical industry for specific patients requiring implants [17].

2.1.2 Issues Regarding Additive Manufacturing

The preferred end result is to have the AM component ready for implementation as built without cumbersome post-process manufacturing methods that would negate the desirable cost and carbon footprint savings. However, the caveat is that the mechanical and fatigue properties of the specimen manufactured by the AM process differ than those of wrought material, and some post-processing would be essential depending on the design

implementation. However, tensile properties do not always differ, for example, titanium components produced by AM processing share comparable tensile properties [7]. For AM components that experience dynamic loading, fatigue is an issue that requires investigation. Metallic components manufactured by AM typically experience lower fatigue strength than wrought material. The lower fatigue strength is typically a result of the roughened surface, microstructure, tensile residual stresses and porosity from the AM process. The quality of the AM components are dependent of the various manufacturing parameters such as laser power and laser scan speed for example and ambient processing conditions e.g. elevated chamber temperature [5,6]. Post-manufacturing processes e.g. shot peening, hot isostatic pressing, post-process machining, and laser gas nitriding (LGN) are examples of methods which are used to alter the material properties to the desirable quality required by the design and intended implementation [18, 19, 20]. For example, surface alloying of titanium using the LGN method increases the wear resistance of titanium components formed by the AM process [3].

2.1.3 Additive Manufacturing for Metallic components

An example of additive manufacturing of metallic components utilizes a laser and a powder bed system such as selective laser melting or selective laser sintering (SLM/SLS). SLM/SLS has the potential to reduce manufacturing costs by producing near-net shape components of powdered alloys which increase material utilization [21]. Another example of additive manufacturing of metallic components is electron beam melting (EBM) which is similar to selective laser melting (SLM) that it uses an electron beam instead of a laser beam as a heat source in a powder bed arrangement [7]. As previously described, the component 3-dimensional information is drawn from a model derived from a three-dimensional CAD model, medical-type scans etc. to process

the net shape component. In this process, powdered metallic material is melted together by a sharply focused laser beam or other heat source e.g. electron beam and the manufactured components are built layer by layer per each cross section of the CAD model. The individual cross sections quickly solidify to form localized volumes that combine to form the final product [21].

Another type of additive manufacturing for metallic components is the 3-D laser cladding process which utilizes a laser and nozzle that delivers the powder while being melted in a bed. This process differs from EBM and SLM that it does not have a powder bed that lowers and rakes powder across the previously formed cross section. Edson Costa Santos et al. [4] concluded that this process creates fully densified parts with mechanical properties that are superior or close to that of material processed using standard procedures such as machining. Hip implants manufactured using a ND: YAG laser using Ti-6Al-4V powder in the 3-D laser cladding process demonstrated tensile and fatigue properties which are similar to wrought material [4]. As a result of the success and viability of additive manufacturing of metallic components, it is possible that aerospace, medical, and automotive industries would adapt to AM which would potentially decrease costs associated with conventional manufacturing and would potentially ultimately decrease power consumption and material waste.

Figure 2-1 and 2-2 depict sample material, fatigue and fracture properties of Ti-6Al-4V produced by two different machines, M280 and ARCAM and used hot isostatic pressing as a post process method to increase ductility and enhance fatigue life [11]. Figure 2-3 includes many of the different types of additive manufacturing processes which are categorized by

powder bed (Figure 2-4), powder fed (Figure 2-5) and wire feed (Figure 2-6) with the respective heat source and build volumes. The powder bed system rakes powder across the work area as each cross section is built. The advantages of the powder bed system is that it maintains dimension control and produces high resolution components. In the powder fed system, the work piece is either stationary while the deposition nozzle moves or the work piece moves while the deposition nozzle is stationary. The ability to repair damaged or worn parts and the larger build volume is an advantage of the powder fed system. In the wire feed system setup, the material source is a wire that is fed and the heat source includes an electron beam, laser beam, and plasma arc. The advantage of wire feed is that it has the capability for a high deposition rate and has larger build volumes. The disadvantage of wire feed deposition is that the components typically require more post process machining than the powder material systems [11]. With respect to the different additive manufacturing processes there are also variables (e.g. powder shape and size, laser speed, laser power) that are able to be adjusted which affect the mechanical and fatigue properties of the formed specimen [21]. Microstructure, surface finish, porosity and residual stresses are influenced by the variables of additive manufacturing such as from localized heating and the effects thereof [22]. Yield and ultimate tensile strengths of AM Ti-6Al-4V typically exceed the values of wrought Ti-6Al-4V and there is some anisotropy associated with build directions. The percentage elongation of typical wrought alloy such as Ti-6Al-4V is typically higher than the AM processed components with post processing heat treatment to improve ductility (Figure 2-1). The porosity in as-manufactured specimens are able to be eliminated using HIP processing which increases fatigue strength [11]. Therefore, if the additive manufactured specimen does not meet the material property and

fatigue strength design requirements, then post processing methods e.g. hot-isostatic pressing, shot-peening, surface laser remelting, annealing, machining post AM should be considered.

	Typical wrought	M280, HIP + solution heat treat		ARCAM, HIP	
Orientation	n/a	*X-Y*	*Z*	*X-Y*	*Z*
YS, MPa	828	887	946	848	841
UTS, MPa	897	997	1010	946	946
Elongation	15%	11.4	13.9	13.2	13.9

Figure 2-1: Static properties of Ti-6Al-4V processed by M280 and ARCAM compared to wrought material [11]

Process	Orientation	Porosity, %	K_{IC}, MPa√m	STD, MPa√m	Fatigue strength at 10^7 cycles, MPa
As-fabricated	*Z*	0.19	78.1	2.3	407
As-fabricated	*X-Y*	0.11	96.9	0.99	441
HIP	*Z*	0.00	83.1	0.09	538
HIP	*X-Y*	0.00	99.0	1.1	607

Figure 2-2: Fatigue and fracture toughness of Ti-6Al-4V processed by ARCAM [11]

System	Process	Build volume (mm)	Energy source
Powder bed			
ARCAM (A2)(a)	EBM	200 × 200 × 350	7 kW electron beam
EOS (M280)(b)	DMLS	250 × 250 × 325	200-400 W Yb-fiber laser
Concept laser cusing (M3)(b)	SLM	300 × 350 × 300	200 W fiber laser
MTT (SLM 250)(b)	SLM	250 × 250 × 300	100-400 W Yb-fiber laser
Phenix system group (PXL)(c)	SLM	250 × 250 × 300	500 W fiber laser
Renishaw (AM 250)(d)	SLM	245 × 245 × 360	200 or 400 W laser
Realizer (SLM 250)(b)	SLM	250 × 250 × 220	100, 200, or 400 W laser
Matsuura (Lumex Advanced 25)(e)	SLM	250 × 250 diameter	400 W Yb fiber laser; hybrid additive/subtractive system
Powder feed			
Optomec (LENS 850-R)(f)	LENS	900 × 1500 × 900	1 or 2 kW IPG fiber laser
POM DMD (66R)(f)	DMD	3,200° × 3°,670° × 360°	1-5 kW fiber diode or disk laser
Accufusion laser consolidation(g)	LC	1,000 × 1,000 × 1,000	Nd:YAG laser
Irepa laser (LF 6000)(c)	LD		Laser cladding
Trumpf(b)	LD	600 × 1,000 long	
Huffman (HC-205)(f)	LD		CO_2 laser clading
Wire feed			
Sciaky (NG1) EBFFF(f)	EBDM	762 × 483 × 508	>40 kW @ 60 kV welder
MER plasma transferred arc selected FFF(f)	PTAS FFF	610 × 610 × 5,182	Plasma transferred arc using two 350A DC power supplies
Honeywell ion fusion formation(f)	IFF		Plasma arc-based welding

Country of Manufacturer: (a) Sweden, (b) Germany, (c) France, (d) United Kingdom, (e) Japan, (f) United States, and (g) Canada

Figure 2-3: Additive manufacturing equipment [11]

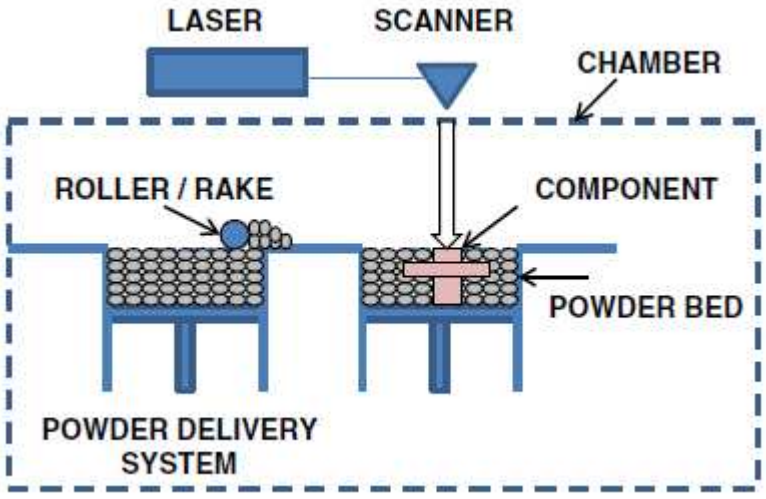

Figure 2-4: Powder bed system [11]

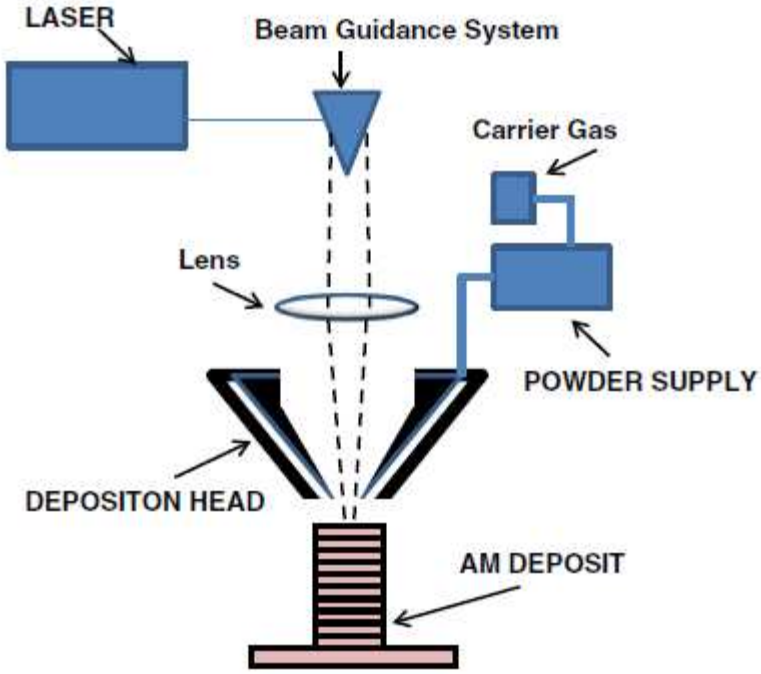

Figure 2-5: Powder feed system [11]

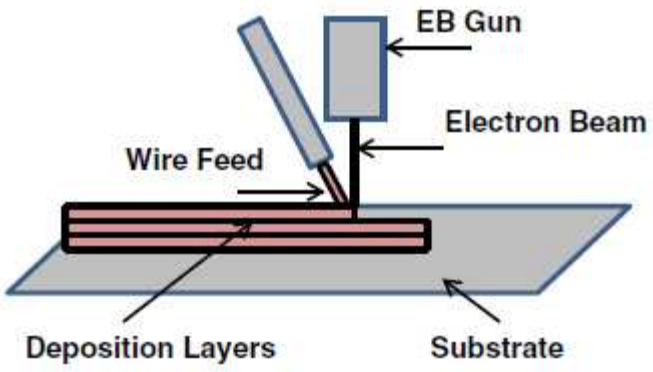

Figure 2-6: Wired fed system [11]

2.1.4 Ferrous and Non-Ferrous Metal Powder

The main focus on this research is the additive manufacture of titanium powder, more specifically Ti6Al4V. However, there are other non-ferrous and ferrous metallic powders that are utilized in additive manufacturing. For example, the additive manufacture of AlSi10Mg by selective laser melting and its associated material properties were investigated [23]. Additionally, additive manufacture of ferrous materials such as AISI 316L stainless steel powder along with nonferrous materials were investigated by Kruth et al [24]. Additionally, Yasa et al investigated SLM and 316L stainless steel [25]. This research demonstrated selective laser melting and laser re-melting to improve the surface finish of the stainless steel. The study additionally indicated that process parameters should be investigated for the desired material properties and microstructure as a result of the selective laser melting process. Another study investigated NiTi shape memory alloy using the selective laser melting process which possesses similar stress-strain characteristics as normal NiTi [26].

2.2 Selective Laser Melting

Selective laser melting (SLM) is an additive manufacturing process that utilizes a laser as a heat source to form specimens from powder and utilizes a powder bed system [7]. SLM is similar to electron beam melting (EBM) which uses a laser instead of an electron beam to construct a specimen. The laser traces the powder-bed melting the powders together following a three-dimensional model that was loaded into the machine. After each cross sectional layers are formed, the specimen is lowered less than approximately 150 micrometers and additional powder is deposited and raked over the previously melted cross section. This process continues to repeat layer-by-layer of the cross section until the three-dimensional specimen is formed. After completion, the excess powder is removed from the finished product [23, 7]. The significance of the powder-bed process of SLM is that the geometry of the specimen has greater accuracy and design flexibility including specimens with complicated geometry compared to other additive manufacturing processes [23]. This layer-by layer method was first used for prototyping in the 1980's. The ability of this process has transformed from constructing simple prototypes into manufacturing suitable net-shape complex parts from three-dimensional computer modeling. The SLM process eliminates expensive tooling and any associated delays related to more conventional methods such as machining and casting of titanium and other expensive materials. This process additionally facilitates the recycle of unused powder for future specimens [27]. This is especially cost beneficial when more expensive base materials are used such as titanium. Additionally, due to the high reactivity of Titanium with oxygen and other gases at high temperatures, the SLM process is conducted in a chamber with inert gases e.g. argon [15].

The static tensile strength of as-built SLM Ti-6Al-4V is comparable to the wrought alloy that is used for conventional methods. According to Koike's study [7], the yield stress and ultimate tensile stress of the Ti-6Al-4V ELI specimens manufactured by the SLM process were comparable to wrought titanium alloy. Additionally, the tensile properties are nearly identical to as-cast Ti-6Al-4V ELI. However, the percentage elongation was significantly less and bulk hardness was greater than that of the wrought alloy [7] (Figure 2-7). The disadvantage of the lower percentage elongation is that the product is more brittle which is related to poor fatigue strength. Just as the above research, a recent study depicted that the tensile and ultimate strengths of the SLM specimens were a little higher than Koike's study, but the percentage elongation were less as depicted in Figure 2-8 and Figure 2-9 [15]. In that study [15], Ti-6Al-4V powder was subjected to a multi-directional laser scan to examine the anisotropic properties of the material. The SLM samples were deposited in the X, Y, and Z directions for comparison of anisotropic behavior. A few samples were additionally subject to post-processed machining to address the issue of the inherently rough surface finish in the as-deposited samples which traditionally correlates to lower fatigue strength. Additionally, an abundance of porosity was observed in all of the samples that also significantly decreases the fatigue strength in relation to their wrought counterparts as seen in Figure 2-11 of the fractured surfaces. Interestingly, this study indicated that by addressing the rough surface, the machined surface SLM specimens did not provide much increased benefit to fatigue testing in comparison with the as-deposited specimens. The post-process machining most likely introduced porosity to the surface and that possibly affected the fatigue strength. In this study [15], the fatigue performance was lower than wrought material by 77 percent regardless of build orientation or surface quality.

Furthermore, the samples that were deposited in the Z direction experienced the least quality of fatigue performance. However, the samples that were built in the x-direction sustained 60 percent higher loads at the same number of cycles to failure compared to the z-direction. The x-direction samples failed at 30% higher loads at the same number of cycles compared to the y-direction. Compared to the wrought material, the fatigue results of the specimens built in the z-direction depicted over 85 percent load reduction at 200k cycles to failure. The low fatigue performance in comparison to wrought material resulted from the rough surface finish, porosity, microstructure and high residual tensile stresses. Residual stresses were measured and are depicted in Figure 2-12 [15]. Furthermore, build orientation with respect to fatigue strength is significant. According to this information, designers or engineers should understand the significance of build direction with respect to component design and implementation.

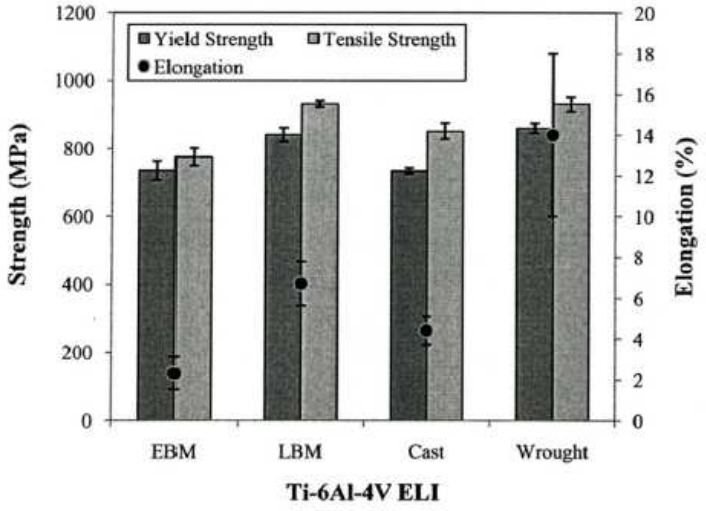

Figure 2-7: [7]

	Average	STDEV
Yield strength (MPa)	910	9.9
Ultimate strength (MPa)	1035	29.0
Elongation (%)	3.3	0.76

Figure 2-8: Tensile properties of SLM [15]

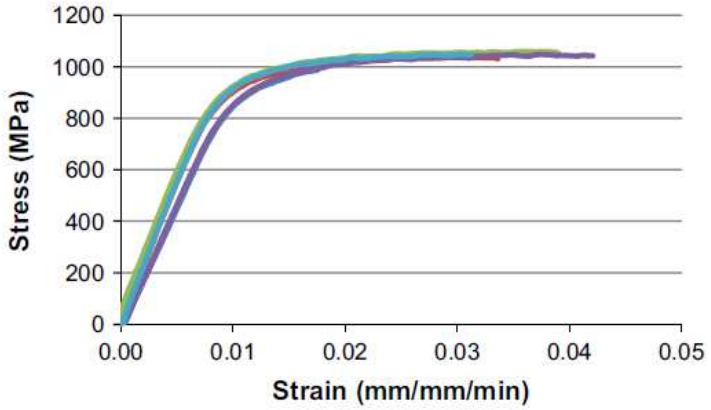

Figure 2-9: Stress vs. strain curves for tensile specimens manufactured in the x-direction as-deposited [15]

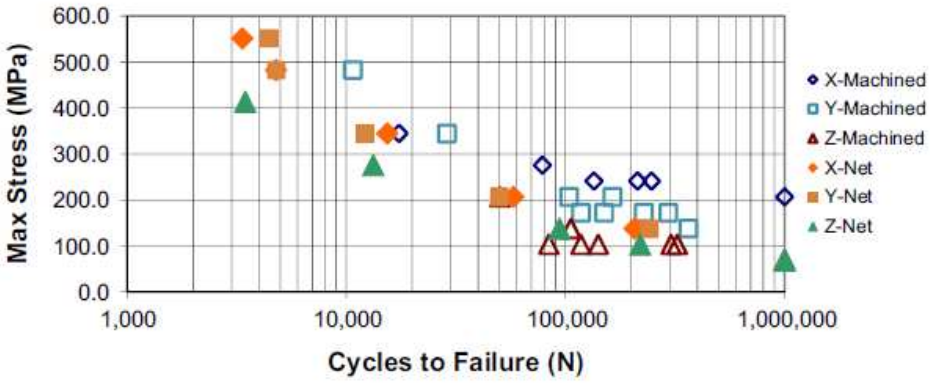

Figure 2-10: Fatigue results R = -0.2 and Kt = 0 [15]

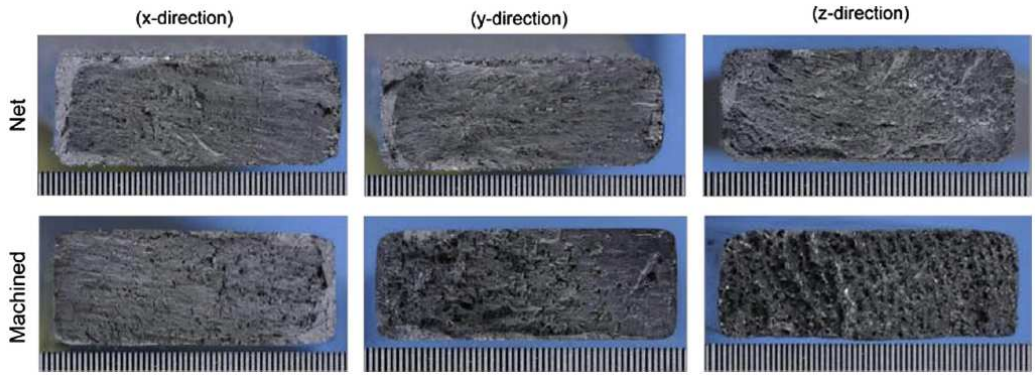

Figure 2-11: Fatigue fracture surfaces [15]

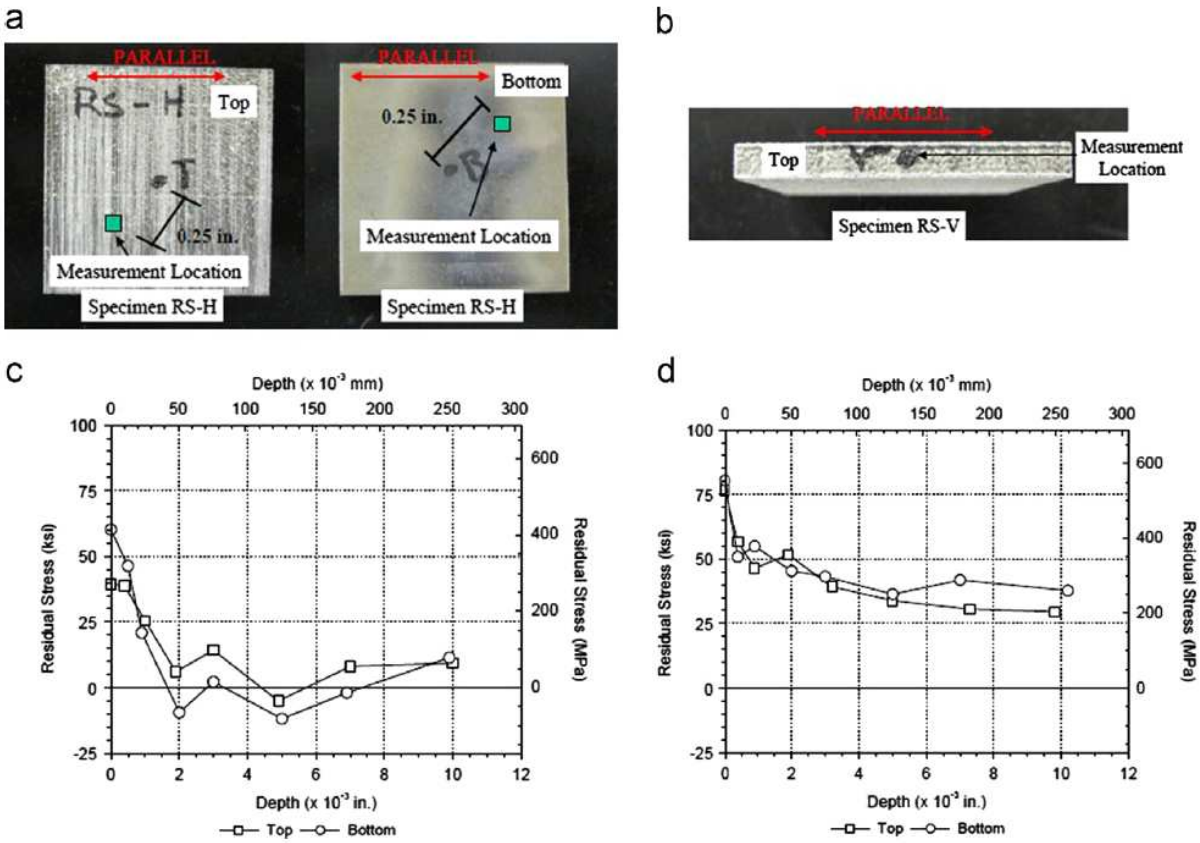

Figure 2-12: Residual stress measurements [15]

According to Leuders et al., fatigue strength is improved by reducing the porosity and residual stress. The porosity and residual stresses are reduced by heat treatment e.g. hot isostatic pressing. Crack initiation is influenced mainly by porosity and crack growth is influenced by

residual tensile stresses [28]. The porosity of parts manufactured by SLM contribute to decreased fatigue life compared to wrought material. The process of SLM results in residual stress due to the low temperature of the build chamber. The temperature differential between the melted section of the specimen in comparison with the already solidified previously layer contributes to the residual tensile stresses on the surface which are detrimental to fatigue life [15]. According to Qiu's study [27], laser power and scan are related to porosity. It was found that the increase of laser power and laser scanning resulted in lower porosity. A post-manufacturing process e.g. hot-isostatic-pressing (HIP) decreases the porosity and the drawback of HIP is that it improves the ductility with the cost of strength and fatigue reduction [27,15]. However, ductility can be improved by heat treating which coarsens the lamellar microstructure and if porosity is present along with other defects, the increased ductility may be associated with an increase in toughness and a decrease in notch sensitivity. The specimen may be less sensitive to crack initiation with respect to porosity due to the increased ductility with heat treatment [15].

The building strategy of SLM induces residual stresses which are unavoidable without any post-processing processing. In comparison to the electron beam melting process, SLM is not preheated to an average temperature of 600 C. The elevated temperature reduces the thermal gradients that influence the residual stress post manufacturing. The microstructure of the specimens are dependent on the ambient temperature and cooling rate. These parameters determine whether the microstructure is lamellar or globular (fine or coarse). Fracture toughness, fatigue crack propagation and oxidation behavior are influenced by a lamellar microstructure, and strength, ductility, and fatigue depend on a globular microstructure. The

SLM process produces specimens with a finer microstructure and higher residual stresses since the solidification rate is higher since the working zone is not preheated [22]. However, in the production of dental implants, the finer surface control of SLM versus EBM is more desirable [7].

2.2 Electron Beam Melting

Electron Beam Melting (EBM) is another additive manufacturing process that is similar to Selective Laser Melting (SLM). Instead of utilizing a laser, EBM uses high speed electrons that are meticulously directed towards the powder according to the 3-dimensional model in the computer. EBM net shape parts are manufactured in a vacuum at elevated temperatures approximately 600 C [8, 29]; which is different than the SLM process that utilizes inert gases e.g. argon at a non-elevated temperature. The focused electrons are electromagnetically scanned onto the powder bed which fuses the powdered material together according to each cross section of the model. Subsequently, gravity is used to feed additional powder from cassettes and is raked across the build platform after each scan continuing the layer-by-layer process of each cross section of the computer model. After each melting cycle the specimen is lowered and additional powder is raked across the bed. Similar to SLM, the EBM process follows the three-dimensional model that is loaded into the machine which could be derived from an MRI image etc. During the manufacturing process of each cross section, the electron beam scans each specific area of the bed to preheat or lightly sinter the powder to circumvent powder spreading. After lightly sintering the powder, the electron beam melts the powder into a molten pool and the molten pool solidifies into the desired net shape according to the cross sections determined by the three-dimensional CAD model. Essentially, the EBM process

methodology is simple as it requires three basic processes: spreading the powder, pre-heating and melting. These three processes are repeated each time the object is lowered after each cross section is formed and additional powder is raked across the building platform [7]. According to Murr [30], the EBM process melts approximately 100 micrometers thick of powdered material together according to each sliced cross section from the three-dimensional CAD model. However, the specific cross sectional thickness and other parameters desired could be tailored to the design implementation of the finished component and the desired mechanical properties.

EBM is similar to SLM that there is freedom in designing and optimization. Traditionally, machined components must contain geometries that are possible of being machined or casted. The EBM process or other additive manufacturing practices provides the possibility to construct non-traditional or structures with cumbersome geometry e.g. non-porous structures or open cellular foams used for biomedical implementation [31, 16, 32]. With respect to conventional manufacturing, the geometries of the specimens manufactured in the machined process typically contains more material which corresponds to more weight and higher costs and carbon footprint. EBM or other AM types permit specimens to be constructed with optimized geometry and amount of material to support the design loading [1]. Just as the other additive manufacturing processes, the mechanical properties and fatigue strength must be determined before implementation. The variables (e.g. power, scan speed) must be optimized for a specific design. Additionally, post-process treatment e.g. hot-iso-static-pressing could alter the fatigue properties for its intended implementation. However, according to Chan's [6] study, the post-process method of electro discharged machining (EDM) of SLM and EBM specimens slightly

improved the fatigue life, but were much less than the wrought titanium alloy. The as-deposited rough surface depicted cavities and gaps that contributed to the lower fatigue strength compared to wrought titanium [6]. Therefore, it is necessary to explore other post processing methods.

According to a recent study [1], material properties of Ti-6Al-4V specimens that were manufactured using the EBM process were assessed. Samples were constructed as-deposited, post-process machined, and post-process machined and peened. Peening is a tool that is utilized to eliminate tensile residual stresses on the surface which are detrimental to fatigue strength. Peening plastically deforms the surface and as a result forms compressive residual stresses which are more beneficial to fatigue life which retards crack growth on the surface. Since EBM for this study was conducted at a high ambient temperature at approximately 700 degrees C in a vacuum build chamber to minimize residual stresses, post-process heat treatment such as hot-isostatic-pressing was not used in this study. The specimens in this study exhibited anisotropic mechanical properties which were related to the directionally dependent microstructure as a result of the build direction. Additionally, there was observed porosity and high surface roughness in the samples (Figure 2-13). The rough surface which contained many possible crack initiation sites and the high porosity possibly contributed to the poor fatigue life compared to the wrought material. The measured residual stresses of the specimens were compressive on the bottom and tensile on the top (last melted section of the EBM process) as depicted in Figure 2-15. On both sides of the specimen at 0.03 mm deep, the residual stress was close to zero. In contrast to SLM processing, the EBM process uses elevated temperatures in the build chamber to minimize the residual stresses which was described above [1].

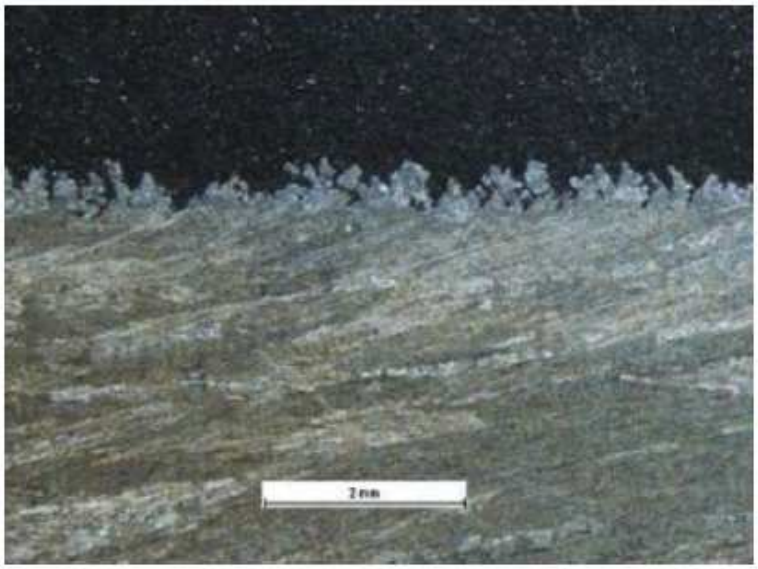

Figure 2-13: Cross section at the surface of sample produced by ARCAM [1]

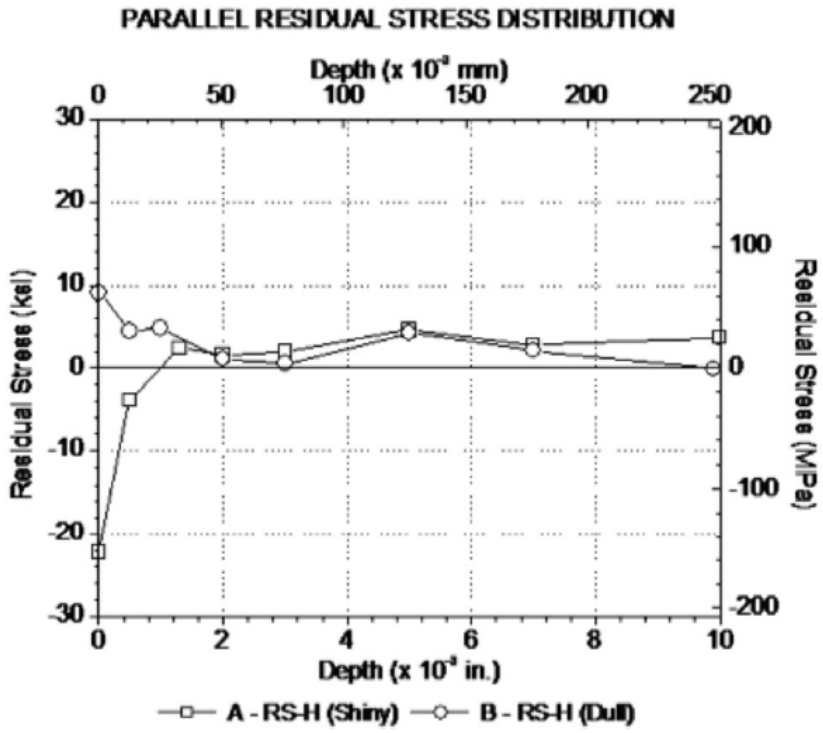

Figure 2-14: Residual stress measurements of the EBM specimens as a function of depth in the x-direction at the top (a) and the bottom (b) [1]

Additionally, the fracture toughness of the EBM specimens were tested per ASTM E 399 (Figure 2-15 and 2-16). The CT specimens were fabricated as blocks using EBM in the horizontal and

vertical orientations and then they were machined per the standard. The fracture toughness results of the EBM specimens were higher than wrought Ti-6Al-4V. However, the EBM specimens tested had higher fracture toughness and lower tensile strengths. Therefore, it is more than likely that a thicker compact specimen would be needed to validate the results [1]. Additionally, fatigue crack growth tests were conducted according to ASTM E647, using CT specimens that were EBM deposited and machined. Additionally, flat bar with low Kt (1.0) high cycle fatigue specimens were fabricated using the EBM process in both the horizontal and vertical orientation. The high cycle fatigue specimens were exposed to maximum stress levels between 100 to 600 MPa at a -0.2 load ratio and were subject to testing per ASTM E466-07 in each category (as-built, machined, machined & peened) as depicted in Figure 2-17. The results indicated that the as-deposited EBM and post-processing samples depicted lower fatigue strength compared to wrought material. The vertical oriented built specimen with post-processing peening and machining demonstrated higher fatigue strength whereas the other orientations with post-processing peening and machining did not exhibit much improvement. Additionally, the post-processing machining did not prove any more beneficial than the as-deposited specimens in this study. The machining most likely brought the internal porosity to the surface which became crack initiation sites just as the rough surface of the as-deposited specimens [1]. Even though additive manufactured components possess lower fatigue strength than the wrought material, it would be beneficial to construct actual components that are to be implemented in industry and test them individually under normal loading conditions. If the part performs without failure, then it would be possible to implement AM processing. However, just as any three-dimensional printing, the size of the specimens are constrained to the size of the

build chamber, but this process would be useful for many components of smaller size. According to the above study [1], the component or structural part that was manufactured by the EBM process was fatigue tested under normal loading conditions using the original fasteners used in the industry. All of the components lasted double the design life at the design load. After double the design life, the components were subjected to double the design load until failure. Not only did the components last more than double the design life, the fasteners failed first and then the component following. It is important to note that the components without any post-processing manufacturing lasted more than double the design life at the design load. Therefore it is important to individually test components according to their design criteria. If they pass comparable to the components tested in the above research, then it is possible that they could be implemented which could replace conventional machining and ultimately save material and energy costs [1].

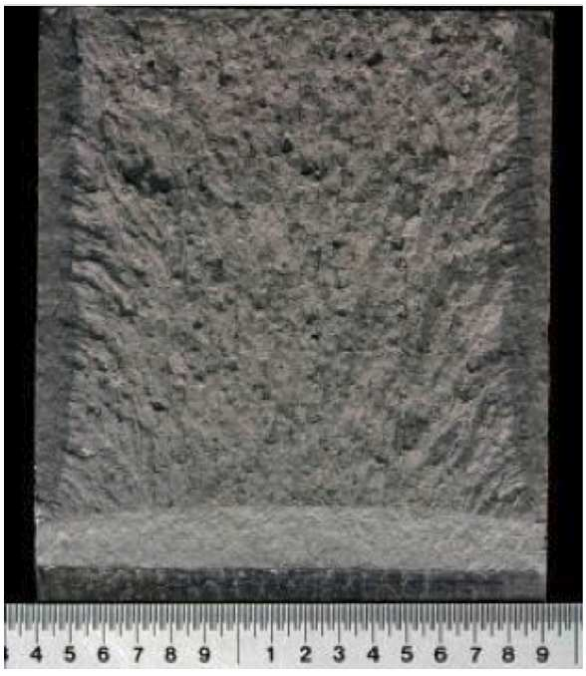

Figure 2-15: Fracture surface of a fracture toughness specimen [1]

Orientation	Kq (MPa√m) Ave	Stdev
Horizontal	110	8.9
Vertical	102	7.4

Figure 2-16: Fracture toughness properties of the EBM Ti-6Al-4V specimens [1]

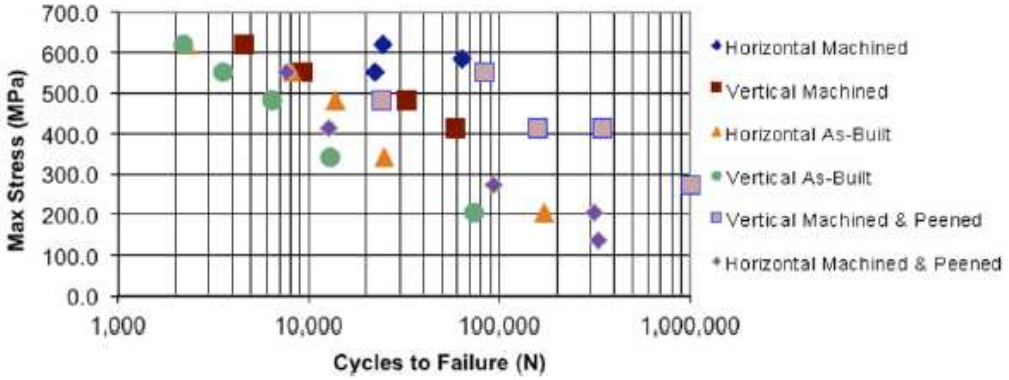

Figure 2-17: Fatigue results of the EBM specimens R = -0.2 and Kt= 1.0 [1]

The tensile properties of the as-deposited specimens in the horizontal and vertical condition are slightly variable which is dependent on the anisotropic properties as depicted in Figure 2-18. Additionally, the as-deposited specimens exhibited much lower percentage elongation compared to wrought titanium which contributes lower ductility of the EBM material [1]. A study provided by Ladani et al provided tensile results of specimens that were manufactured by an ARCAM machine in three different orientations (Figure 2-19). This author also addresses the anisotropic material properties and compares the values with other literature values. According to the stress versus strain curves of each orientation, the specimens manufactured in the top orientation exhibited higher tensile and ultimate strengths but less percentage elongation (Figure 2-20. The top built specimen exhibited much less tensile strengths with percentage elongation that was almost comparable to the side built. Therefore, the anisotropic behaviors

of the different build orientations of the EBM specimens are significant and designers should consider this when they design for implementation. Additionally, Ladani et al provided a comparison the values obtained with other literature (Figure 2-21) [33].

	UTS (MPa)		0.2% YS (MPa)		Elong %	
Orientation	Ave	Stdev	Ave	Stdev	Ave	Stdev
Horizontal	833	22	783	15	2.7	0.4
Vertical	851	19	812	12	3.6	0.9

Figure 2-18: Tensile properties of the EBM Ti-6Al-4V specimens [1]

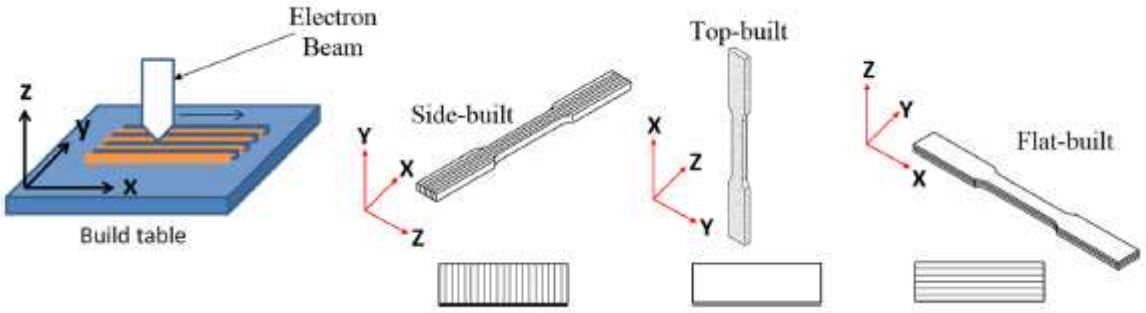

Figure 2-19: EBM dog bone samples produced in three different orientations by the ARCAM machine [33]

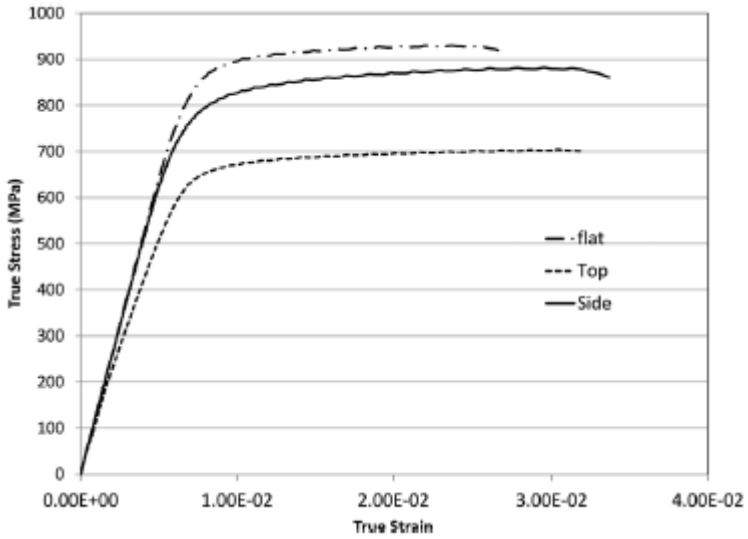

Figure 2-20: Stress-strain curves for the flat, top and side built orientations [33]

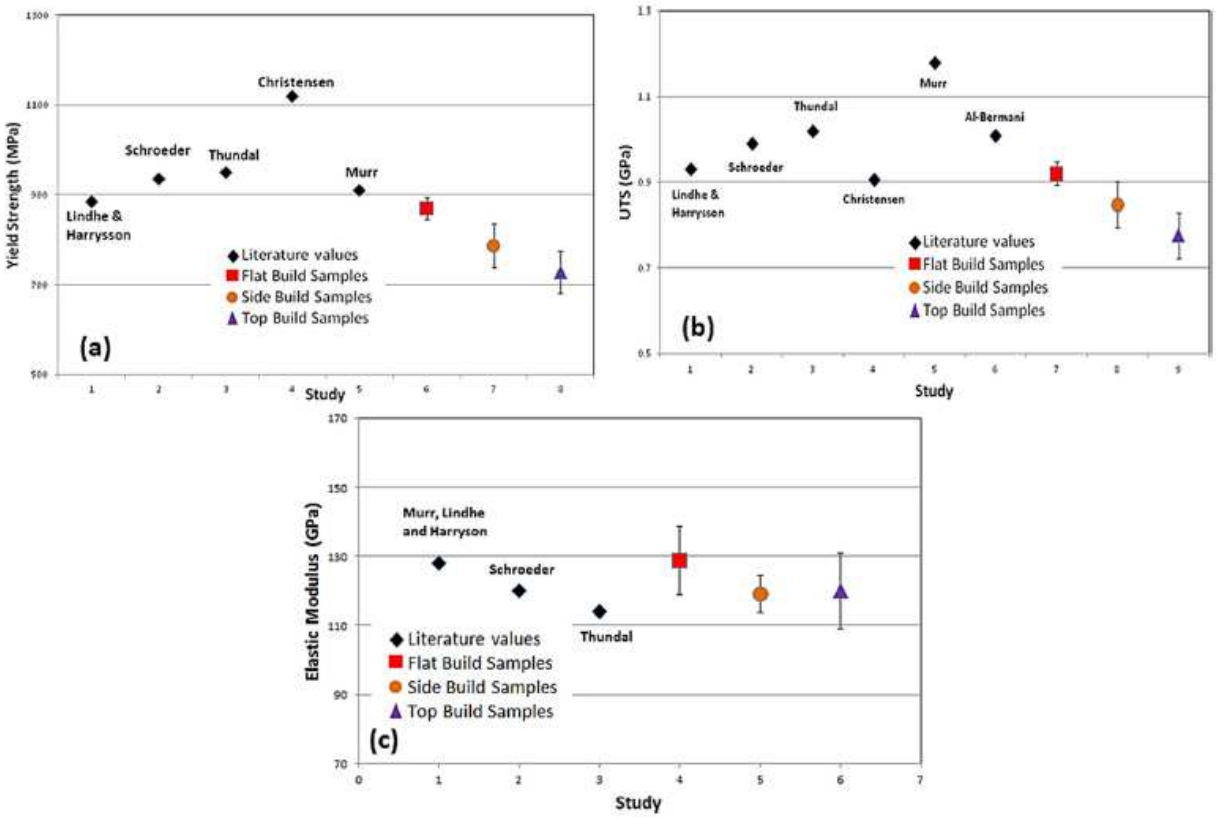

Figure 2-21: Comparison with other literature values of yield strength (a), ultimate tensile strength (b), and elastic modulus (c) [33]

Additional studies examined the mechanical properties of specimens manufactured by EBM. According to Koike's study [7], it was determined that the static tensile strength of the EBM Ti-6Al-4V ELI manufactured specimens was also comparable to cast and wrought Ti-6Al-4V ELI just as the SLM components (Figure 2-22). Furthermore, the bulk hardness of the EBM specimens was higher than that of LBM, cast and wrought material (Figure 2-23). Furthermore, Facchini et al [29] indicated that EBM produced specimens with 99.4 percent density and an increase in density increases the fatigue resistance. This study indicated that the fatigue resistance of as-built Ti-6Al-4V alloy is comparable to cast materials and lower than wrought materials. However, hot-isostatic pressing (HIP) increased the fatigue resistance. The microstructure is slightly coarsened by the HIP process which decreases the strength and increases the elongation at fracture. As a result, the fatigue strength is significantly improved. [29].

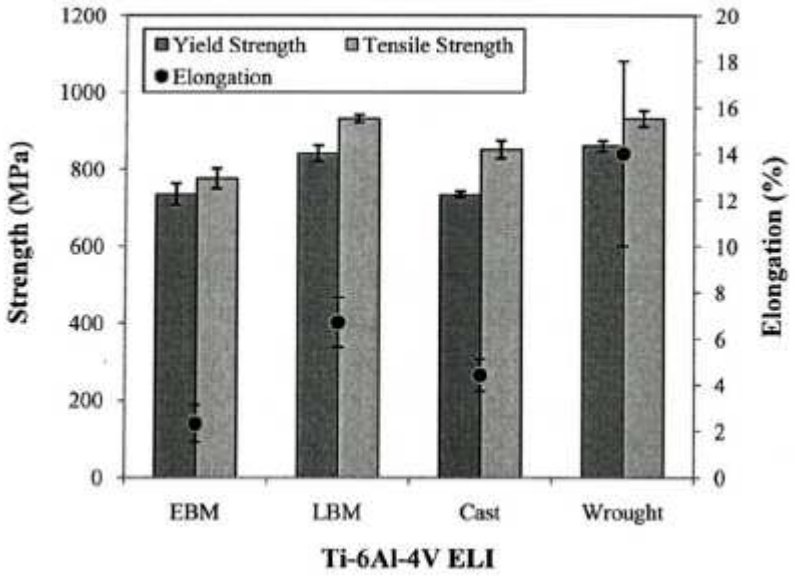

Figure 2-22: [7]

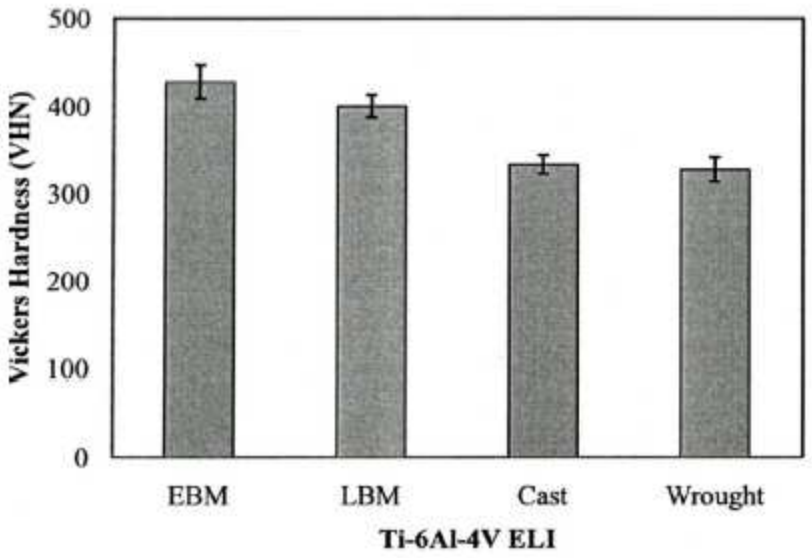

Figure 2-23: Bulk hardness [7]

Electron beam melting along with other additive manufacturing processes is an exciting technological advance. The possibilities are endless with respect to design and implementation. The tensile properties of Ti-6Al-4V are comparable to wrought material. With some post-process heat treatment or other processes the fatigue strength and ductility could be improved from the as-built specimens. The ease of manufacturing along with cost savings from material wasting, this manufacturing process will revolutionize current manufacturing practices [12].

Chapter 3: EBM Component

3.1 Material Properties

The components in this study were manufactured by an Arcam EBM system using Ti-6Al-4V powdered alloy. The EBM components were manufactured using the same parameters as were used in a previous study to manufacture EBM coupon samples that depict the tensile properties in Table 3-1. It was assumed that the material properties of the coupon samples were identical to the components manufactured using the same parameters and ambient conditions. Arcam indicated that Young's Modulus for EBM Ti-6Al-4V was 120 GPa. Table 3-2 depicts Young's Modulus that was obtained from other literature studies [8, 33].

Table 3-1 Tensile properties [1]

Orientation	UTS (MPa)	O.2% YS (MPa	% Elongation
Horizontal	833	783	2.7
Vertical	851	812	3.6

Table 3-2 Young's modulus

Source	Young's Modulus (MPa)
Arcam	120
Ladani	127
Schroeder	120
Thundal	120

3.2 EBM Components Tested

The specimens that were used in the monotonic and cyclic testing procedures were fabricated from powdered Ti-6Al-4V using electron beam melting with material properties indicated in Section 3.1. The novelty of this research was to test and investigate an actual structural component in its intended design function. Essentially, if the actual component experienced the

design loading conditions without failure, then it would be possible to use EBM components in the industry even though the coupon samples demonstrated lower fatigue strength compared to wrought material.

As described in the literature study, the main potential benefit of additive manufacturing would be the ability to manufacture components and to implement them in their respective design without being subjected to any post process manufacturing processing which increase costs. This potential benefit was investigated by subjecting EBM components to testing that were not exposed to major expensive post processing methods with the exception of post-process machining.

There were a total of eight components used in this study as indicated in Table 3-3. Four of them were manufactured using EBM and were not subjected to any post processing methods. An additional four components were manufactured using EBM and were subjected to post process machining. The post process machining was used to determine whether the smoother surface finish in comparison to the rough as built surface finish impacted the fatigue life. Fatigue crack propagation is typically enhanced by a rough surface finish which decreases the fatigue strength of the structure. However, post-process machining does not decrease the inherent porosity from the electron beam melting process as indicated in the literature study. As previously described in the literature study, there are methods that could be used to enhance mechanical and fatigue properties of additive manufactured parts. However, these processes increase production time, energy, and costs. For this purpose, the raw as built component and the as built with post processing machining were investigated.

The test samples were the same exact design and dimensions of the actual machined structural component used in the aviation industry. Therefore, the test samples were subjected to the same loading conditions as their machined counterparts in the industry. Figure 3-1 depicts the conventional machined wrought Ti-6Al-4V which is currently used in the industry. Figure 3-2 depicts the as built EBM component and Figure 3-3 depicts the EBM component that was subjected to post process machining to smooth the rough surface that was inherent of the EBM operation. Note the rough surface of the EBM as built component (Figure 3-2) compared to the conventional machined and EBM with post process machining components.

Table 3-3 Total of components tested

	As-machined	EBM	EBM Post-machining
Total components	1	4	4

Table 3-4 Number of components per test

	As-machined	EBM	EBM Post-machining
monotonic	1	2	2
cyclic	0	4	4

Figure 3-1: Conventional Machined Ti-6Al-4V

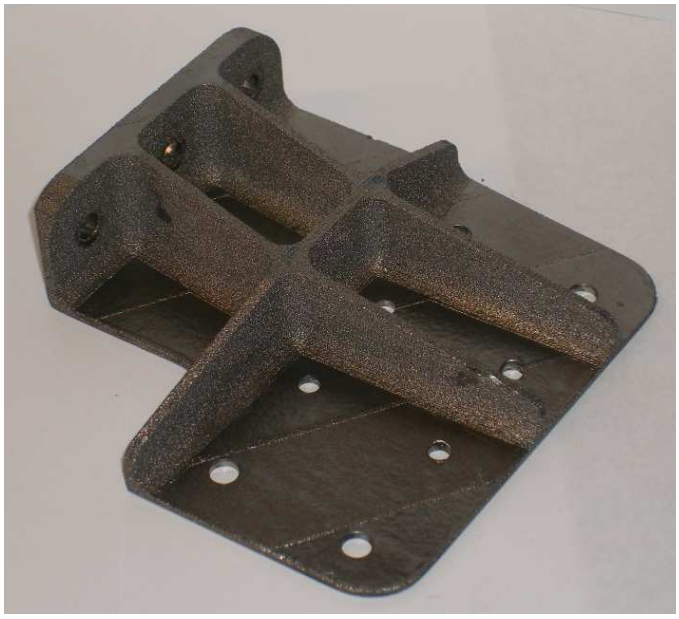

Figure 3-2: EBM Net Ti-6Al-4V

Figure 3-3: EBM Machined Ti-6Al-4V

3.3 Fasteners

As the objective of this study of this study, previously described was to investigate whether additive manufacturing would be a viable option for industry and to determine whether the components manufactured by electron beam melting would survive the designed loading conditions. As a result of this objective, the sponsor provided the exact fasteners used in service for the designed application. These fasteners were used to fasten the EBM components to the test fixture for testing. The fasteners that were used were manufactured from a nickel alloy, Inconel 718, and a titanium alloy, Ti-6Al-4V. There were a total of three Inconel 718 fasteners with a 6.35 mm (0.25 inch) diameter, and there were four Ti-6Al-4V fasteners with a 6.35 mm diameter. Additionally, there were four Ti-6Al-4V fasteners with a 4.83 mm (0.19 inch) diameter. The material properties for the fasteners were provided by the manufacturer depicted in Table 3-5. Figure 3-4 depicts the Ti-6Al-4V fastener with a 4.83 diameter the other

fasteners were similar in shape. Figure 3-5 depicts the fastener locations by number and Table 3-6 indicates the type of fastener at each location of the component.

Table 3-5 Fastener material properties

	Young's Modulus	Yield Strength	Ultimate Strength
		Mpa	
Inconel 718	203k	1034	1276
Ti-6Al-4V	117k	924	979

Figure 3-4: Ti-6Al-4V Hex-nut and bolt

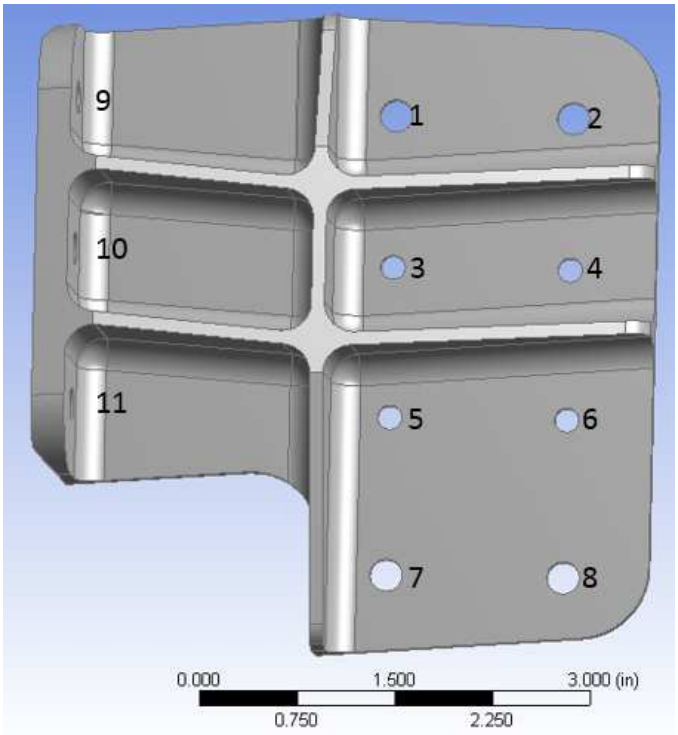

Figure 3-5: Fastener location numbering

Table 3-6 Fastener locations per Figure 3-5

Location	Fastener Type
1	Ti-6Al-4V (6.35 mm)
2	Ti-6Al-4V (6.35 mm)
3	Ti-6Al-4V (4.83 mm)
4	Ti-6Al-4V (4.83 mm)
5	Ti-6Al-4V (4.83 mm)
6	Ti-6Al-4V (4.83 mm)
7	Ti-6Al-4V (6.35 mm)
8	Ti-6Al-4V (6.35 mm)
9	Inconel 718 (6.35mm)
10	Inconel 718 (6.35mm)
11	Inconel 718 (6.35mm)

Chapter 4: Monotonic Testing

4.1 Static Tensile Testing Setup

Four samples were subjected to monotonic tensile loading on the entire fixture structure including the fasteners and two fixture pieces (fixture and base plate) after the cyclic loading tests. Two samples from each manufactured condition, EBM and EBM machined, were tested on the Instron 5585H located at the University of Washington in the mechanical engineering building. The Instron 5585H load frame had a 250 kN capacity. The samples were fixed to the same fixture that was used in the cyclic loading tests and were mounted onto the load frame depicted in Figure 4-1. The rigid linkage (used in the cyclic loading tests) was eliminated in the setup since there was no place located on the machine to include it. Pure tension was applied at a 1.27 mm/min strain rate (constant crosshead speed) to the entire assembly. The monotonic testing continued until fracture of the specimen, fasteners or the fixture occurred.

Figure 4-1: INSTRON 5585H with fixture and component

4.2 Static testing results

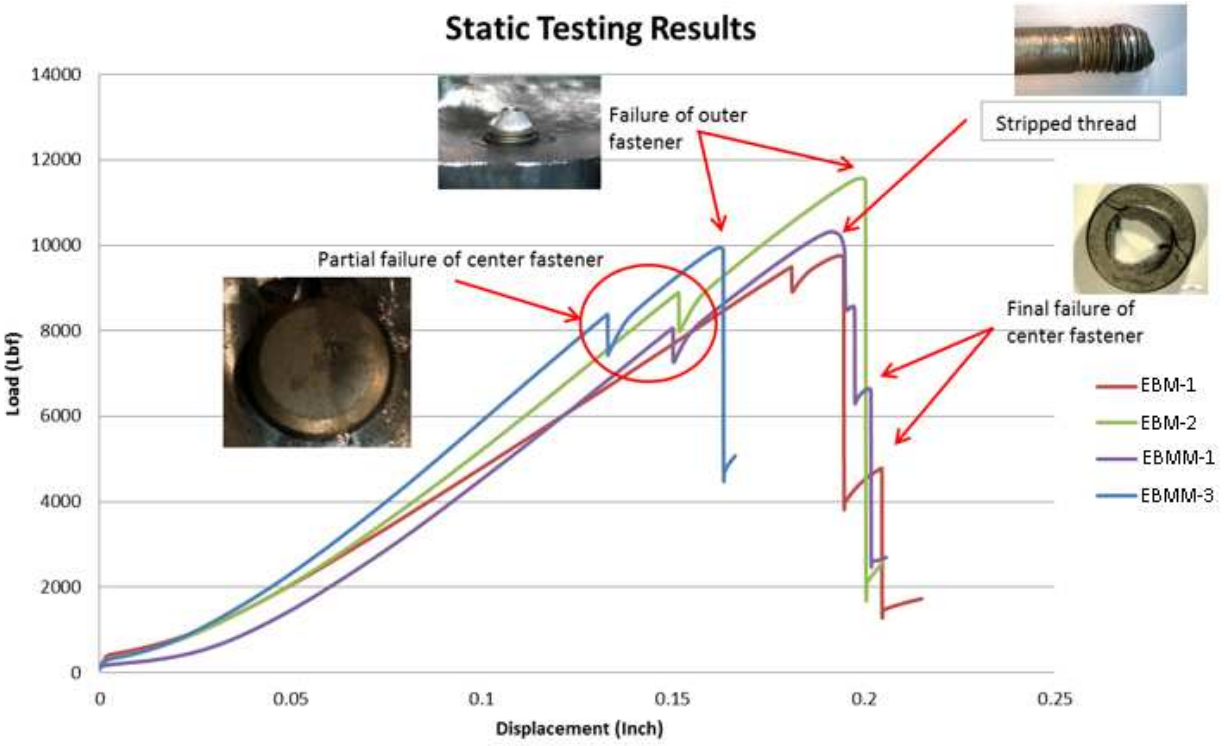

Figure 4-2: Force and displacement curve for static testing

Figure 4-2 depicts the load and displacement curve for the four samples used in the static testing. Fastener 10 (center Inconel 718 fastener) in all of the four cases, was the first to have a partial fracture at an approximately 35.6 KN (8000 lbs) load. The partial fracture occurred at the non-threaded section of the fastener which interfaced with the fixture towards the loading direction. Additionally, there was some variance regarding fastener 10 which had a partial failure when Fastener 10 on EBM-1 experienced a partial fracture near the 44.5 KN (10,000 lbs) load mark. Furthermore, fastener 10 experienced a partial failure at the non-threaded section.

Following the partial failure of fastener 10, fastener 11 was the next fastener to fail in the assembly. Fastener 11 in the EBM-2 and EBMM-3 (EBM with post-process machining) samples

completely failed with ductile failure. The fastener failed at the threads and experienced a ductile fracture as indicated by the cone at the end of the fastener depicted in Figure 4-3. In the other two samples, fastener 11 experienced failure at the threads by stripping of the bolt and the nut. After fastener 11 failed, the load force of the test dropped and the continued displacement finished the failure of fastener 10.

Figure 4-2 generally depicts the same behavior from the beginning of the test until approximately 35.6 KN (8000 lbs) load when there is a partial failure at fastener 10. This is the elastic region of the assembly in the static loading test. The displacement of the system was measured as the machine head displacement, and the load force was measured by the machine load cell. All four samples did not depict the exact same behavior in each test as evident in the fasteners which depicted different types of failures and other failures occurred at different load forces. If future tests were to be conducted, it would be necessary to use more samples with the use of additional instrumentation such as strain gauges and video equipment. However, as depicted in the cyclic loading tests, the fasteners failed instead of the components manufactured using electron beam melting technology. This is an indicator that this technology is a viable option for implementation in the industry.

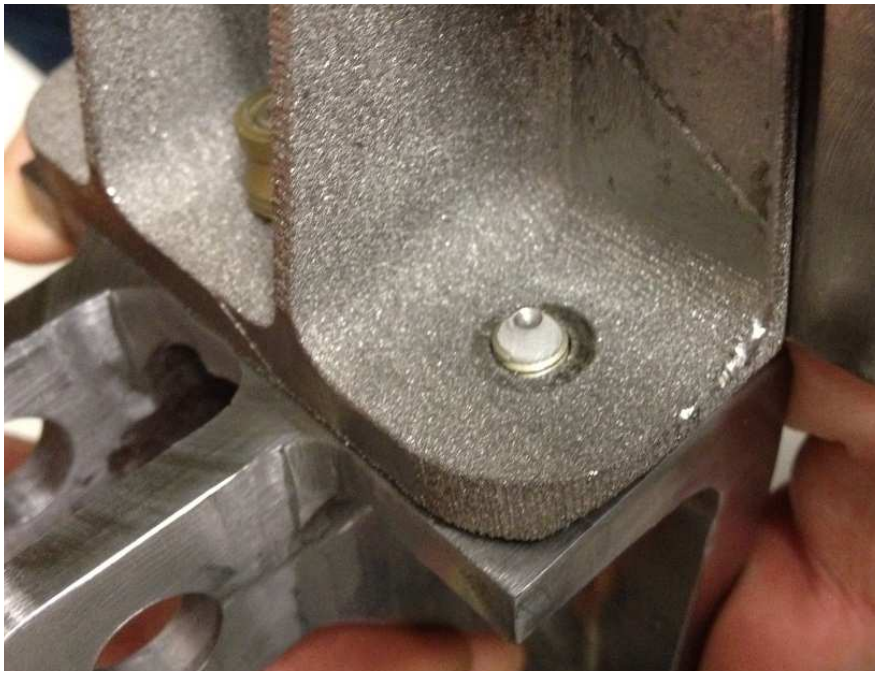

Figure 4-3: Fastener 11 Failure

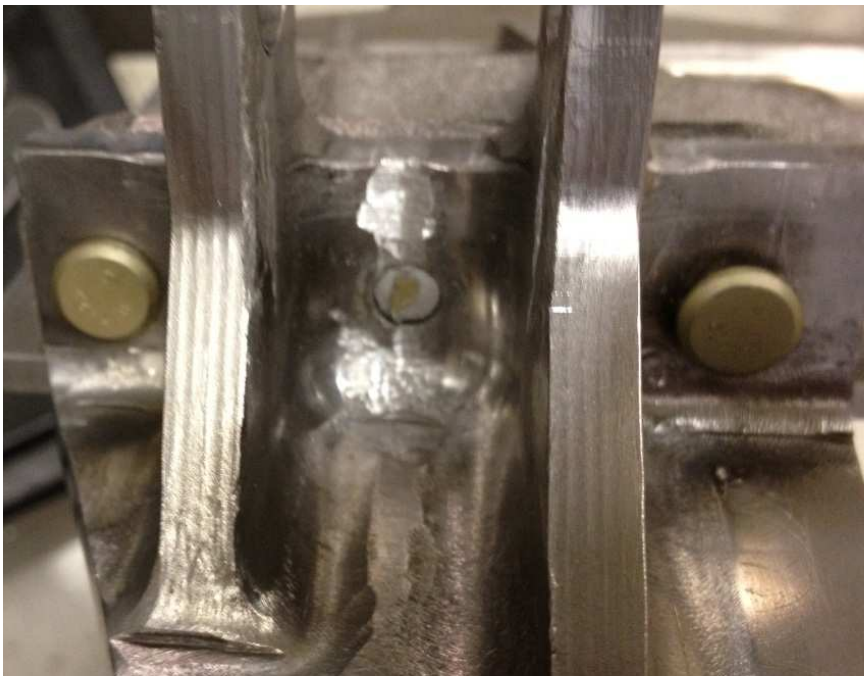

Figure 4-4: Fastener 10 Failure

Table 4-1 Failure locations on each tested specimen

Sample	Static Testing
EBM-1	Fastener 11 and 10 failure
EBM-2	Fastener 11 and 10 failure
EBMM-1	Fastener 11 and 10 failure
EBMM-3	Fastener 11 and partial 10 failure

Chapter 5: Cyclic Loading Testing

5.1 Testing Fixture

Preparation for the testing required manufacturing a fixture that would attach the specimen to the cyclic loading machine. The fixture was designed such that the specimen would experience similar loading conditions as it would in actual service. The first fixture (Figure 5-1) that was designed and used on the cyclic loading machine produced an eccentric force on the machine. This was evident due to the location of the three nickel fasteners (fasteners 9, 10, and 11) which induced bending to the structural system. The cyclic loading machine malfunctioned and stopped the testing when the original fixture was used. The original loading fixture induced an eccentric force onto the machine. After a few thousand cycles with the original fixture the procedure was aborted to avoid damage to the equipment. The original fixture (Figure 5-1) was made from steel using conventional machining and welding. It became apparent that the fixture should be modified or replaced in order to address the eccentric loading.

Figure 5-1: First designed fixture

The new fixture (Figure 5-2) included a mechanism link that transferred the eccentric force of the load to the frame of the MTS. The new fixture was machined out of lescalloy stainless steel and excluded welding to ensure durability during entire span of the cyclic loading tests. Authorization from sponsor allowed the change anticipating minimal differences in the end result. The fixture and the component were assembled together with the Inconel 718 and Ti-6Al-4V fasteners (Figure 5-3), and was placed on the cyclic loading machine with the rigid link attached to the frame of the machine (Figure 5-4).

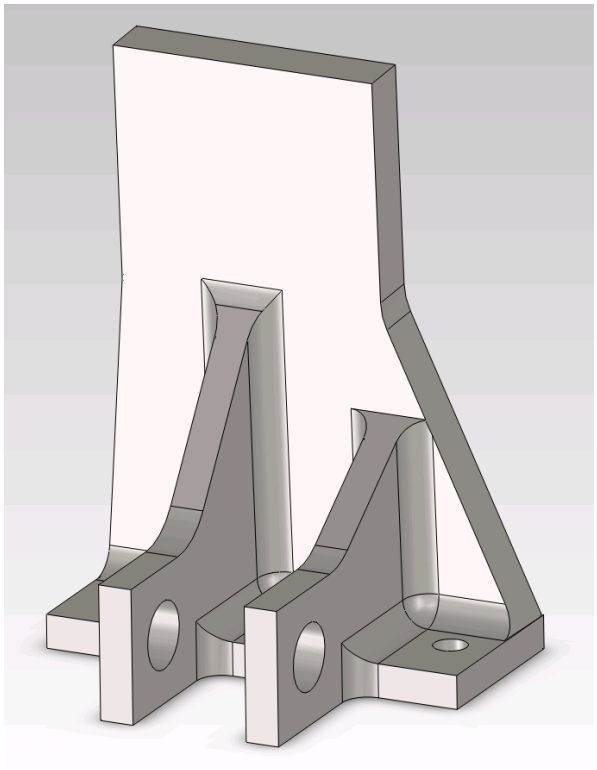

Figure 5-2: Fixture for rigid link as designed in Solidworks

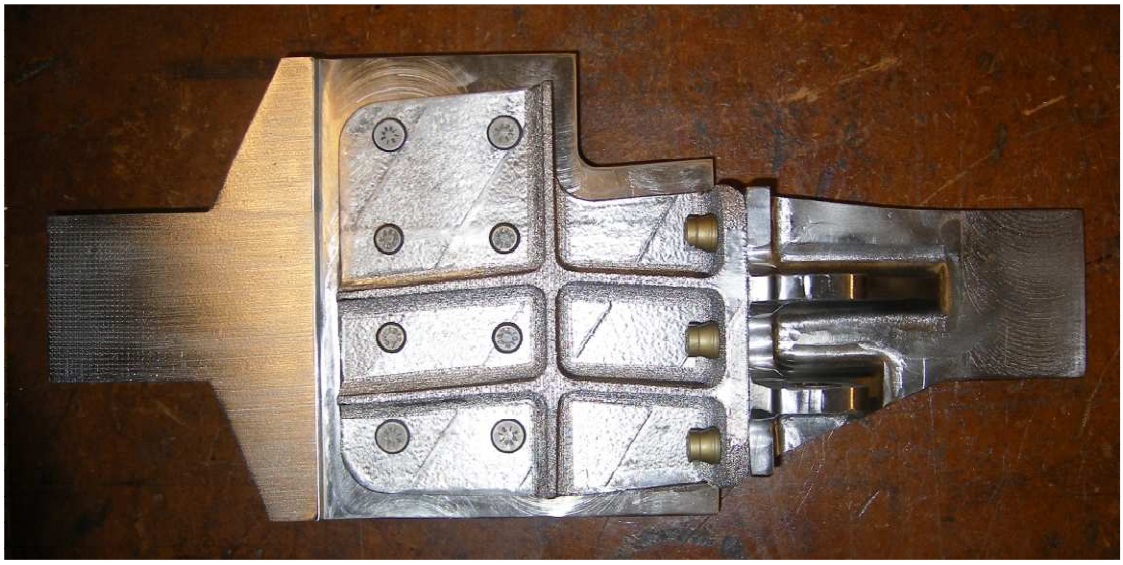

Figure 5-3: Fixture and Specimen Assembled with Fasteners

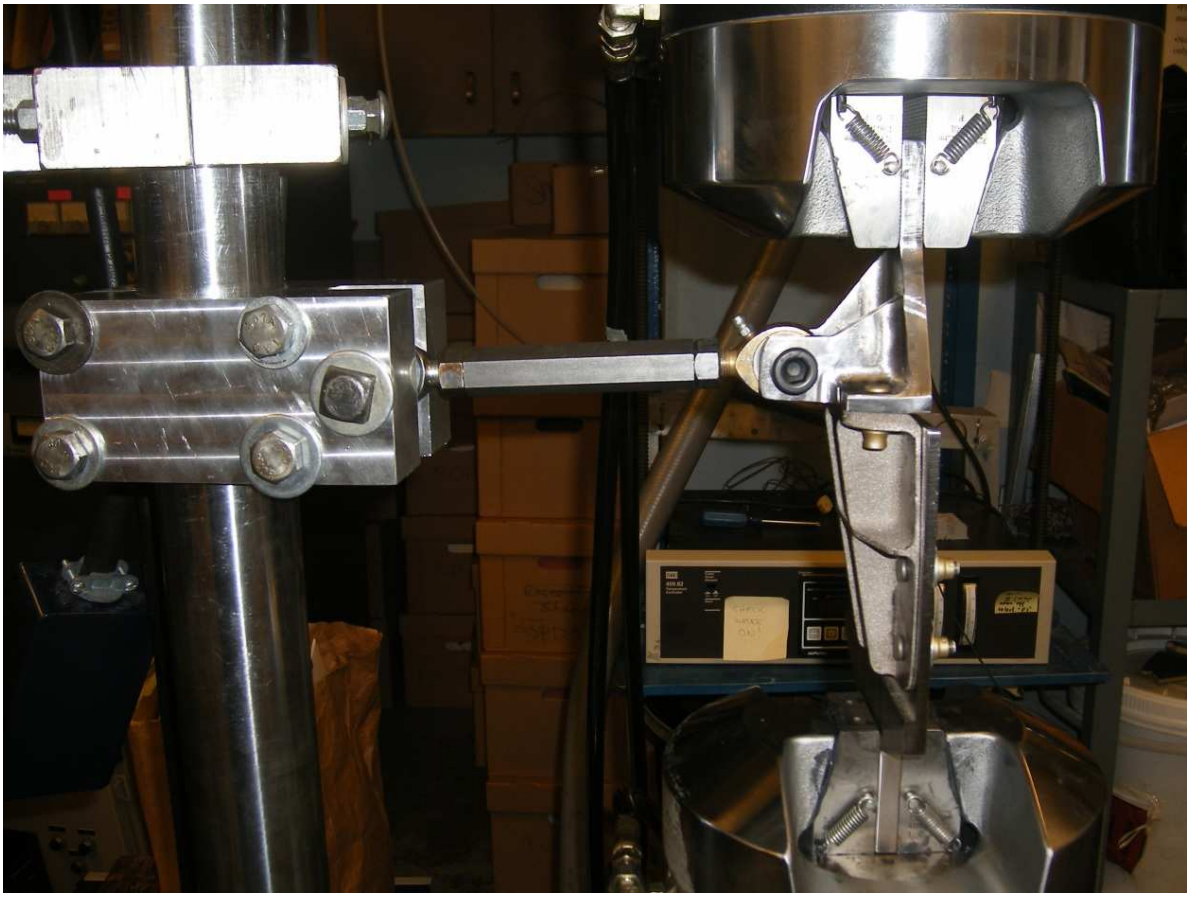

Figure 5-4: Rigid link and assembly on the cyclic loading machine

5.2 Servo Hydraulic

The cyclic loading equipment included the MTS servo hydraulic loading frame and a 458.20 MicroConsole Controller included in Figures 5-5 and 5-6 respectively. The ambient temperature was considered to be room temperature. The samples were attached to the testing fixture using the supplied fasteners. The testing fixture was mounted onto the MTS cyclic loading machine, and the load cell was balanced using the controller. The fixture was mounted to the upper collar and undesirable movement of the eccentric collars was eliminated by adjusting the collars after closing the lower hydraulic grip. The rigid link was secured to the MTS frame and the remaining slack was eliminated (Figure 5-7).

Figure 5-5: MTS

Figure 5-6: 458.20 MicroConsole Controller

Figure 5-7: Specimen with Rigid Link Fixated to MTS

The cyclic loading was defined by a sinusoidal loading profile, and the frequency was set to 10 Hz. The loading ratio was -0.39 and the tensile and compressive loads were set as per design loads provided by the sponsor indicated in Table 5-1. Each test was set to endure 500k cycles which is double the service life. The machine automatically terminated the cyclic loading test after the 500k cycle design limit or when there was added displacement e.g. fracture or failure. Following the design load cyclic testing, select samples were subjected to double the design load up to 250k cycles or up to failure of the specimen or fasteners.

Table 5-1 Design Loading (R = -0.39)

	Tension	Compression
	Newtons	
Design Load	9653	-3765
Double Design Load	19305	-7529

5.3 Cyclic Loading Results

As previously described, the designed service life of the structural component was 250k cycles. All eight samples including the fasteners survived double the service life without showing any visible signs of failure. As a result of the success of the cyclic loading tests of all eight samples (EBM and EBM with post-process machining), three samples (EBM-4, EBMM-2 and EBMM-4) were subjected to additional cycles at double the design load with the same design loading ratio of -0.39. When the design load was doubled, the number 11 fastener (Inconel 718) failed after at least 100k cycles on the three samples that were tested. Sample EBM-4, as built, underwent cyclic loading up to 177k cycles until fastener 11 failed and a crack was initiated. As fastener 11 failed each time it failed further up the shank suggesting bending and crack propagation of the EBM structural component. The fastener was replaced and the test was run to 32k cycles until it failed again. This process repeated for 26k cycles and 18.5k cycles which completely opened the crack to fracture. Additionally, EBMM-4 (electron beam melted and post process machining) sample had a fastener failure at 104k cycles at the double the design loading, and the testing of EBMM-2 was terminated at 191k cycles. Figure 5-8 depicts the results and respective fastener failures at location 11 for the three structural components that underwent double the design load. Figures 5-9 and 5-10 depict the crack that started at where the fastener is located and propagated to the edge on EBM-4. The crack is a through thickness crack and it does not run parallel to the horizontal sintered layers, and the crack traversed several layers linearly.

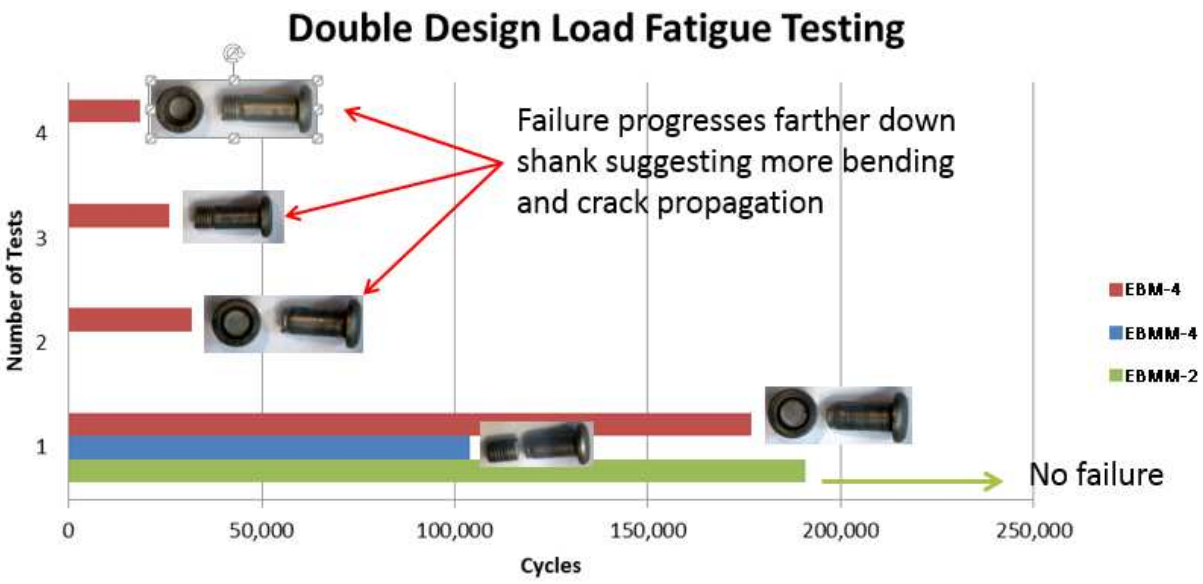

Figure 5-8: Double design load fatigue testing results

Figure 5-9: Failed Fastener 11 on EBM-4

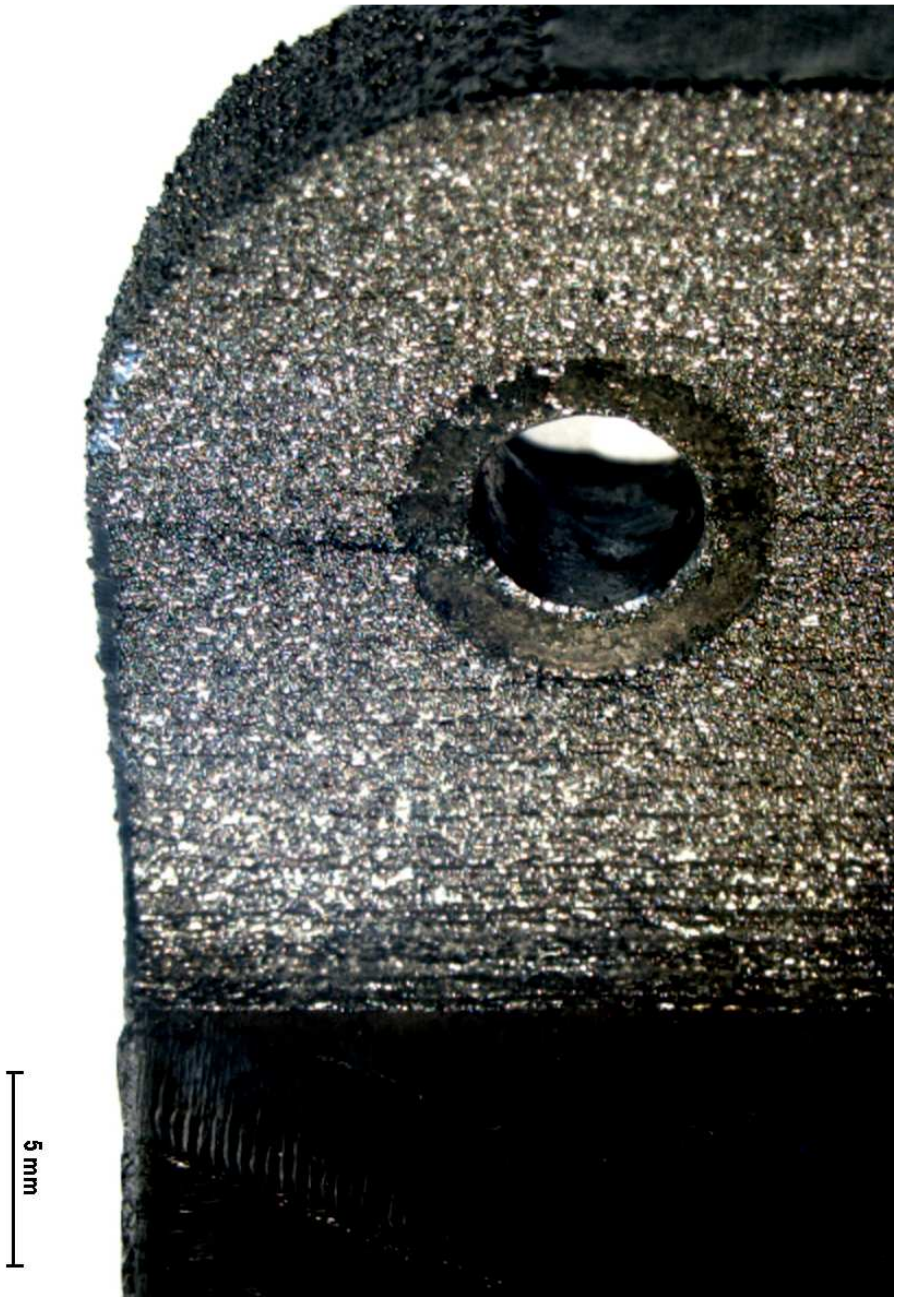

Figure 5-10: EBM-4 Crack

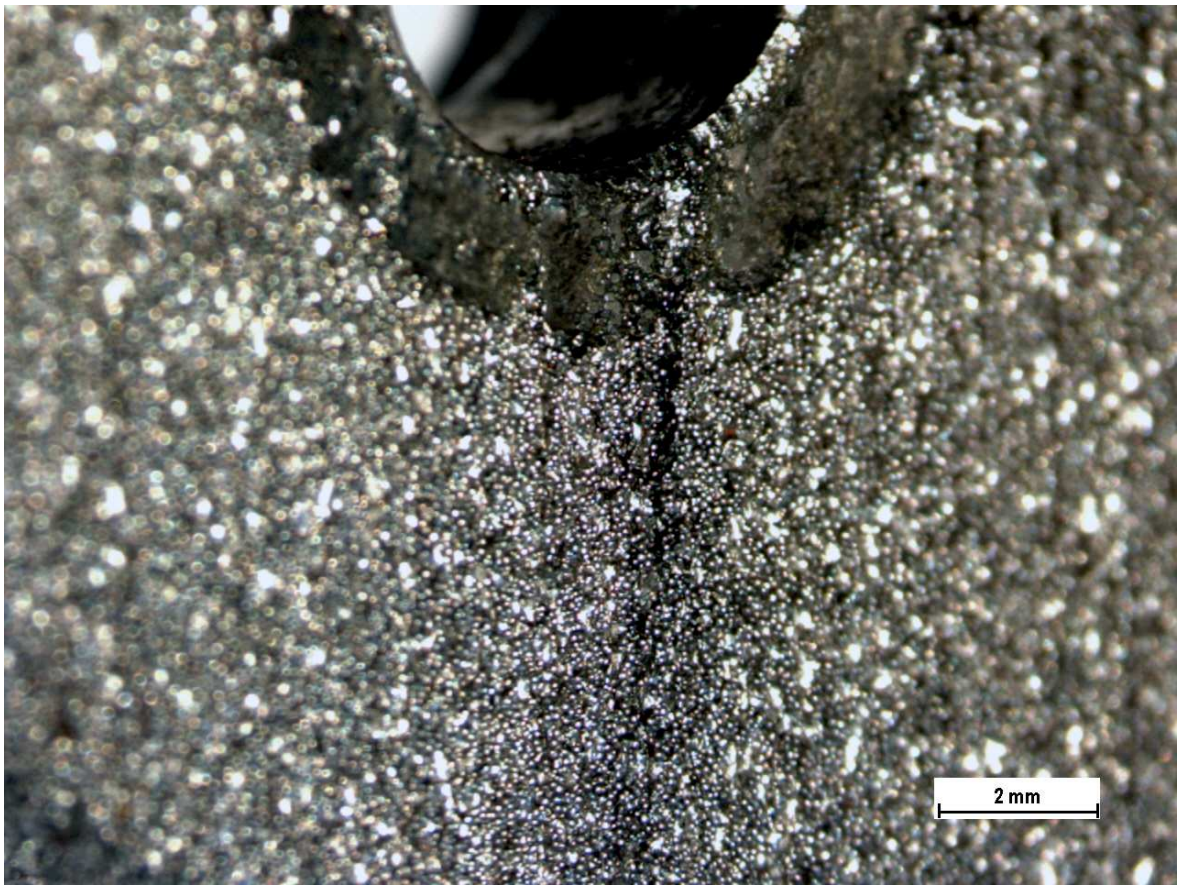

Figure 5-11: EBM-4 crack close-up

As described previously, Fastener 11 on EBMM-4 failed at 104k cycles when the design load was doubled. There were no visual signs of fracture on the structural component to the unaided eye. The test was repeated for EBMM-2 up to 191k cycles until the machine was manually stopped due to signs of scarring on the ram. The cyclic loading could not continue with the current loading as machine wear and damage was imminent.

All eight specimens did not experience failure at the design load. Three of the components that underwent additional cyclic loading testing at double the design load survived up to over 100k cycles without any visible failure. The design life was 250k cycles and the components survived at least twice that amount. If it would have been known beforehand that doubling the design

load would cause premature wear to the MTS, it would be beneficial to test the structural components up to failure at the design load. As a result of the cyclic loading tests, it was evident that the fasteners were the first to fail, but the initial crack propagating possibly increased the displacement and stress on the fastener. However, the cyclic loading tests demonstrated that the structural component did not fail at twice the design life.

Table 5-2 Cyclic loading results

Sample	Design Load R = -0.39 9.65 kN (tension) -3.77 kN (compression)	Double Design Load R = -0.39 19.3 kN (tension) -7.54 kN (compression)
EBM-1	500k cycles – no failure	
EBM-2	500k cycles – no failure	
EBM-3	500k cycles – no failure	
EBM-4	500k cycles – no failure	Fastener 11 failure: 177k, 32k, 26k, 18.5k cycles with crack detected in the component
EBMM-1	500k cycles – no failure	
EBMM-2	500k cycles – no failure	191k cycles no failure
EBMM-3	500k cycles – no failure	
EBMM-4	500k cycles – no failure	fastener 11 failure 104k

Chapter 6: Finite Element Modeling

6.1 Introduction

ANSYS Worbench 14 was used to model the fixture and component to represent the loading conditions during the cyclic loading and monotonic loading tests. The research license for ANSYS Workbench v14 was used on an HP mobile workstation equipped with Windows 7 Professional 64 bit operating system, Intel i7 quad core CPU, 8 GB RAM, and an NVIDIA Quadro with CUDA graphics unit.

The objective of the finite element modeling was to attempt to model, in the linear elastic region, the stress distributions of the component that underwent testing and to assess the failures that occurred during testing. The finite element modeling did not include plasticity. The approximate assumed boundary conditions were applied to the model. Additionally the assumed contact mechanics were applied to the model along with the material properties of each geometry body of the assembly.

6.1.1 Modeling

The tested component was modeled in Catia which was provided by the sponsor. It was converted to a Solidworks model using the resources available at the University of Washington Mechanical Engineering department. The test fixture was modeled in Solidworks and assembled with the specimen and fasteners. The fasteners were modeled as one body without the threads to simplify the FEA (Figure 6-1). In the physical world, the threads interfacing with nut and assembly served as a stress concentration factor as evident in the failures at the threads in testing previously described. The finite element model was to serve as a tool to

understand trends in the applied loading that would assist in interpreting the results of the physical testing. The fasteners as modeled in this research facilitated simple contact mechanics between the fixture and the specimen to decrease computational time. The objective of the finite element model was to obtain an understanding of the stress distribution throughout the assembly in its entirety.

An attempt was made to represent the loading conditions of the physical tests in the finite element analysis study. The assembly of the test fixture, specimen, and fasteners in Solidworks 3D CAD model were converted to line data or an SAT file type. This file type organized the line data of the geometry for the finite element program. When the line data was imported into the FEA program, ANSYS Workbench v14, it generated a solid assembly on which the boundary conditions, contact mechanics, and meshing were applied. Figure 6-2 depicts that all of the lines, fillets, bodies that were modeled in Solidworks appeared to remain in the FEA program for analysis. Other file types e.g. IGES excluded main geometry aspects when they were imported into Workbench. As a result, those file types were avoided.

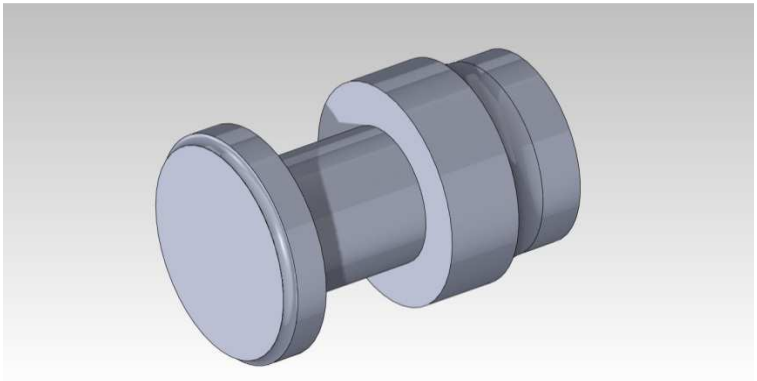

Figure 6-1: Titanium 1/4" Fastener

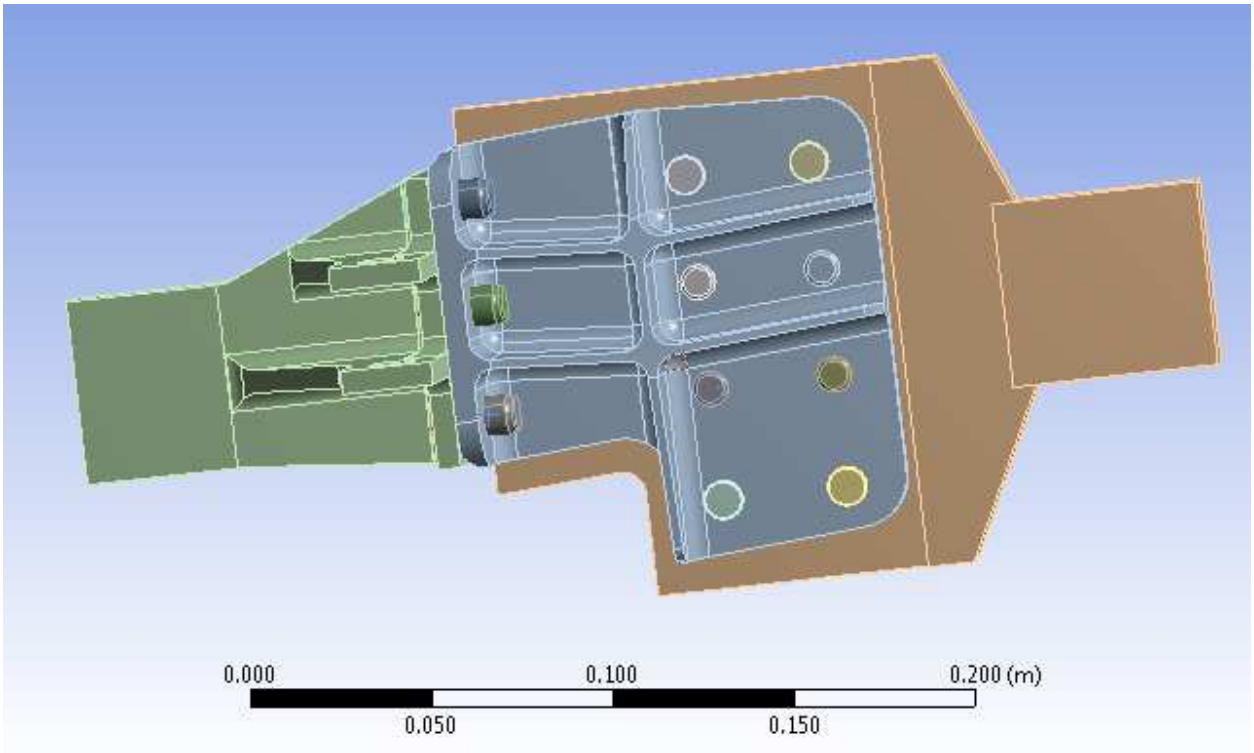

Figure 6-2: Assembly in ANSYS Workbench 14

The material properties used for the parts in the assembly in the finite element modeling are indicated in Table 6.1. For this model, the EBM specimen was assumed to be isotropic. The material properties of the fixture and backing plate were for Lescalloy high strength steel [34]. Additionally, the material properties of the nickel and titanium fasteners were provided by the manufacturer and were inputted into the program. The coefficients of friction were included in the model. The fixture facilitated the direction in which the design loads were transferred through the specimen. Note that the model in the finite element program investigated the linear elastic region of the assembly. However, an attempt was made to utilze the linear elastic model to understand trends of the applied loads and associated stress distributions.

Table 6-1 Material properties of the parts in FEA assembly

	Young's Modulus (GPa)	Poisson's Ratio	Coefficient of Friction
EBM component	120	0.3	0.3
Ti-6Al-4V fasteners	116.5	0.3	0.3
Inconel 718 fasteners	202.7	0.3	0.5
Testing Fixture	213	0.3	0.3

Figure 6-3 includes the mesh that was generated automatically using the available generate mesh function. The mesh generator provided a mesh that was appropriate for the geometry. There were a total of 101,305 nodes and 49,841 elements. The relevance center, smoothing and span angle were all set to medium.

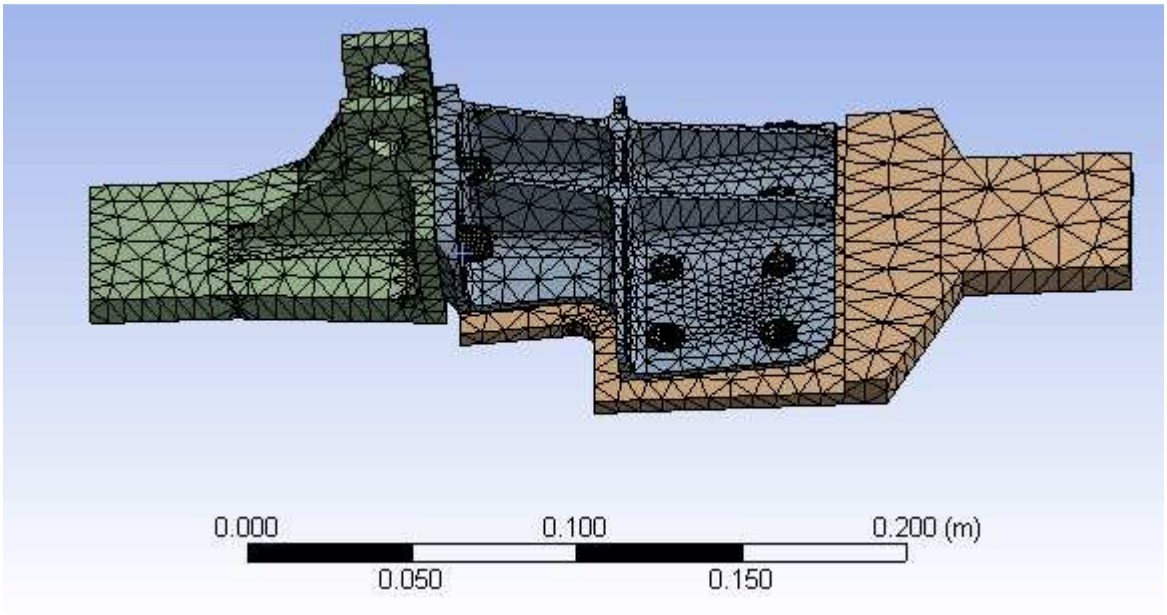

Figure 6-3: Mesh with 101,305 nodes and 49,841 elements

The assembly that was imported to Workbench included a total of seventeen different parts. As a result, connections or contacts were required in order for the loads to transfer through the system appropriately. The nickel fasteners in locations 9, 10, and 11 were imported into the model as two separate pieces each (Figures 6.4 and 6.5). The bonded contact was used to

contact the shank of the fastener and the head or nut as one piece. The contacts of the other pieces of the assembly were assumed frictional. The frictional coefficient of titanium against titanium and steel was assumed 0.3, and the frictional coefficient of nickel against steel and titanium was 0.5 [35, 36, 37]. All of the other options such as behavior, trim contact, formulation, detection method, penetration tolerance, elastic slip tolerance, normal stiffness etc. regarding frictional contact in Workbench were set to program controlled. The coefficient of friction of the materials was assumed constant in the model. Additionally as an informative aside, the scope mode, behavior and other advanced options are available if the user decides to control the contact mechanics for composites, welding, etc.

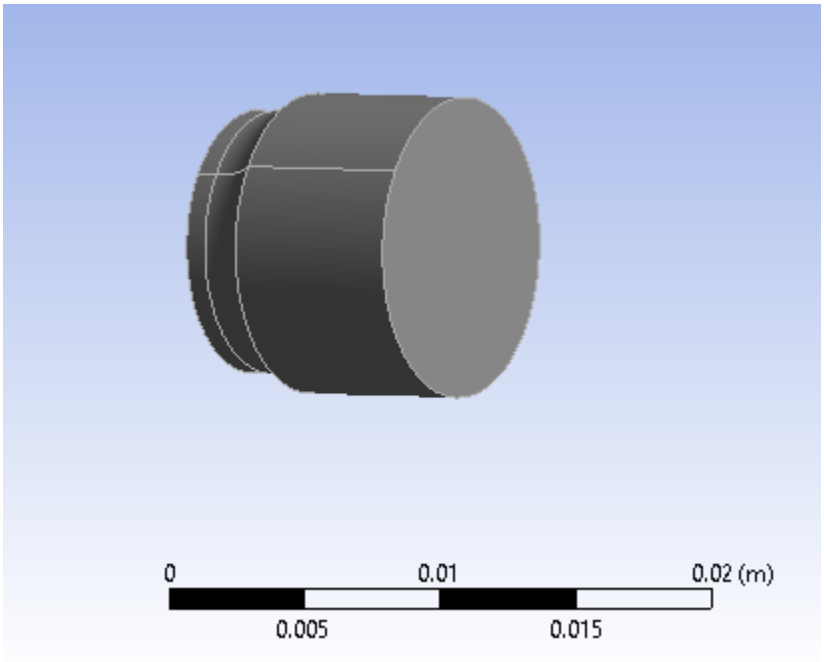

Figure 6-4: Inconel 718 fastener head

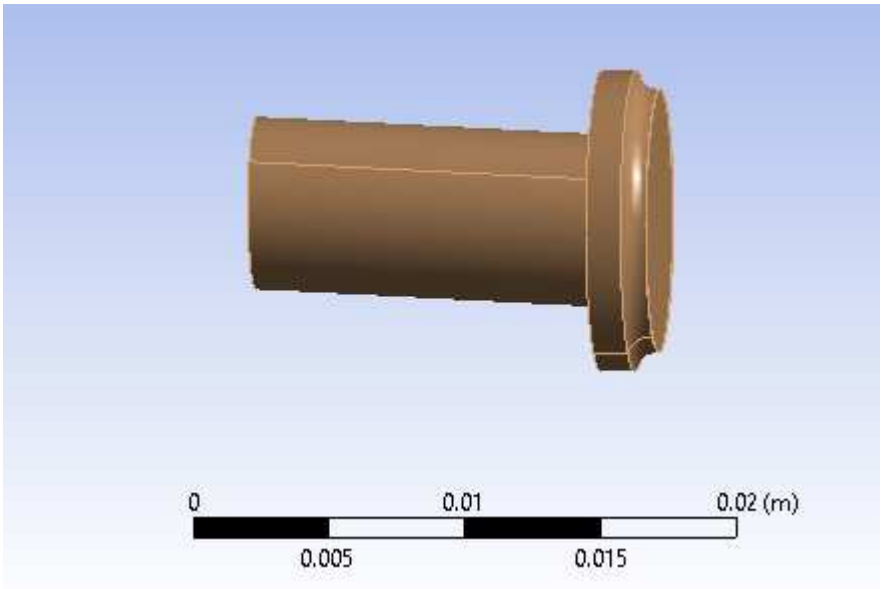

Figure 6-5: Inconel 718 fastener shank

6.1.2 Boundary Conditions

The assumed boundary conditions that were applied to the assembly represented the collars on the MTS and the rigid link between the fixture and the MTS. Additionally, the clamps of the monotonic tensile testing machine (Instron) were included in the boundary conditions. The location on the backing plate and the fixture where the clamps of the machines were placed were added to the geometry faces to increase the accuracy of the boundary conditions of displacement and fixed. In the finite element model, a fixed support was applied to the end of the backing plate on both faces (Figure 6-6). A constrained displacement for the other end of the assembly was applied fixing it in one direction normal to the clamping faces and was set to free in the other two directions including the direction of the movement of the hydraulic collar (Figure 6.7). The described boundary conditions regarding the collars were the same for the cyclic loading and the monotonic loading tests. In the dynamic loading model, zero displacement was applied in the direction of the rigid link and it was free in the other two

directions. Due to the geometry and the degrees of freedom of the rigid link, it is probable that the rigid link allowed pivoting. In the finite element model, 0 displacement was set as the boundary condition to the two faces on the fixture where it interfaced with the rigid link (Figure 6-8). In both the cyclic loading and static testing model, the applied force was applied as a distributed load along the faces where the clamps connect with the assembly and were assigned in the direction of the clamp loading direction (Figure 6-9).

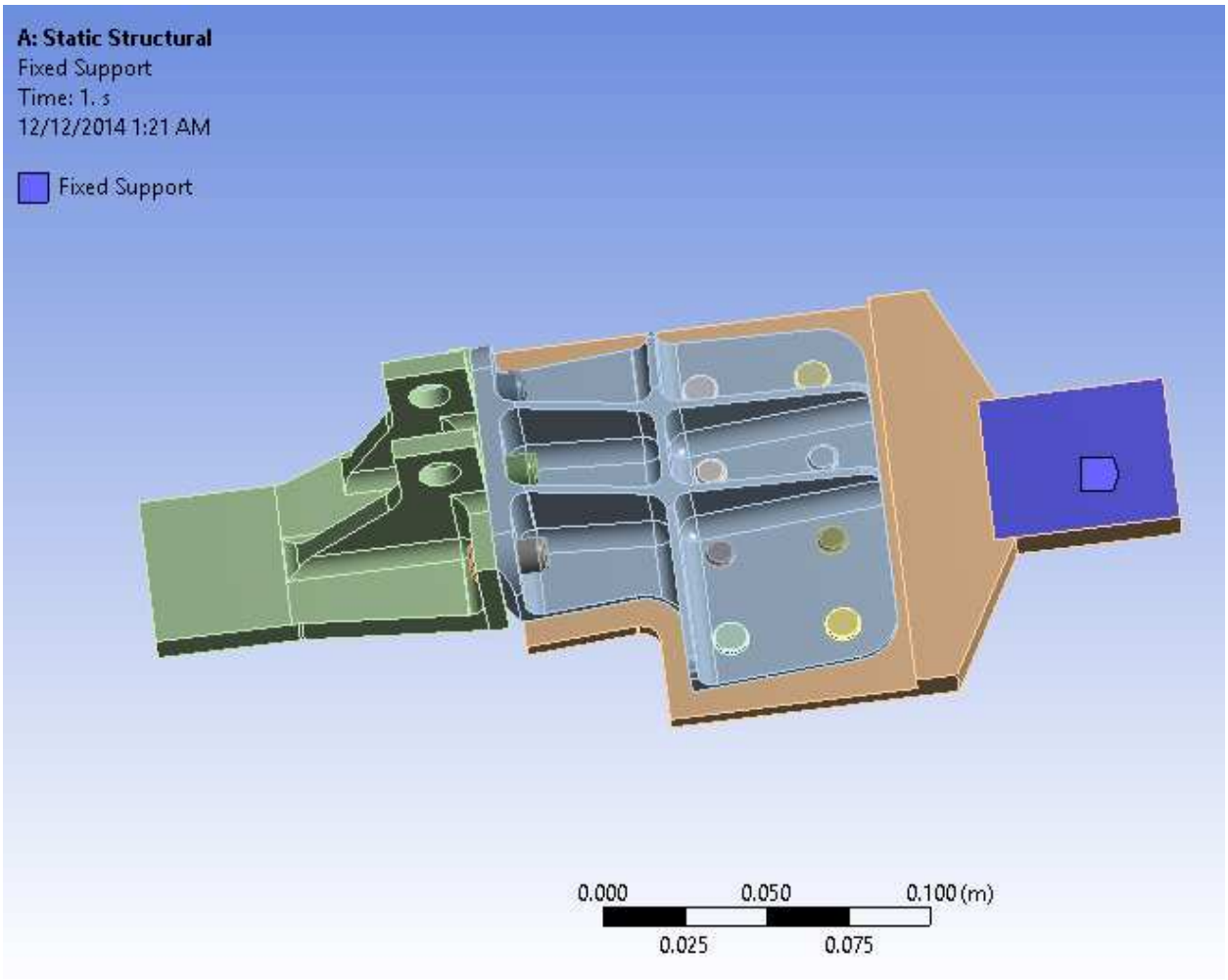

Figure 6-6: Fixed boundary condition on the backing plate

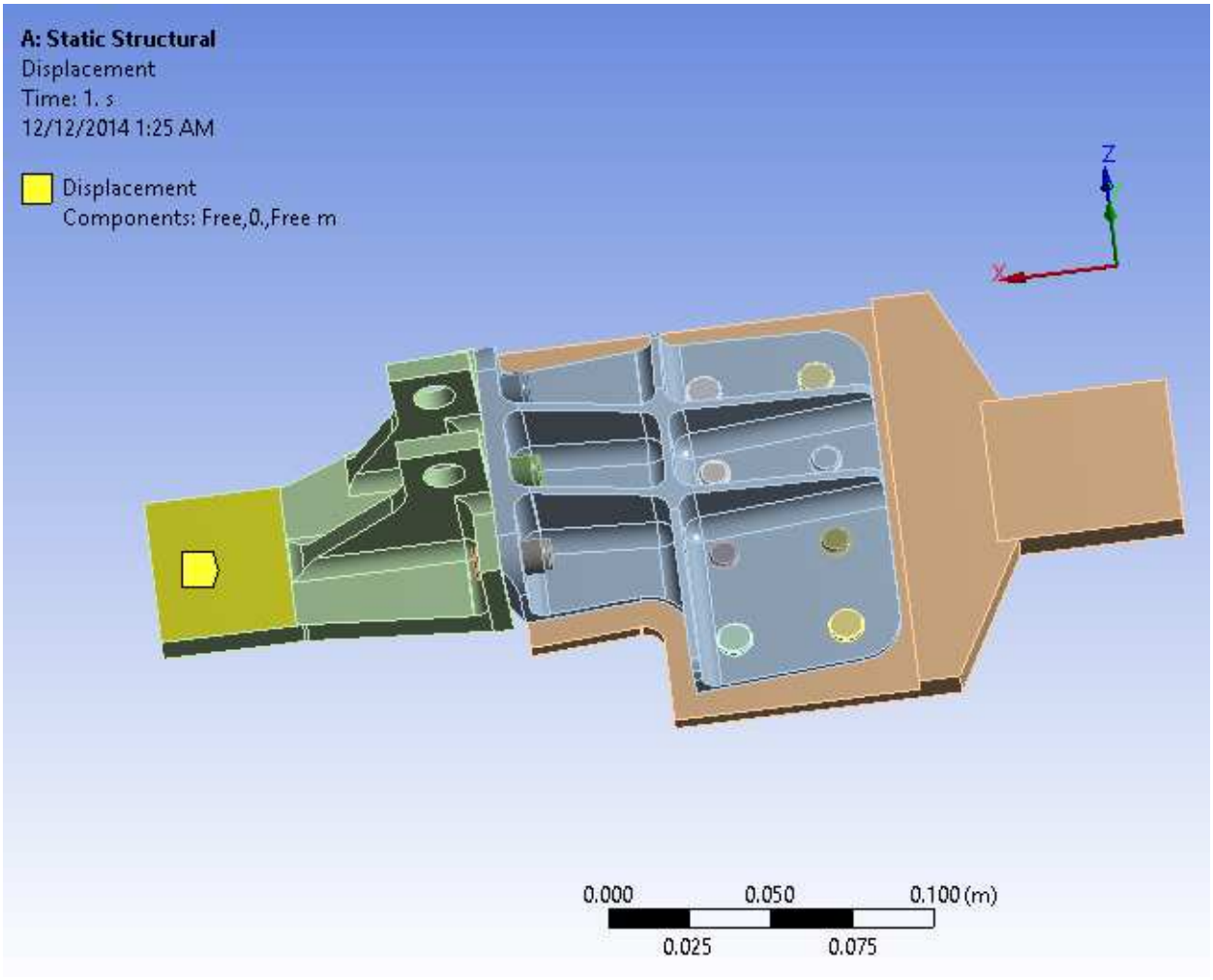

Figure 6-7: Displacement boundary condition on the fixture (fixed in y-direction and free in x and z)

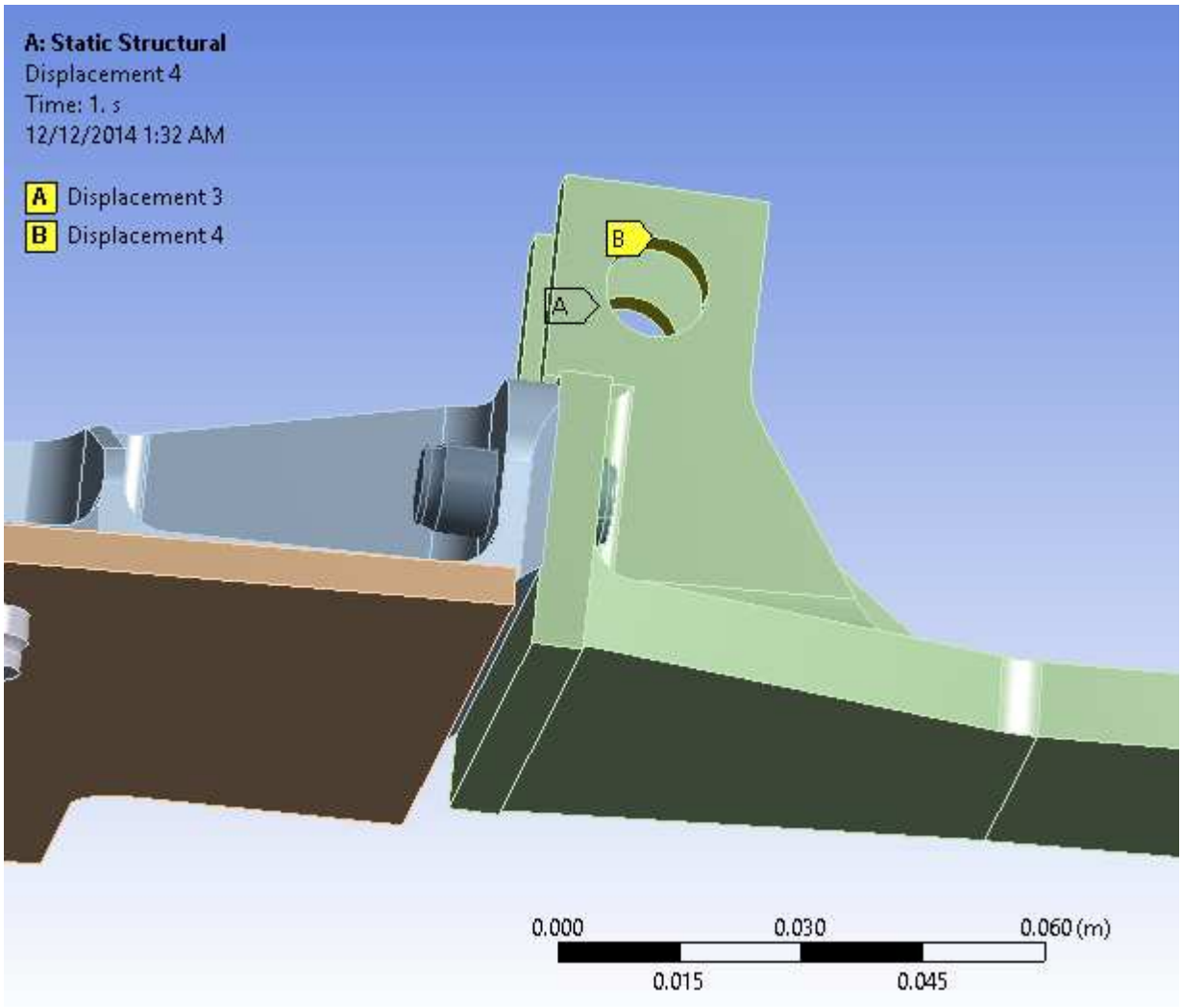

Figure 6-8: Displacement boundary conditions for rigid link

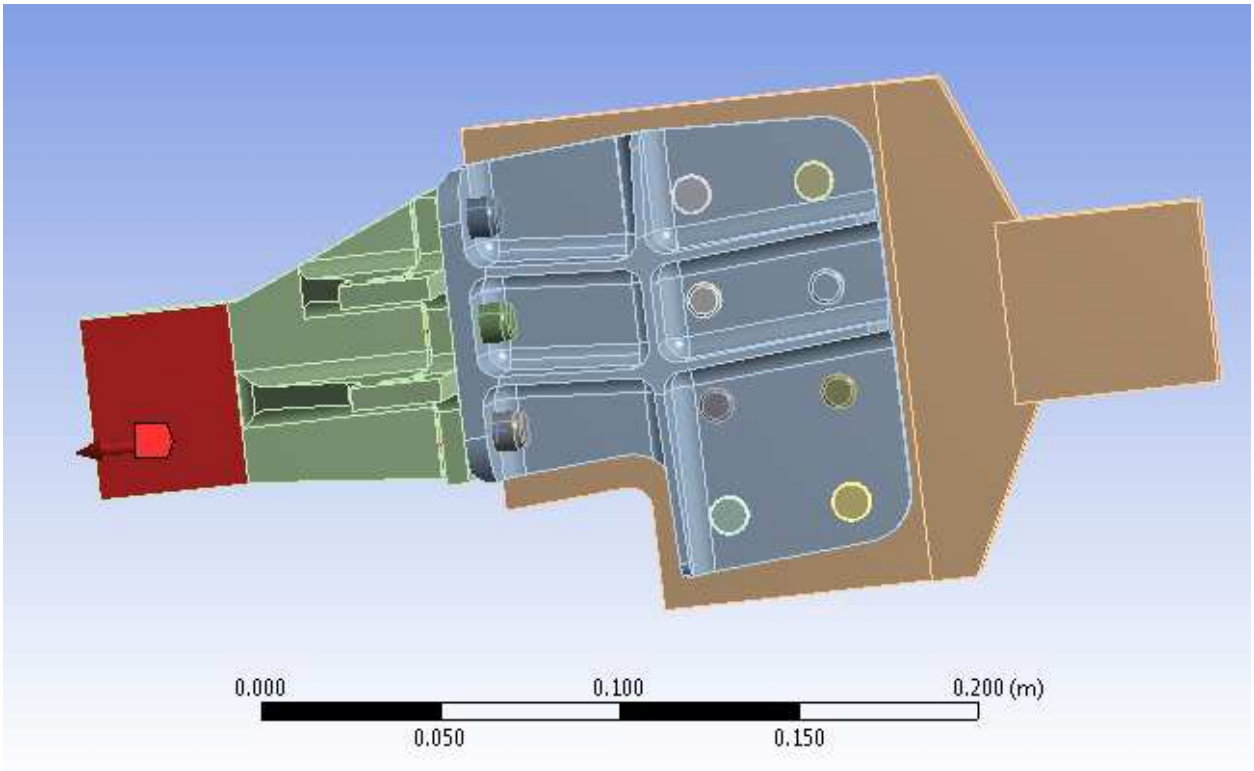

Figure 6-9: Applied load on the two faces of the fixture

As a result of the nonlinear contact mechanics, the analysis settings were manipulated to obtain convergence. The model does run or converge with the current boundary conditions and contact mechanics without including 10 initial substeps and 10 maximum substeps. The auto time stepping function is engaged which facilitates the nonlinear analysis of the frictionless contact mechanics thus allowing the force to increment by substeps (Figure 6-10).

Details of "Analysis Settings"	
Step Controls	
Number Of Steps	1.
Current Step Number	1.
Step End Time	1. s
Auto Time Stepping	On
Define By	Substeps
Initial Substeps	10.
Minimum Substeps	1.
Maximum Substeps	10.

Figure 6-10: Step controls for the non-linear contacts

6.2 Monotonic Loading FEA Results

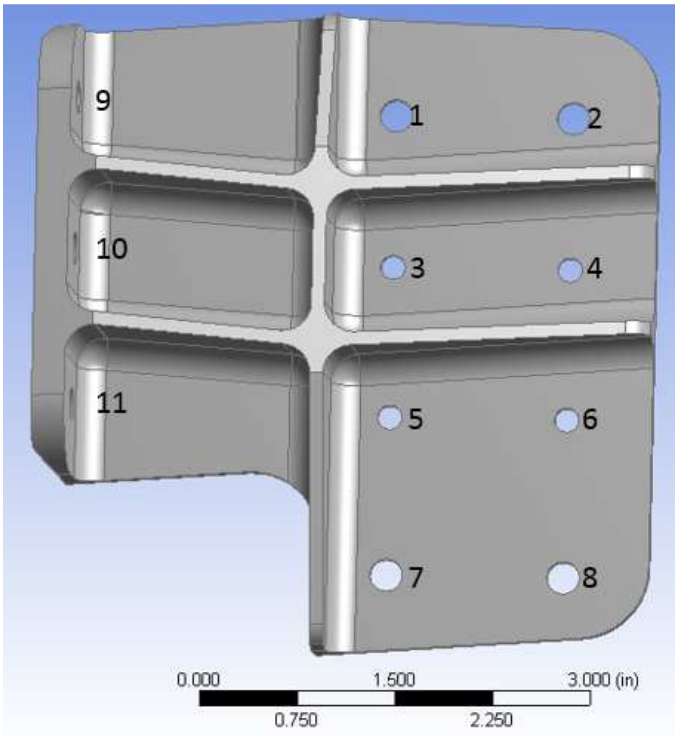

Figure 6-11: Fastener location by number on EBM component

As previously described in the cyclic loading model, the static loading FEA model included the same assumptions regarding the boundary conditions. As previously indicated, the static model did not include the rigid link. That boundary condition was eliminated in this model. The FEA, as

modeled, only included the elastic region of the analysis. This analysis was used to obtain a general understanding of the trends regarding the static loading test of the entire assembly.

According to Figure (4-2), the static testing curve was mostly linear up to 35.6 kN (8000 lbs) load cell force . The finite element model was to analyze that region and the model was run at 8.9 kN, 17.8 kN, 31.1 kN and 35.6 kN (2000, 4000, 7000, and 8000 lb) force. There was a convergence issue at the 26.7 kN (6000 lb) force model, therefore 31.1 kN was run to plot the data for comparison. Figure 6-12 depicts the nickel fasteners maximum equivalent stress versus load force. The results are linear as expected. The maximum stress on fastener 11 went from the shank to the head as the load increased. For this purpose, the maximum stress of the nut (head) and the shank were recorded. Additionally, the maximum equivalent stress of the titanium fasteners and the component at the eleven fastener locations were recorded (Figures 13, 14 and 15).

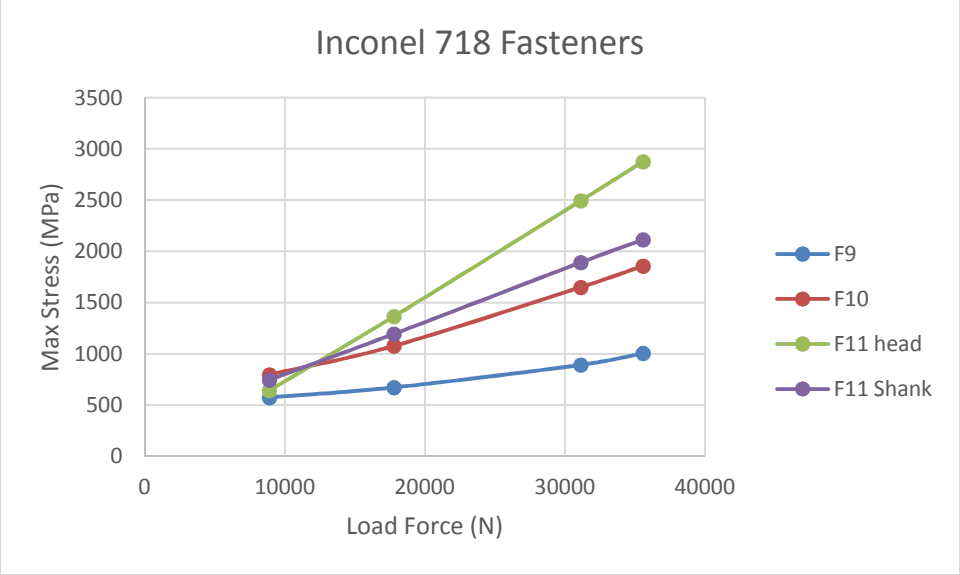

Figure 6-12: Max equivalent stress at Inconel 718 fasteners

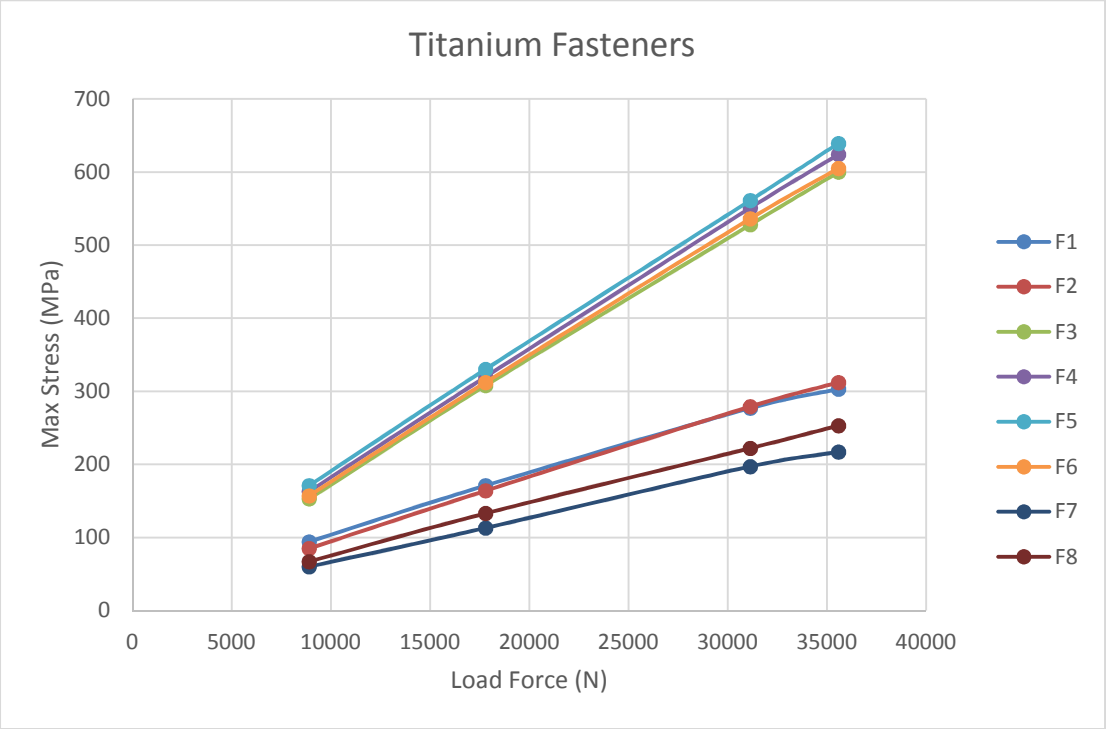

Figure 6-13: Max equivalent stress at titanium fasteners

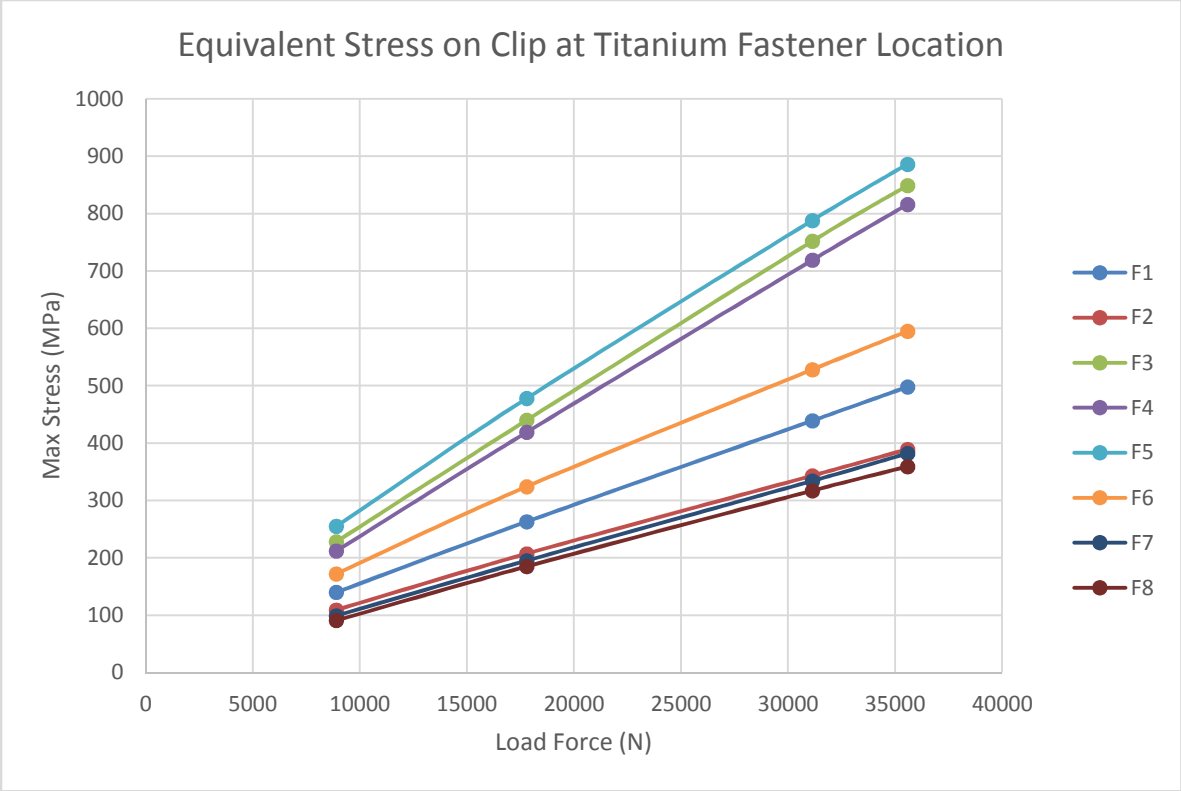

Figure 6-14: Max equivalent stress on component at titanium fastener location

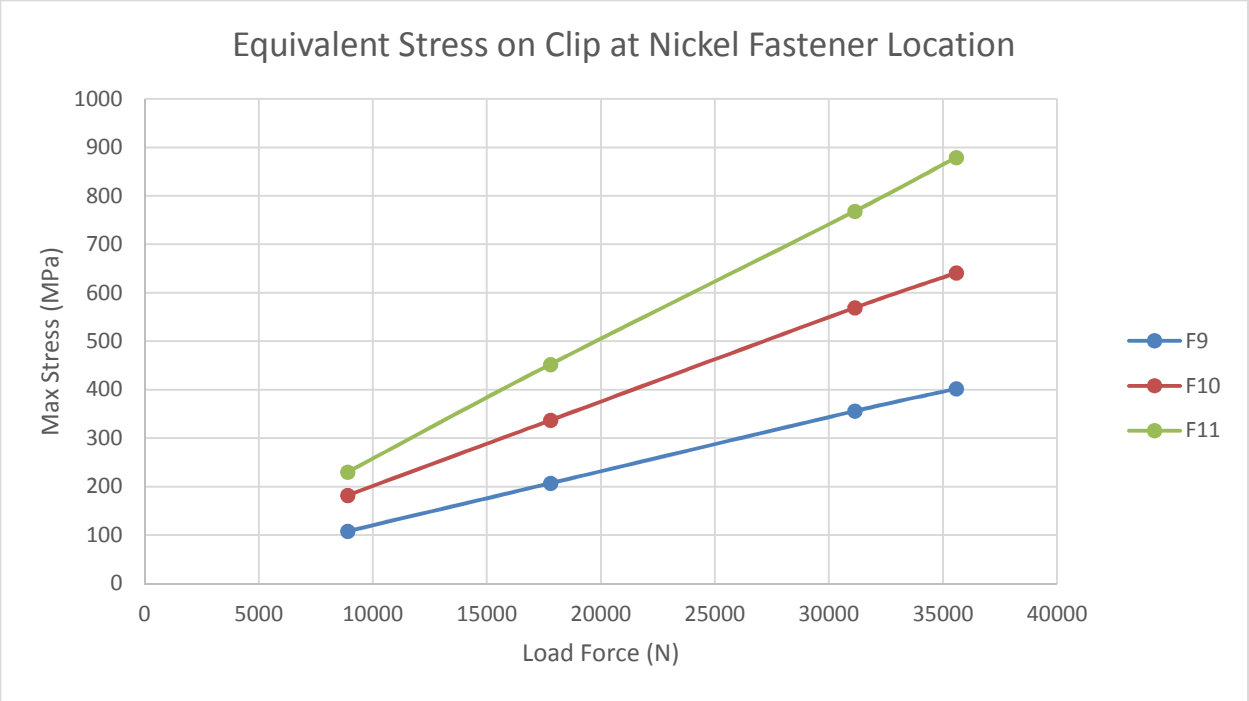

Figure 6-15: Max equivalent stress on component at Inconel 718 fasteners

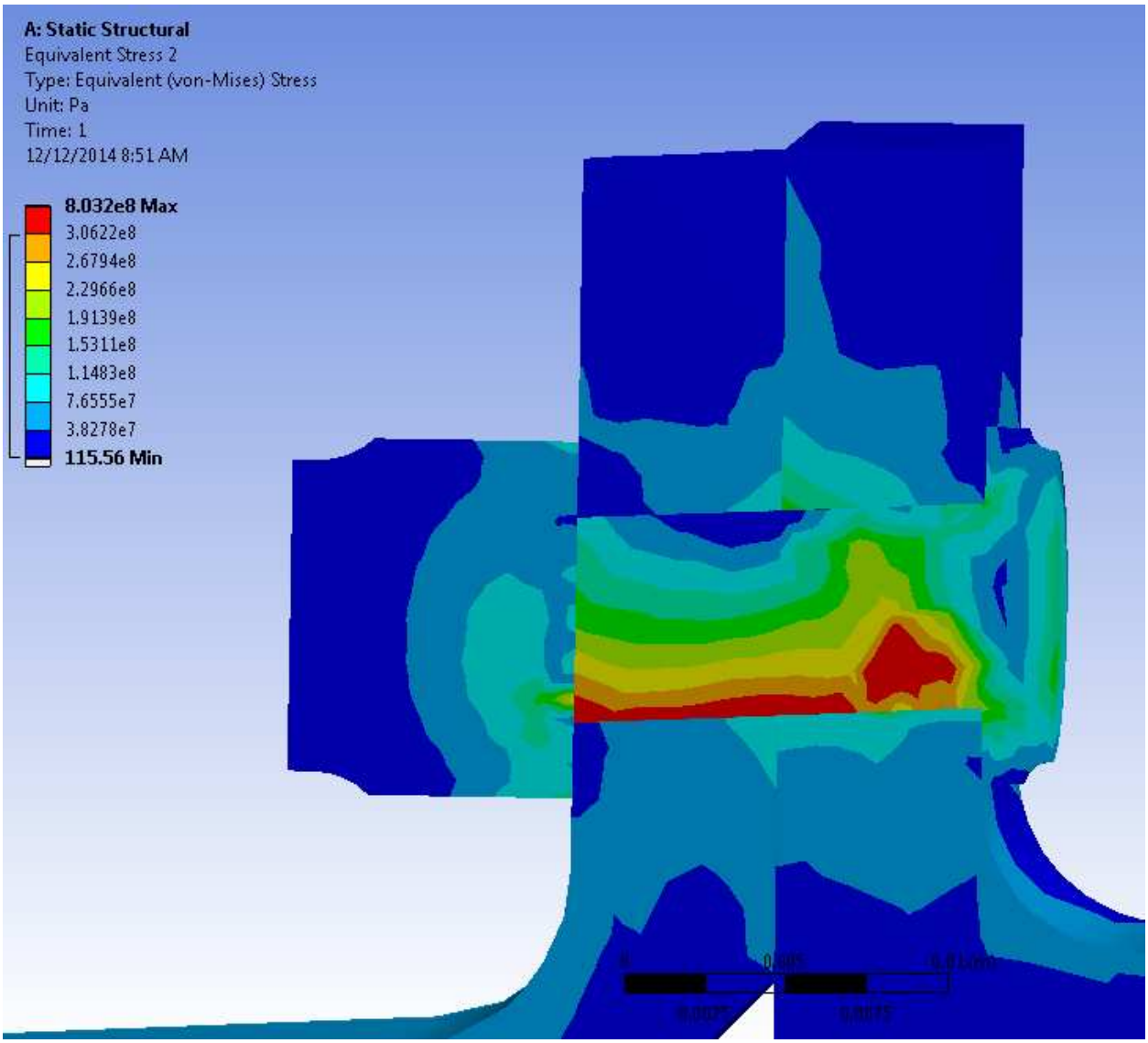

Figure 6-16: Section plane of fastener 11 at component (left) and fixture (right) with 8.9 kN load force

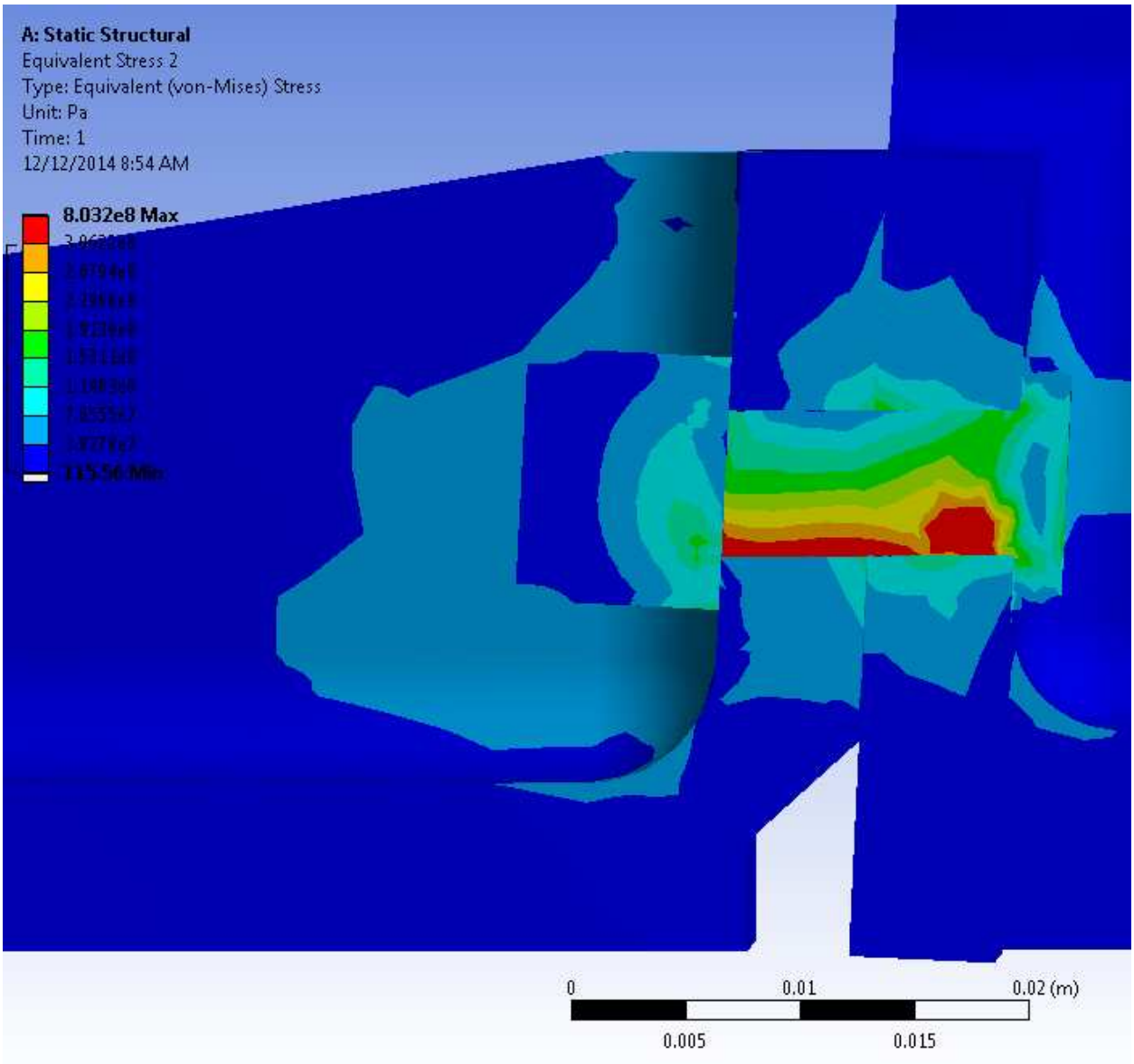

Figure 6-17: Section plane of fastener 10 at component (left) and fixture (right) with 8.9 kN load force

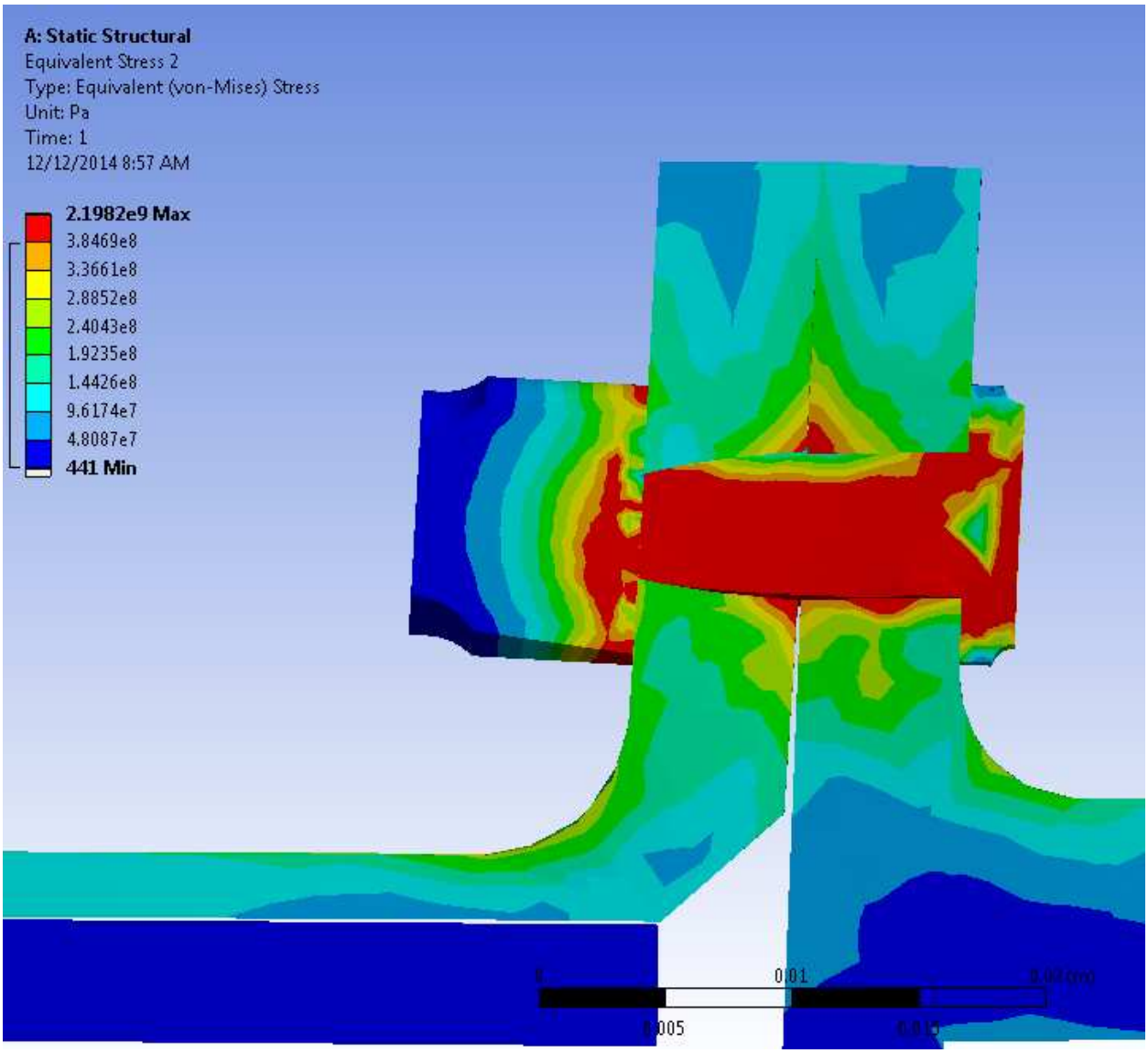

Figure 6-18: Section plane of fastener 11 at component (left) and fixture (right) with 35.6 kN load force

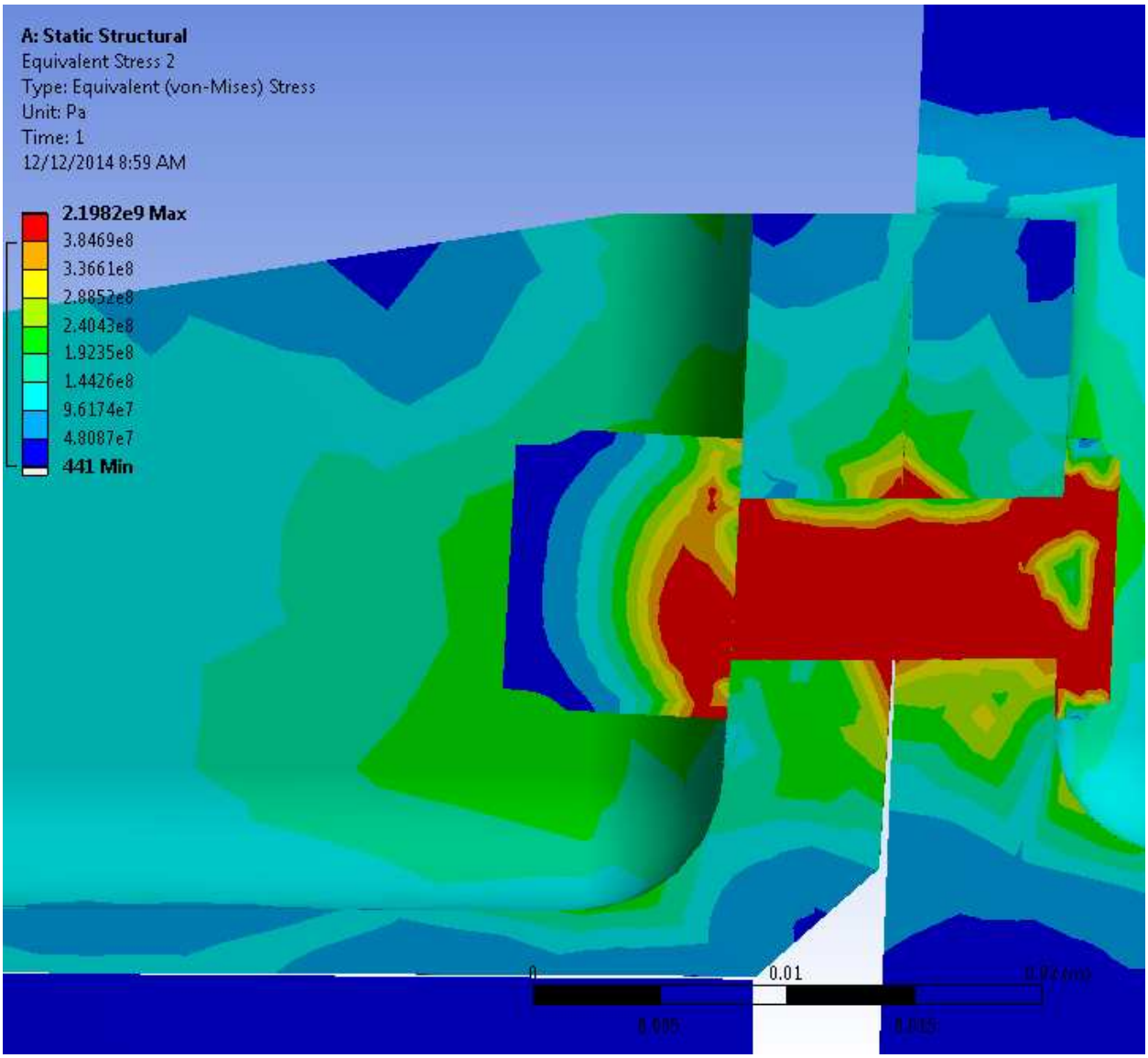

Figure 6-19: Section plane of fastener 10 at component (left) and fixture (right) with 35.6 kN load force

Fastener 10 and 11 were the only items in the assembly to fail. As previously described, the fastener at location 10 partially failed and was followed by fastener 11 total ductile failure. Fastener 11 failed at the threads, and the finite element model depicts that the maximum equivalent stress was located at the fastener head (nut). The finite element model did not include the threads to simplify the analysis. However, modeling the threads in fastener 10 and 11 would facilitate a better understanding of the failed fasteners.

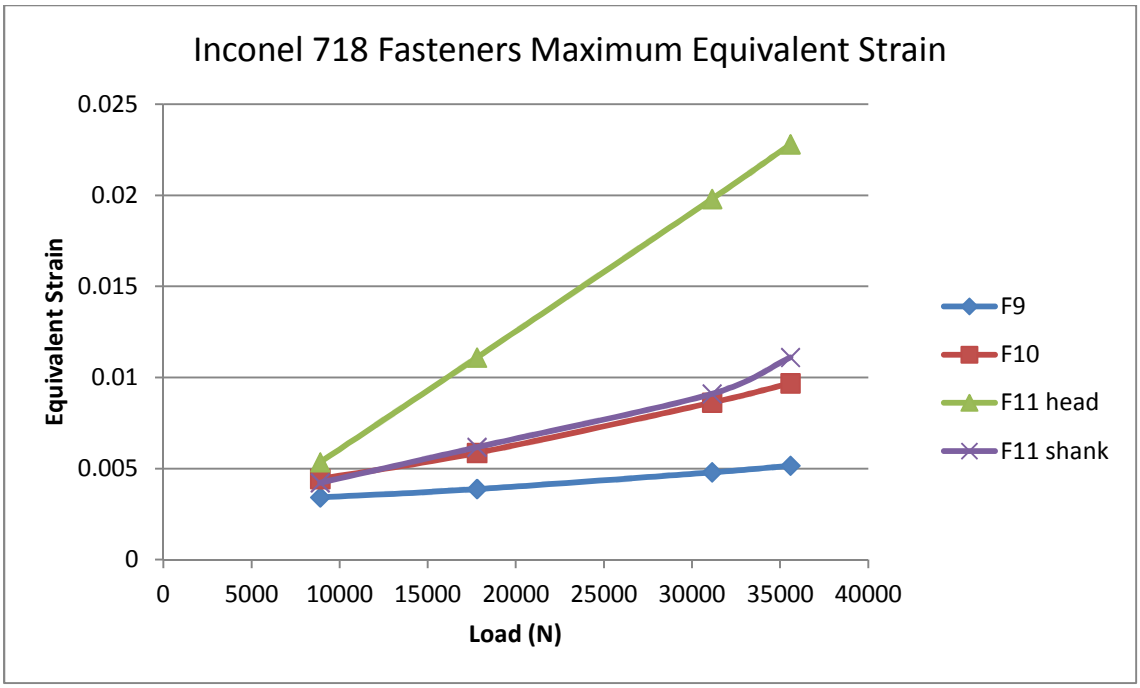

Figure 6-20: Maximum equivalent strain at Inconel 718 fasteners

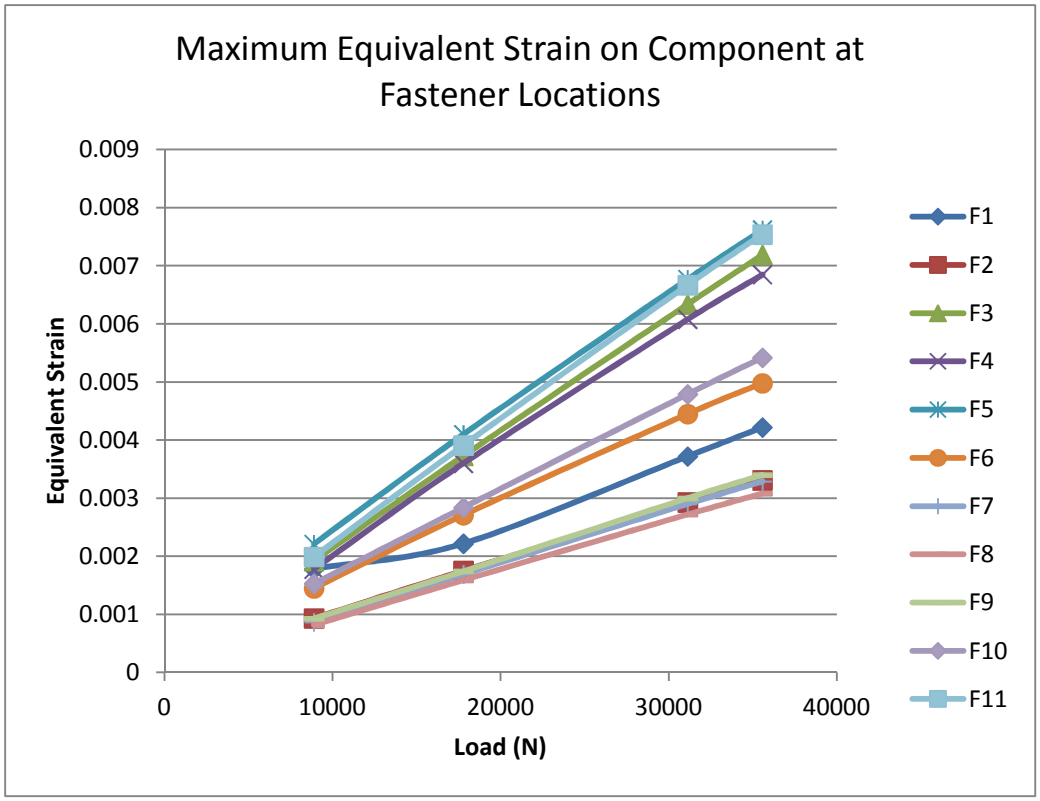

Figure 6-21: Maximum Equivalent Strain on Component at fastener locations

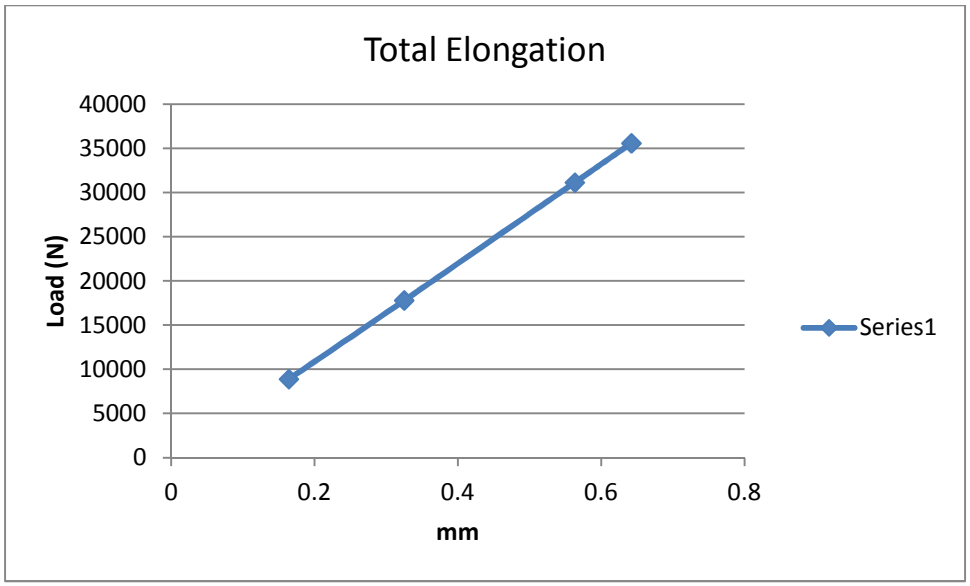

Figure 6-22: Total elongation (machine head displacement) in the elastic range

Figure 6-20 depicts the nickel fasteners maximum equivalent strain and Figure 6-21 depicts the maximum equivalent strain at all of the fastener locations on the component. Figure 6-22 depicts the elongation of the linear elastic region modeled in FEA. There is a linear relationship between the strain and load which was expected in the linear elastic region. Fastener 11 head depicted the most maximum strain as depicted in Figure 6-23. According to Figure 4-2 (in chapter 4), the total elongation up to the 8000 pound (35.6 kN) load was approximately 0.15 inches (3.81 mm). The finite element model indicated that the total elongation in the linear-elastic region in the x-direction was approximately 0.025 inches (0.635 mm) which is approximately 6 times less than the physical results. However, the displacement recorded on the experiment was machine head displacement. It is possible that could have attributed to the imprecision of the model and experiment. Additionally, future testing using other types of measuring equipment would be warranted for matching results between the model and experiment.

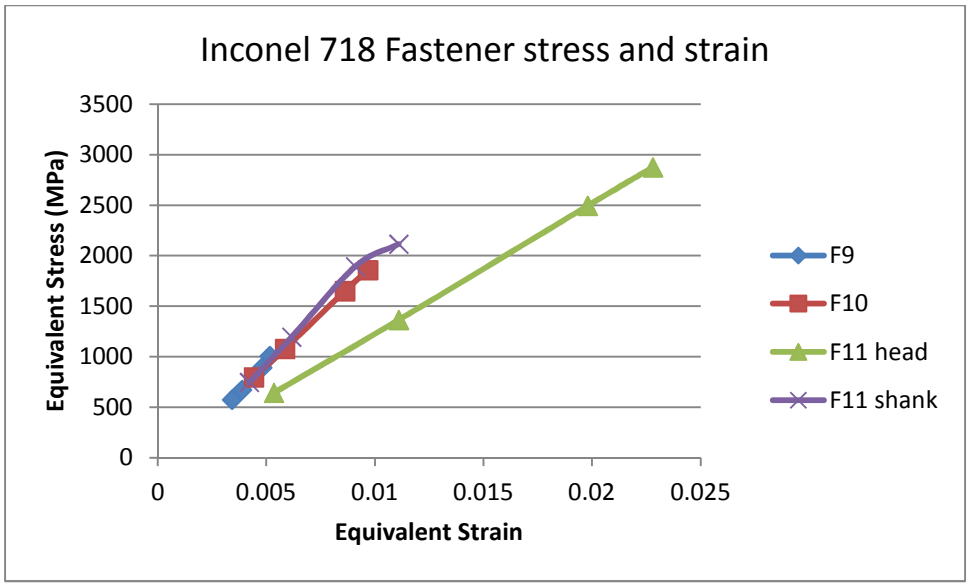

Figure 6-23: Equivalent stress and strain at Inconnel fasteners

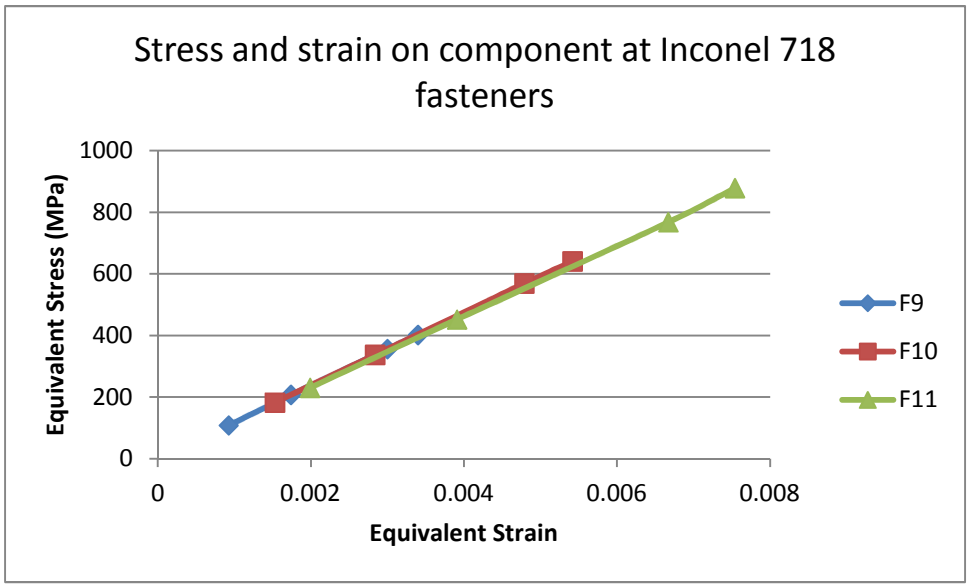

Figure 6-24: Equivalent stress and strain at Inconel fastener locations on EBM component

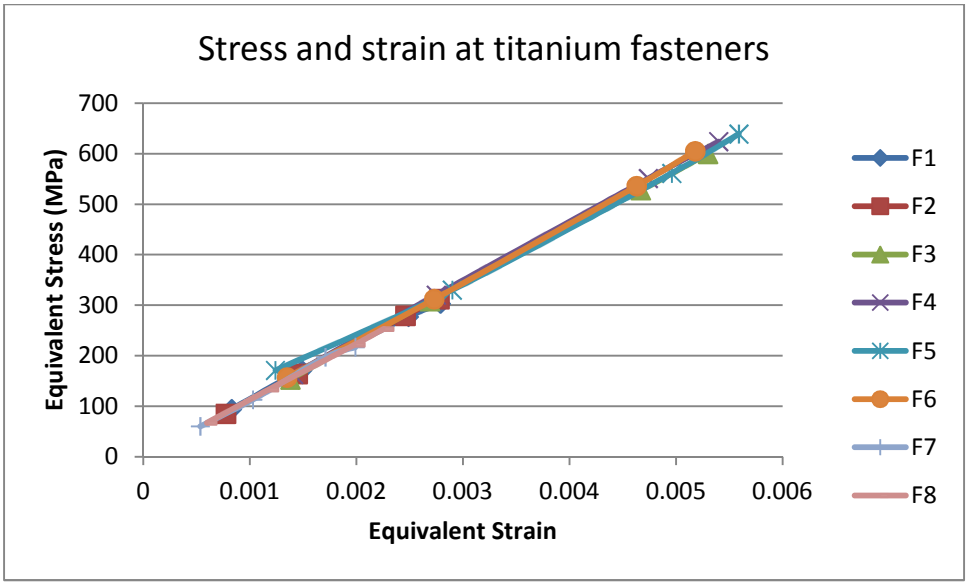

Figure 6-25: Equivalent Stress and strain at titanium fasteners

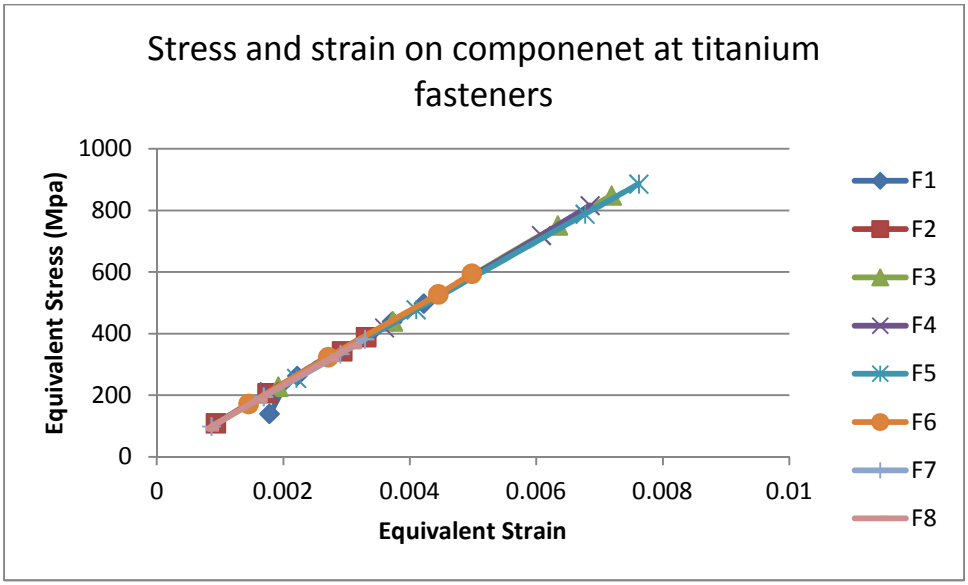

Figure 6-26

6.3 Cyclic Loading FEA Results

As previously described, an attempt was made to model the assembly in the finite element analysis program, ANSYS Workbench v14. The load and boundary conditions, contact mechanics were applied to the assembly as was indicated in the monotonic loading. An

additional boundary condition as described earlier, indicated that the rigid would restrict displacement in the y-direction (normal to the clamp faces as depicted in Figure 6-27.

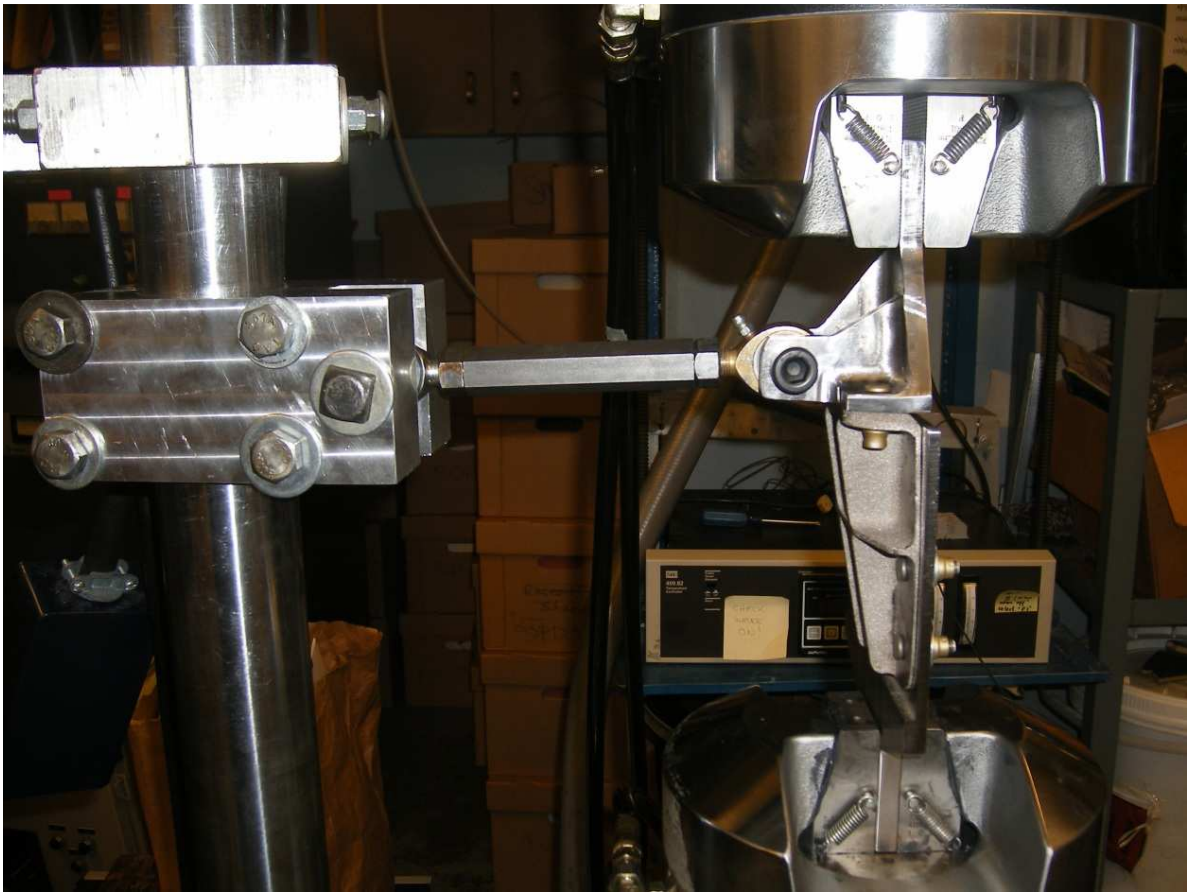

Figure 6-27: Cyclic loading test setup with the rigid link on the load frame and fixture

As previously indicated, a total of eight specimens were subject to the design load at 500k cycles which was double the design life. The loading ratio was -0.39 which included a tensile load and a compressive load. Firstly, the design load and double the design load are depicted in Figures 6-28 through 6-40. According to the FEA, it is indicated that fasteners 10 and 11 experienced the greatest stress of the assembled model (Table 6-2). None of the EBM components failed during the cyclic loading at the design load and double the design life. It is indicated in table 6-2 that the Inconel fastener in location 10 was 38 MPa greater than fastener

11. However, during the testing at double the design load until failure, fastener 11 failed. In the maximum tension in the cyclic loading, the FEA results indicate that the greatest stress occurred at Fastener 11 at above the yield strength of 1034 MPa and below the ultimate strength of 1276 MPa. This data only accounts for the tensile aspect of the fatigue sinusoidal cycle. During cyclic loading there are typically residual stresses that remain after loading, but these data attempted to verify the failed fastener at location 11 in the tests. In the double the design load stress distribution, it is indicated that the max stress occurred on the head or bolt of fastener 11. This is the location where it failed during cyclic testing.

Table 6-2 Max equivalent stresses at tensile load

	Tensile Load	
	9.56 N	19.1 N
Fastener 10	710 Mpa	880 Gpa
Fastener 11	672 Mpa	1,195 Mpa

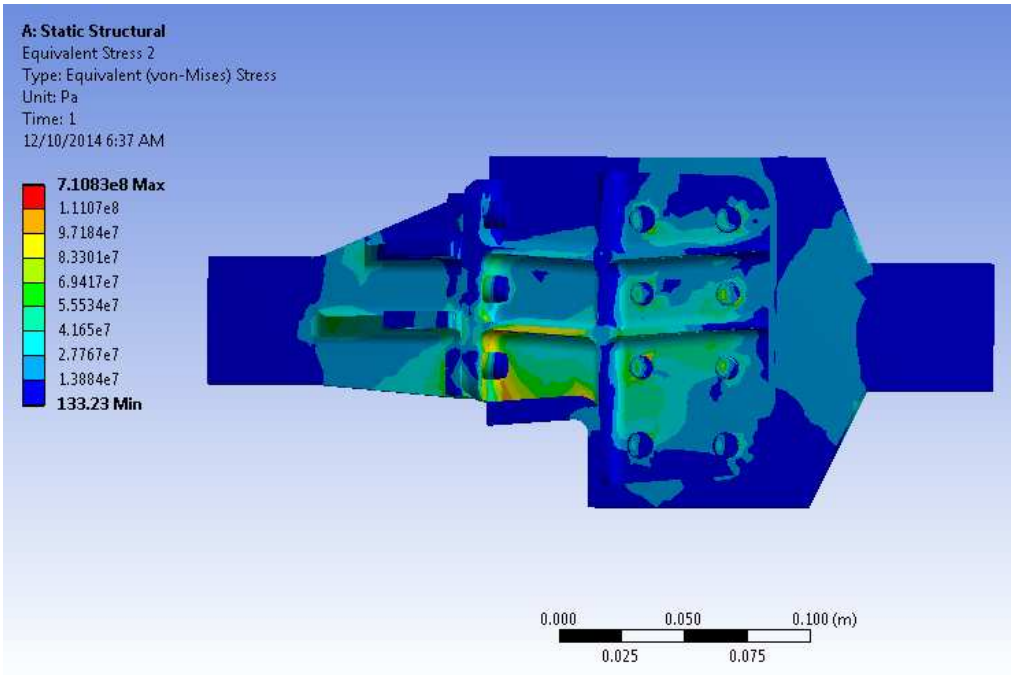

Figure 6-28: Top view of assembly of equivalent stress at design load (tension)

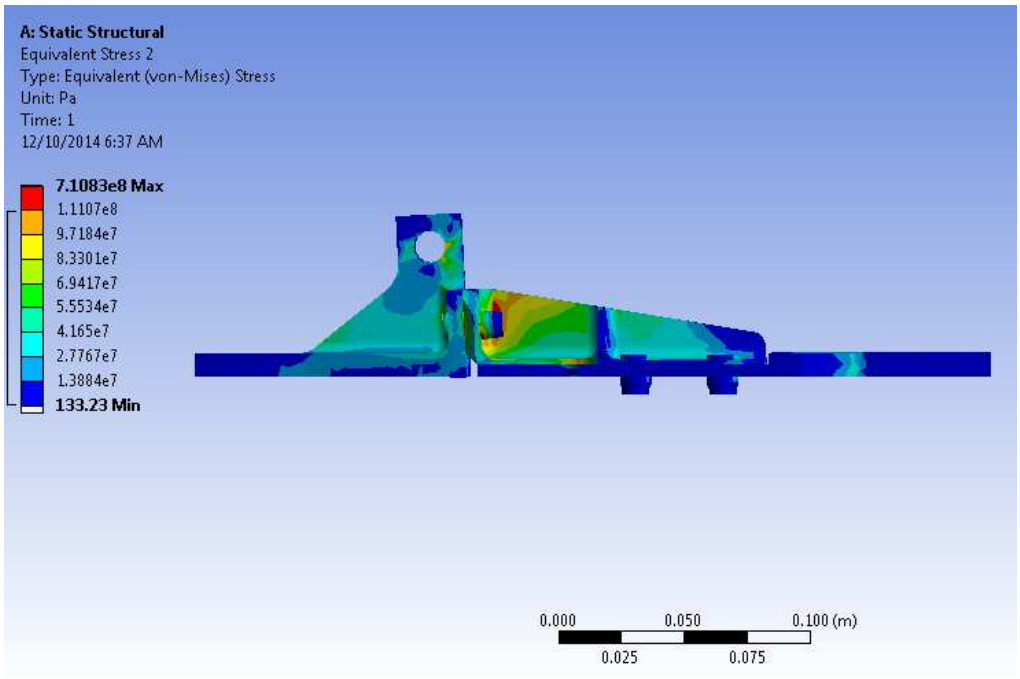

Figure 6-29: Side view of assembly of equivalent stress at design load (tension)

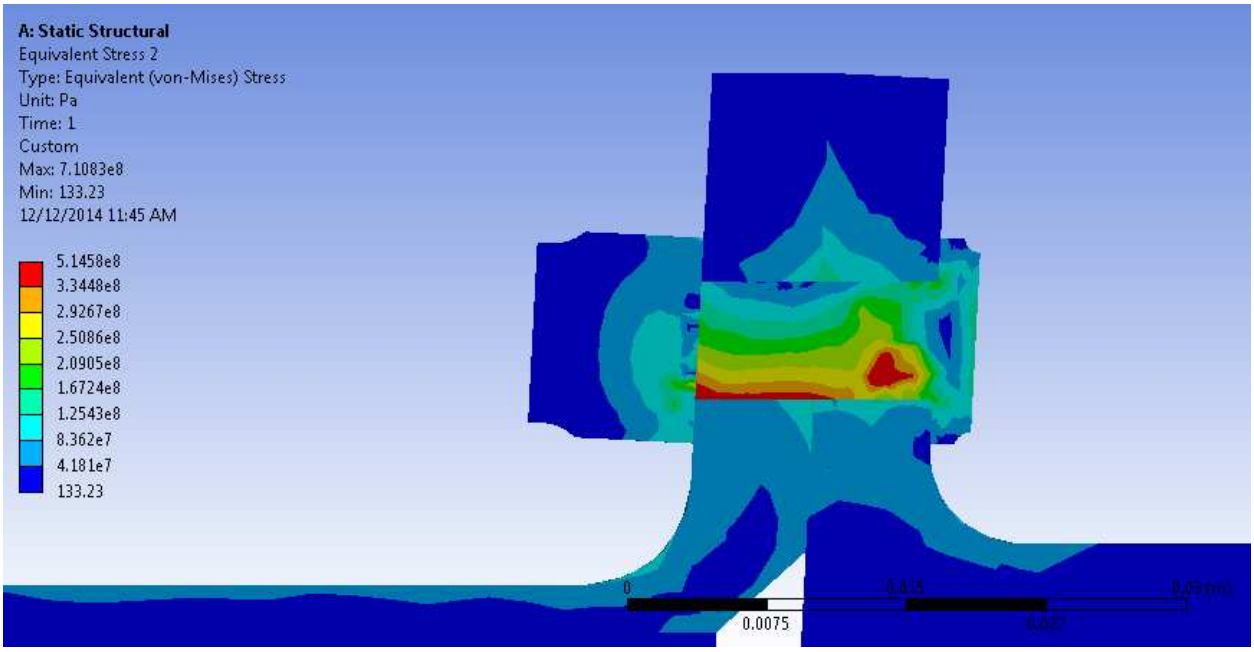

Figure 6-30: design load at fastener 11 at design load (tension)

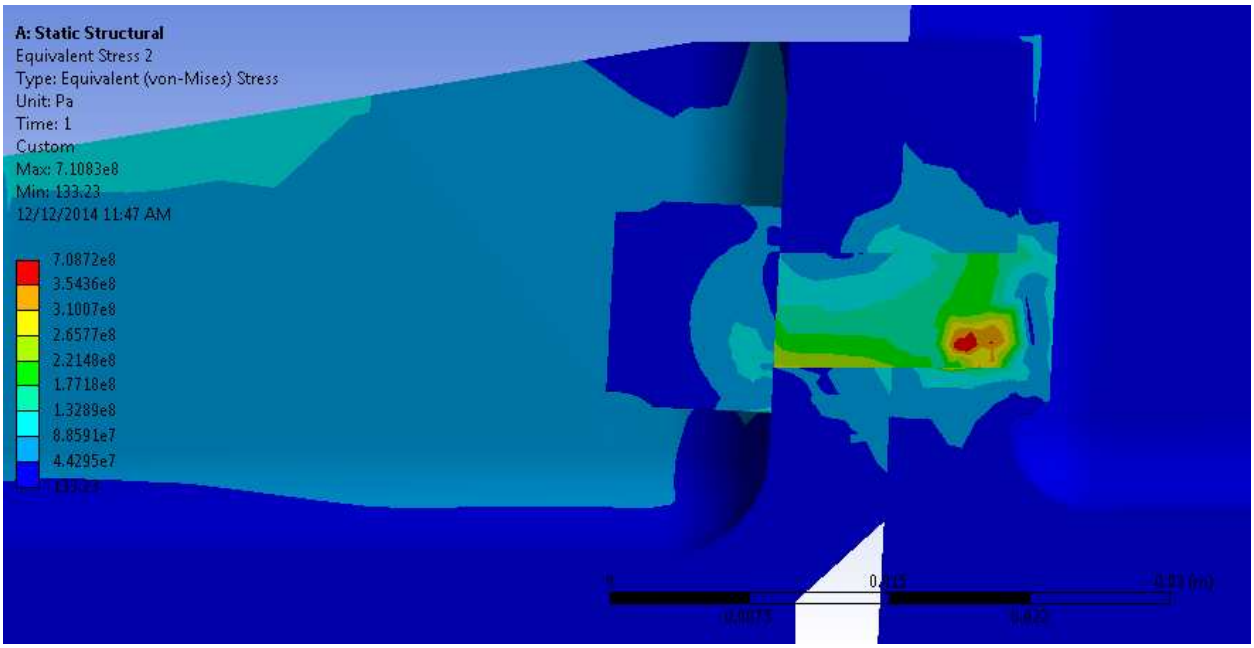

Figure 6-31: design load at fastener 10 at design load (tension)

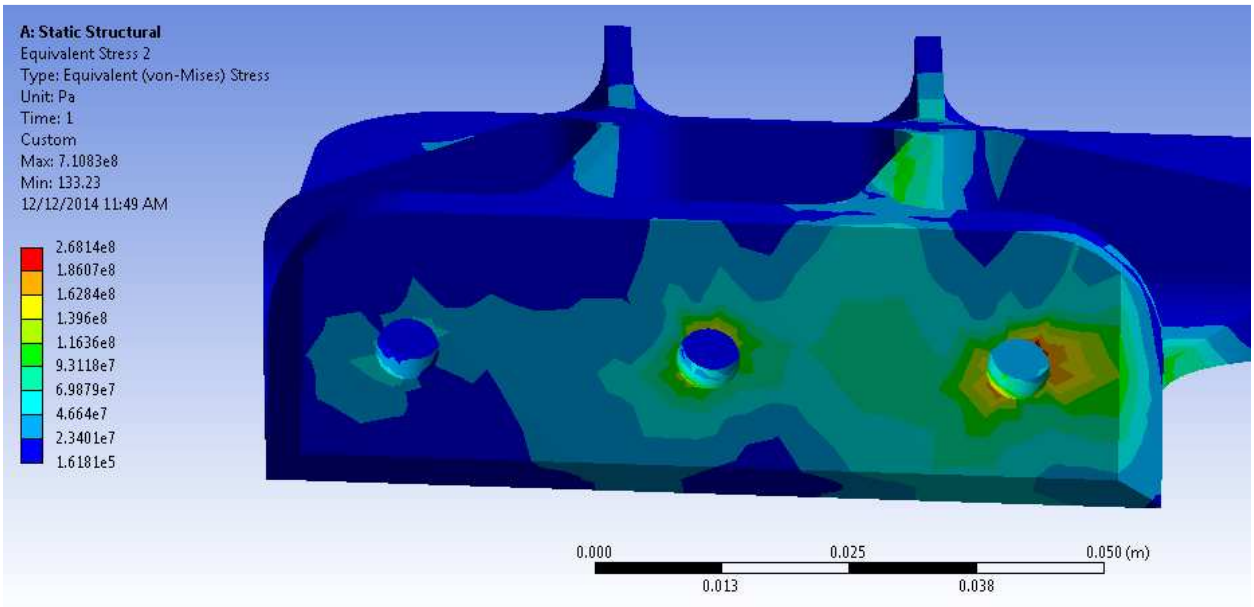

Figure 6-32: Design load component fastener locations 9, 10, 11 at design load (tension)

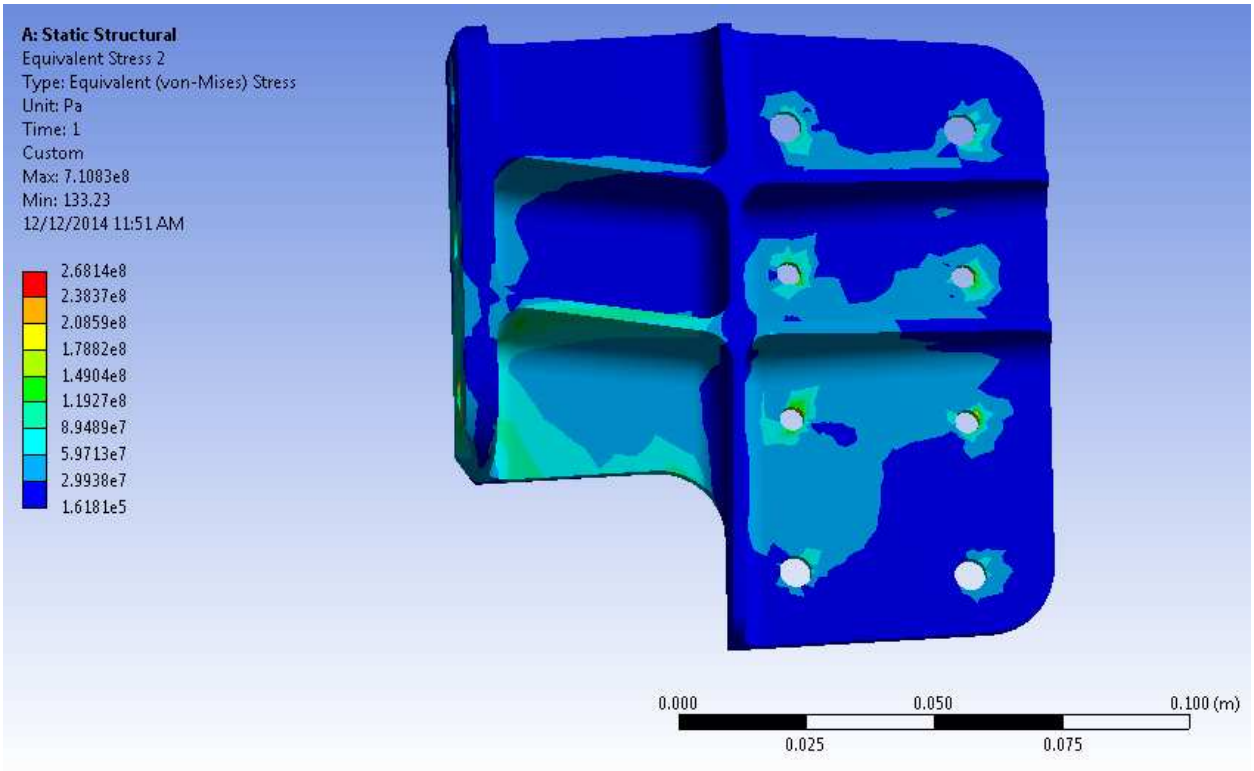

Figure 6-33: Design load at fastener location 1-8 (at design load tension)

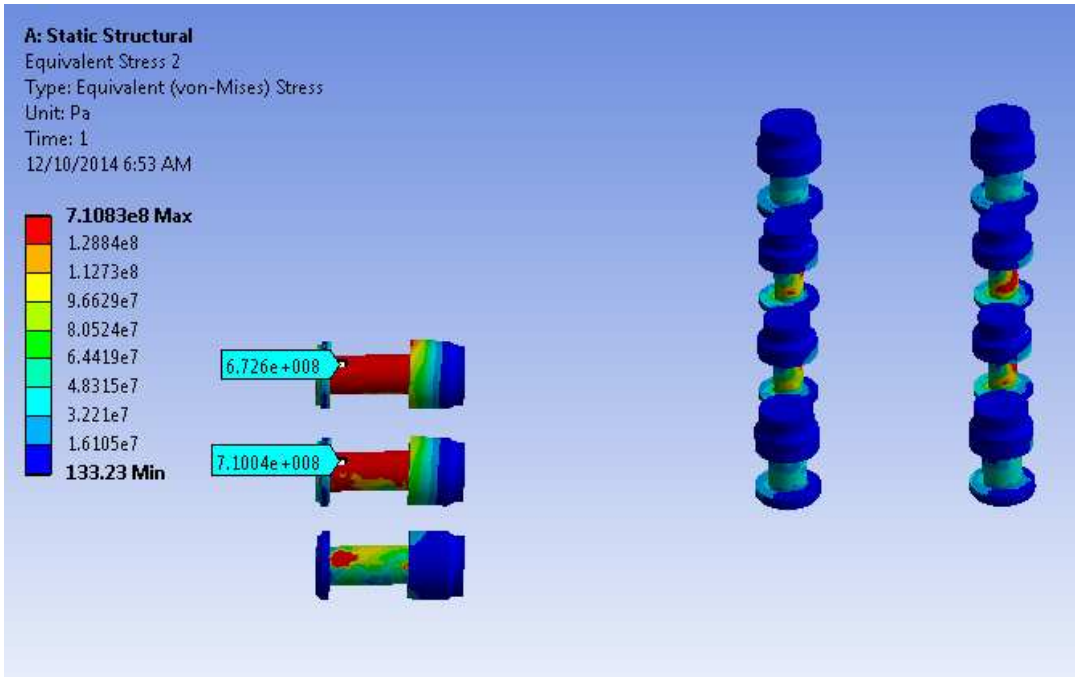

Figure 6-34: Maximum equivalent stress at fastener 11 (672 MPa) and fastener 10 (710 MPa) at design load (tension)

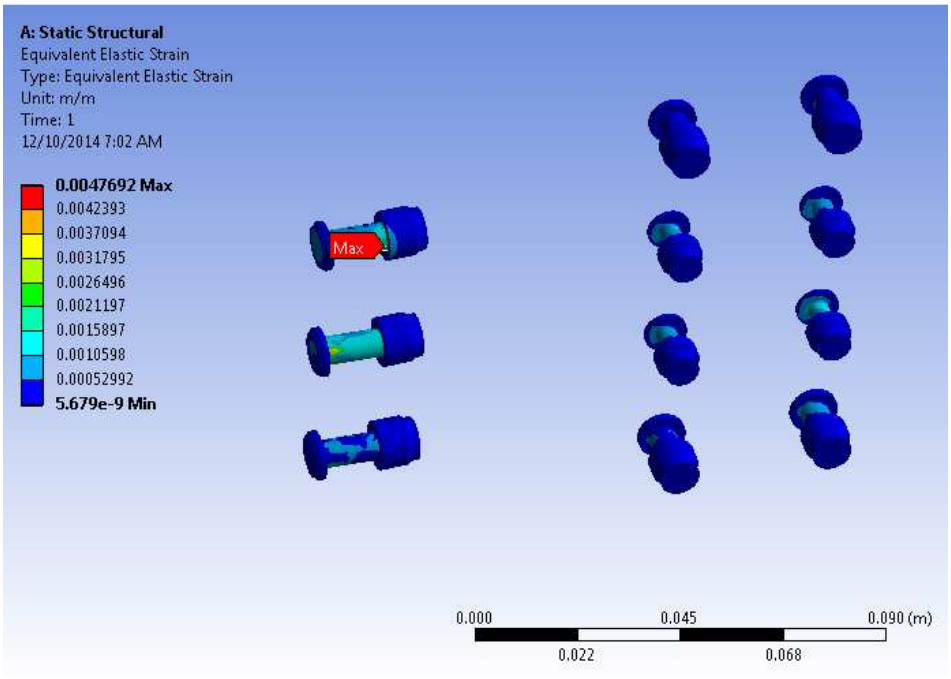

Figure 6-35: Max equivalent elastic strain at fastener 11 at design load (tension)

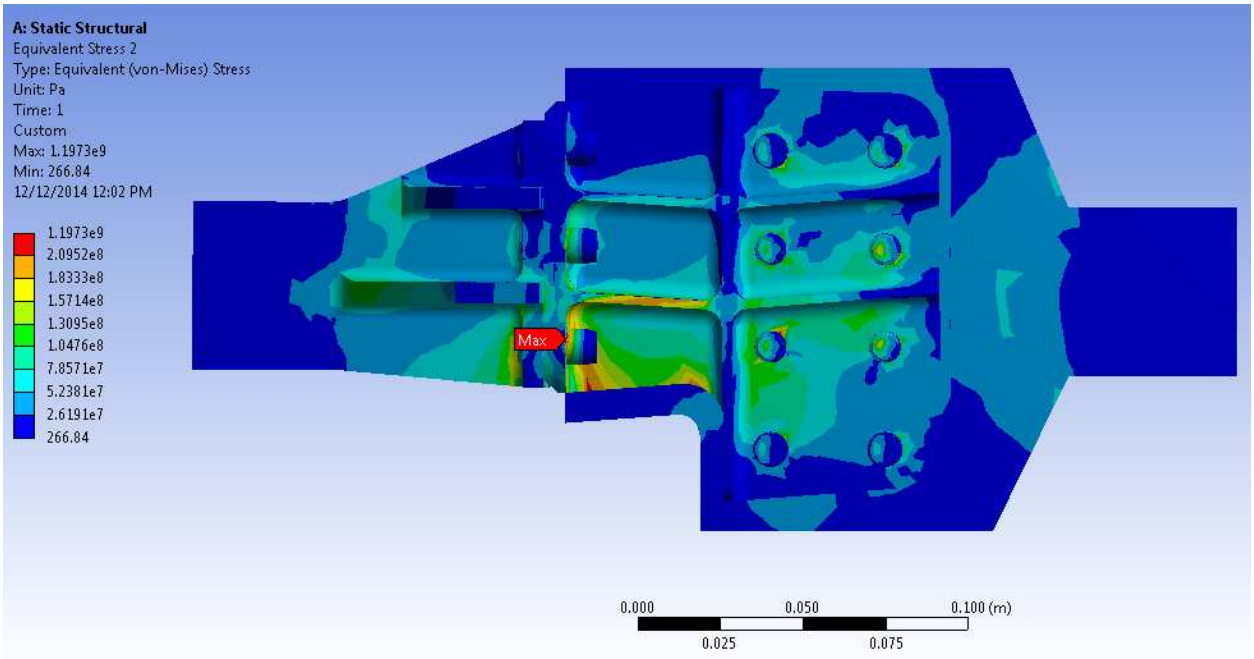

Figure 6-36: double design load equivalent stress distribution

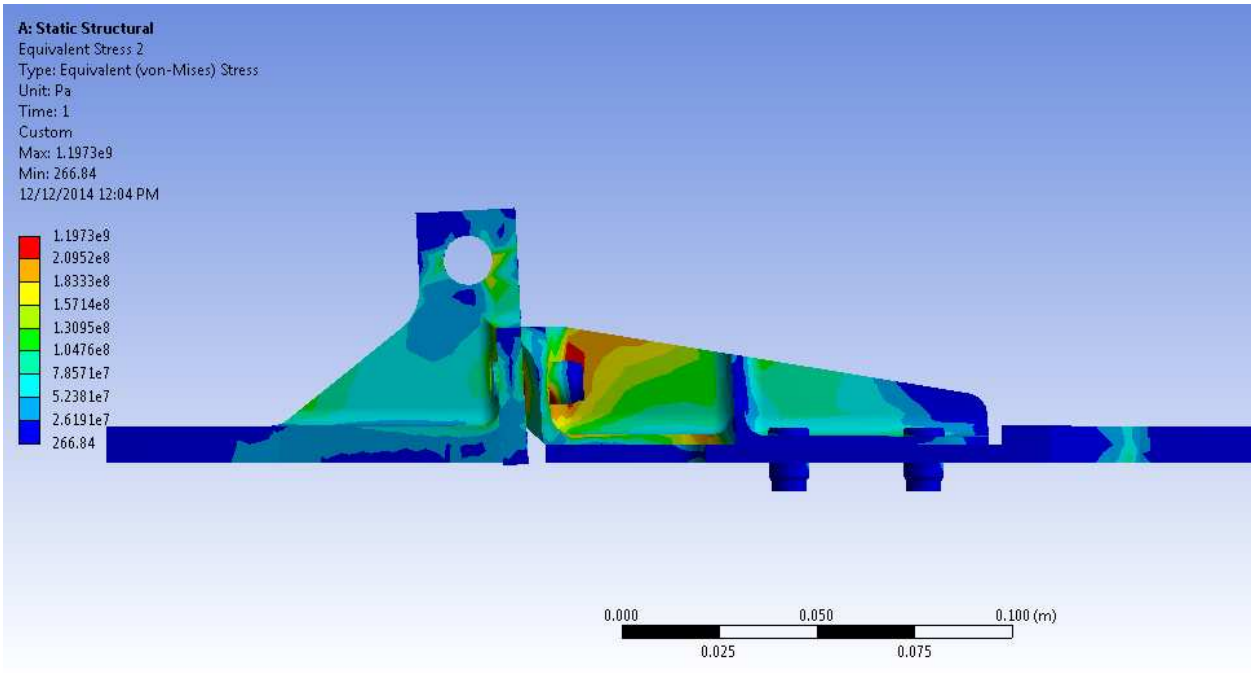

Figure 6-37: Double design load

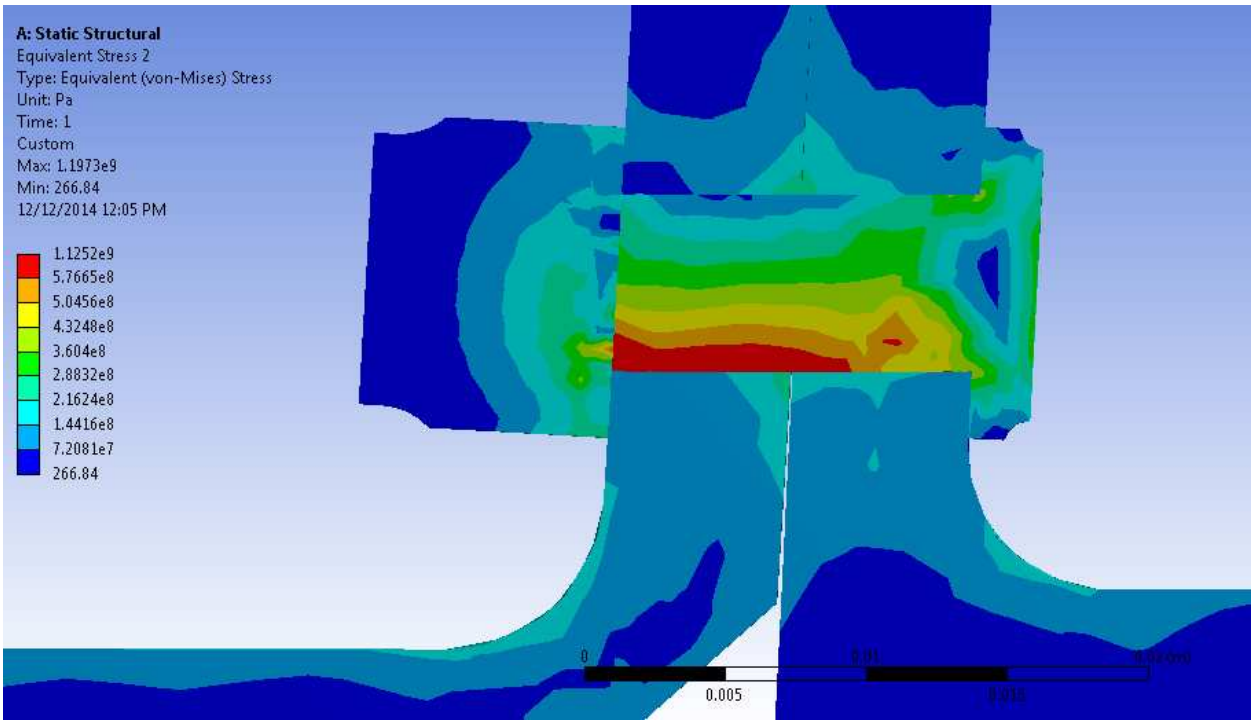

Figure 6-38: Double design load at fastener 11 section plane

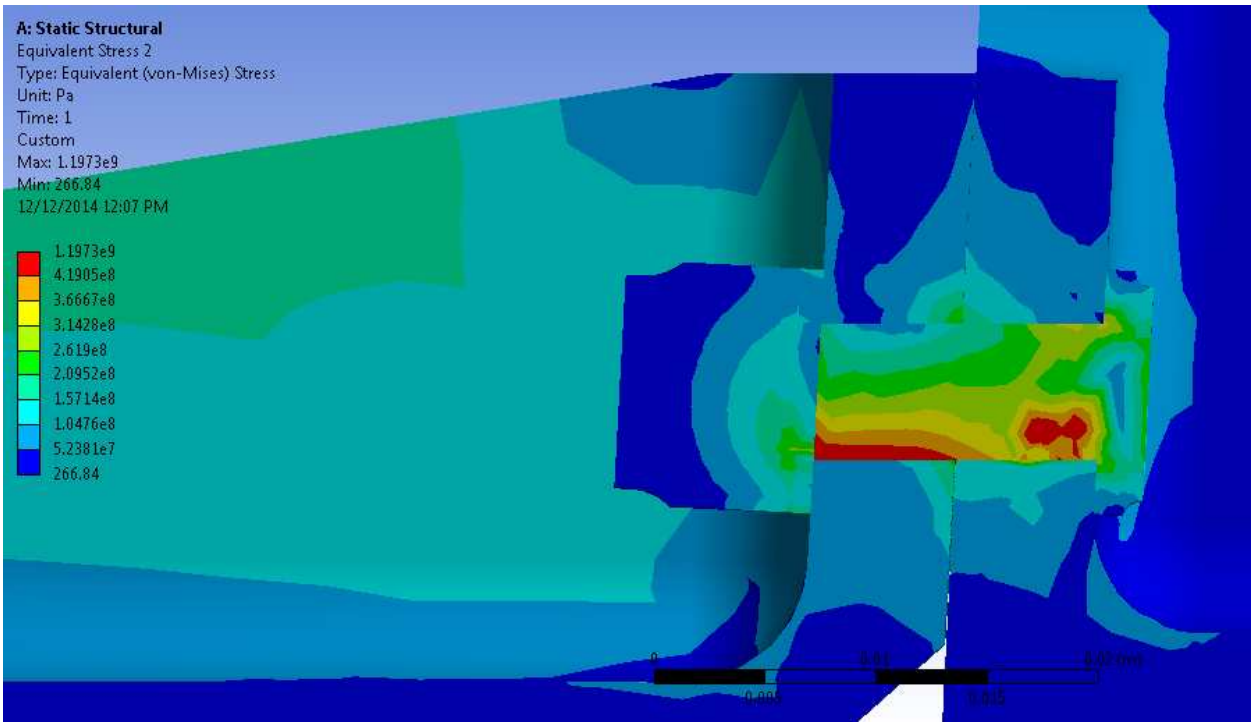

Figure 6-39: Double design load fastener 10 section plane

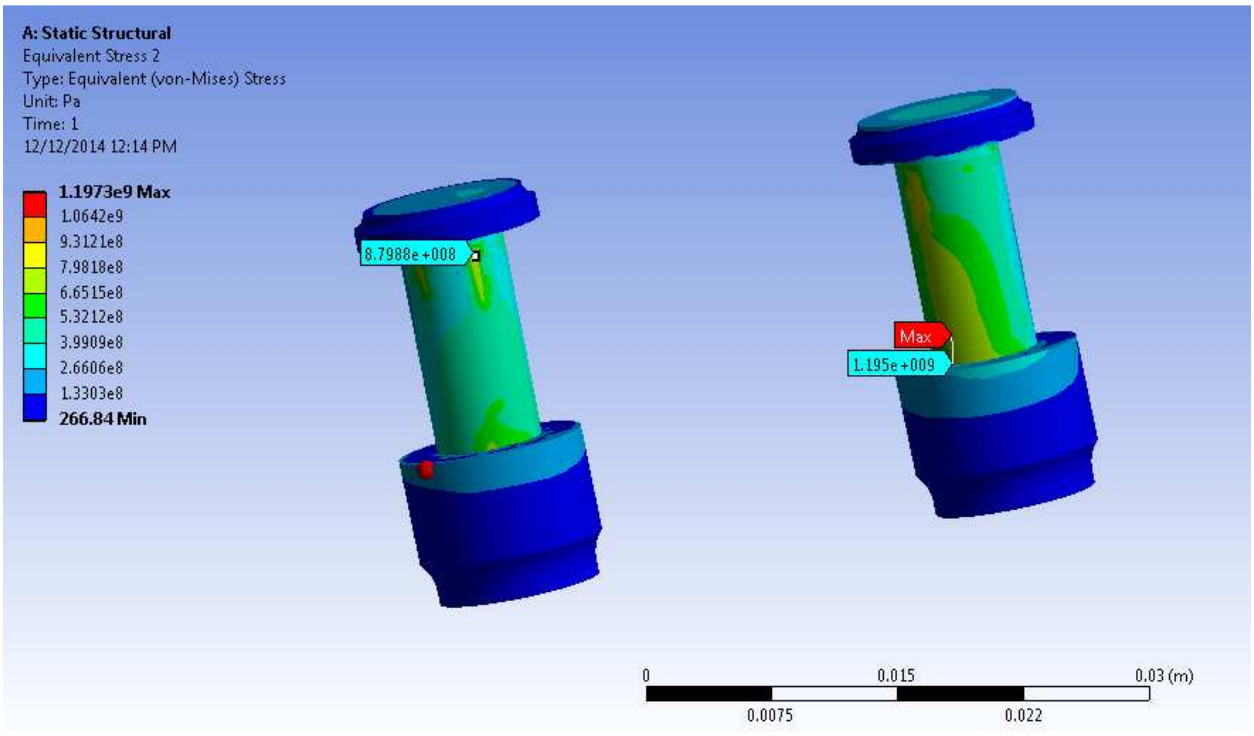

Figure 6-40: Double the design load (tension) at fastener 10 (880 Mpa) and fastener 11 (1,195 MPa)

Chapter 7: Conclusion and Recommendations

Titanium components were manufactured using a form of additive manufacturing, electron beam melting and were subjected to testing. The EBM components did not fail prematurely as expected by coupon testing.

- All of the eight components including the fasteners did not experience failure at 500k cycles at the design load of 9.56 kN with a loading ratio of R = -0.39 (double the design life)
- Three EBM components were subjected to double the design load (19.1 kN with R = -0.39) following the design load cyclic testing. EBM-4 had a fastener fail at location 11 at 177k cycles. EBMM-4 (EBM with post process machining) had a fastener failure at 104k cycles. EBMM-2 was aborted at 191k without any signs of failure. It was determined that the machined surface did not contribute much benefit to the EBM component in the cyclic loading test.
- Four EBM components were subjected to monotonic loading until failure. Fasteners 10 and 11 failed in the testing, and there was no sign of failure on the EBM component.
- This was a preliminary study and the first attempt to model this type of system in FEA with an EBM component. Therefore, FEA model at best was an approximation for monotonic loading near yield range. Further study needed to study not only cyclic loading but also the materials elastic-plastic range to predict the failure.

7-1 Recommendations

Further work upon this study would possibly include additional testing to increase the statistical confidence of the results due to the amount of scatter and relatively few data points. Furthermore, future testing of components that are subjected to post processes for example, hot isostatic pressing, peening etc. should be considered to compare with the as built components from this study. Any future testing should use measuring techniques such as strain gauges or video equipment on the component and assembly.

The finite element model was assumed linear elastic and isotropic. No plasticity was used in the modeling and the right boundary conditions regarding the loading must be used in a future study. Additionally, the fasteners at location 10 and 11 should be modeled with the threads to provide more information.

References

1. Edwards, P., A. O'Conner, and M. Ramulu. "Electron Beam Additive Manufacturing of Titanium Components: Properties and Performance." *Journal of Manufacturing Science and Engineering* 135.6 (2013): 061016
2. E.C. Santos, F. Abe, Y. Kitamura, K. Osakada, M. Shiomi, “Mechanical Properties of Pure Titanium Models Processed by Selective Laser Melting”, Proc. SFF Symp., Austin: (2002), pp. 180–186
3. Edson Santos et al., ”Fabrication of Titanium Dental Implants by Selective Laser Melting”, Proceedings of the SPIE (2004), Vol. 5662: 268-273
4. Edson Costa Santos et al., “Rapid Manufacturing of Metal Components by Laser Forming”, International Journal of Machine Tools & Manufacture (2006), Vol 46: 1459-1468
5. Laoui, Tahar, et al. "Properties of titanium dental implant models made by laser processing." *Proceedings of the Institution of Mechanical Engineers, Part C: Journal of Mechanical Engineering Science* 220.6 (2006): 857-863
6. Chan, Kwai S., et al. "Fatigue Life of Titanium Alloys Fabricated by Additive Layer Manufacturing Techniques for Dental Implants." *Metallurgical and Materials Transactions A* 44.2 (2013): 1010-1022
7. Koike, Mari, et al. "Evaluation of titanium alloys fabricated using rapid prototyping technologies—Electron beam melting and laser beam melting." *Materials* 4.10 (2011): 1776-1792
8. www.arcam.com

9. Baufeld, Bernd, Erhard Brandl, and Omer Van der Biest. "Wire based additive layer manufacturing: comparison of microstructure and mechanical properties of Ti–6Al–4V components fabricated by laser-beam deposition and shaped metal deposition." *Journal of Materials Processing Technology* 211.6 (2011): 1146-1158
10. Blackwell, P.L. et al., “Laser-Aided Manufacturing Technologies; Their Application to the Near-Net Shape Forming of a High-Strength Titanium Alloy”, Journal of Materials Processing Technology (2005), Vol. 170: 268-276
11. Frazier, William E. "Metal Additive Manufacturing: A Review." *Journal of Materials Engineering and Performance* 23.6 (2014): 1917-1928
12. Beyer, Christiane. "Strategic Implications of Current Trends in Additive Manufacturing." *Journal of Manufacturing Science and Engineering* 136.6 (2014): 064701
13. Y W Seo et al., “Machinability of Titanium Alloy (Ti-6Al-4V) by Abrasive Waterjets”, Journal of Engineering Manufacture (2003), Vol. 217 no. 12: 1709-1721
14. Boyer, R. R. "An overview on the use of titanium in the aerospace industry." *Materials Science and Engineering: A* 213.1 (1996): 103-114
15. Edwards, P., and M. Ramulu. "Fatigue performance evaluation of selective laser melted Ti–6Al–4V." *Materials Science and Engineering: A* 598 (2014): 327-337
16. Li, S. J., et al. "Compression fatigue behavior of Ti–6Al–4V mesh arrays fabricated by electron beam melting." *Acta Materialia* 60.3 (2012): 793-802
17. Murr, L. E., et al. "Microstructure and mechanical behavior of Ti–6Al–4V produced by rapid-layer manufacturing, for biomedical applications." *Journal of the mechanical behavior of biomedical materials* 2.1 (2009): 20-32

18. Suo, Hongbo, et al. "Microstructure and Mechanical Properties of Ti-6Al-4V by Electron Beam Rapid Manufacturing." *Rare Metal Materials and Engineering* 43.4 (2014): 780-785

19. Kocan, Marcin, Alfred Ostertag, and Lothar Wagner. "Shot Peening and Roller-Burnishing to Improve Fatigue Resistance of the (α+ β) Titanium Alloy Ti-6Al-4V." *Shot Peening* (2003): 461-467

20. Biswas, Amit, et al. "Laser surface nitriding of Ti-6Al-4V for bio-implant Application." *Trends in Biomaterials & Artificial Organs* 20.1 (2006): 68-71

21. Kobryn, P. A. et al., "The Laser Additive Manufacture of Ti-6Al-4V", JOM (2001), Vol. 53 Issue 9: 40-42

22. Facchini, Luca, et al. "Ductility of a Ti-6Al-4V alloy produced by selective laser melting of prealloyed powders." *Rapid Prototyping Journal* 16.6 (2010): 450-459

23. Brandl, Erhard, et al. "Additive manufactured AlSi10Mg samples using Selective Laser Melting (SLM): Microstructure, high cycle fatigue, and fracture behavior." *Materials & Design* 34 (2012): 159-169

24. Kruth, Jean-Pierre, et al. "Part and material properties in selective laser melting of metals." *Proceedings of the 16th International Symposium on Electromachining*. 2010

25. Yasa, Evren, and Jean-Pierre Kruth. "Microstructural investigation of Selective Laser Melting 316L stainless steel parts exposed to laser re-melting." *Procedia Engineering* 19 (2011): 389-395

26. Meier, H., C. Haberland, and J. Frenzel. "Structural and functional properties of NiTi shape memory alloy produced by selective laser melting." *Innovative Developments in*

Design and Manufacturing: Advanced Research in Virtual and Rapid Prototyping (2011): 291-296

27. Qiu, Chunlei, Nicholas JE Adkins, and Moataz M. Attallah. "Microstructure and tensile properties of selectively laser-melted and of HIPed laser-melted Ti–6Al–4V." *Materials Science and Engineering: A* 578 (2013): 230-239
28. Leuders, S., et al. "On the mechanical behaviour of titanium alloy TiAl6V4 manufactured by selective laser melting: Fatigue resistance and crack growth performance." *International Journal of Fatigue* 48 (2013): 300-307
29. Facchini, Luca, et al. "Microstructure and mechanical properties of Ti-6Al-4V produced by electron beam melting of pre-alloyed powders." *Rapid Prototyping Journal* 15.3 (2009): 171-178
30. Murr, L. E., et al. "Microstructures and mechanical properties of electron beam-rapid manufactured Ti–6Al–4V biomedical prototypes compared to wrought Ti–6Al–4V." *Materials Characterization* 60.2 (2009): 96-105
31. Murr, L. E., et al. "Characterization of Ti–6Al–4V open cellular foams fabricated by additive manufacturing using electron beam melting." *Materials Science and Engineering: A* 527.7 (2010): 1861-1868
32. Murr, Lawrence E., et al. "Next generation orthopaedic implants by additive manufacturing using electron beam melting." *International journal of biomaterials* 2012 (2012)

33. Ladani, Leila, Jafar Razmi, and Soud Farhan Choudhury. "Mechanical Anisotropy and Strain Rate Dependency Behavior of Ti6Al4V Produced Using E-Beam Additive Fabrication." *Journal of Engineering Materials and Technology* 136 (2014): 031006-1
34. www.matweb.com
35. http://www.roymech.co.uk/Useful_Tables/Tribology/co_of_frict.htm
36. http://blog.mechguru.com/machine-design/typical-coefficient-of-friction-values-for-common-materials/
37. http://www.engineeringtoolbox.com/friction-coefficients-d_778.html

Appendix A: Fatigue Fixture Drawings

Figure A-1: Assembled Fixture and Component

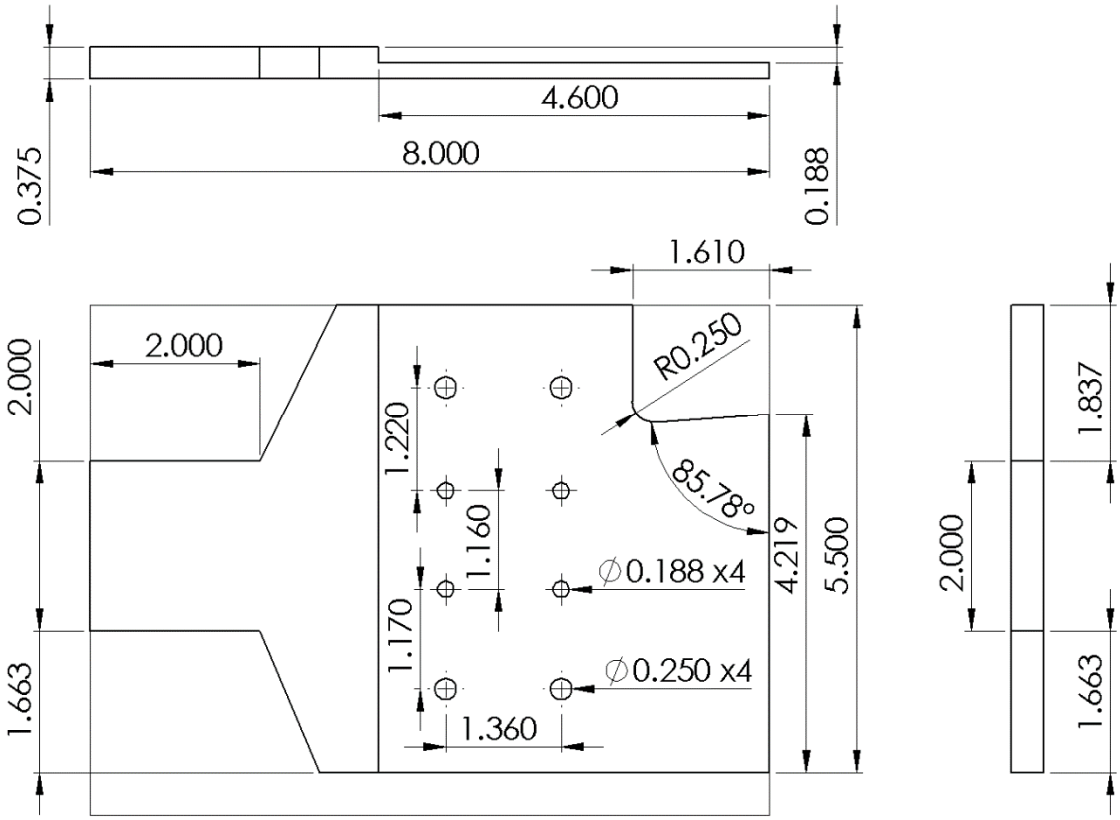

Figure A-2: Backing Plate Drawing

Figure A-3: Upper Fixture Drawing

Appendix B: Finite Element Results at 89.0 kN without Rigid Link

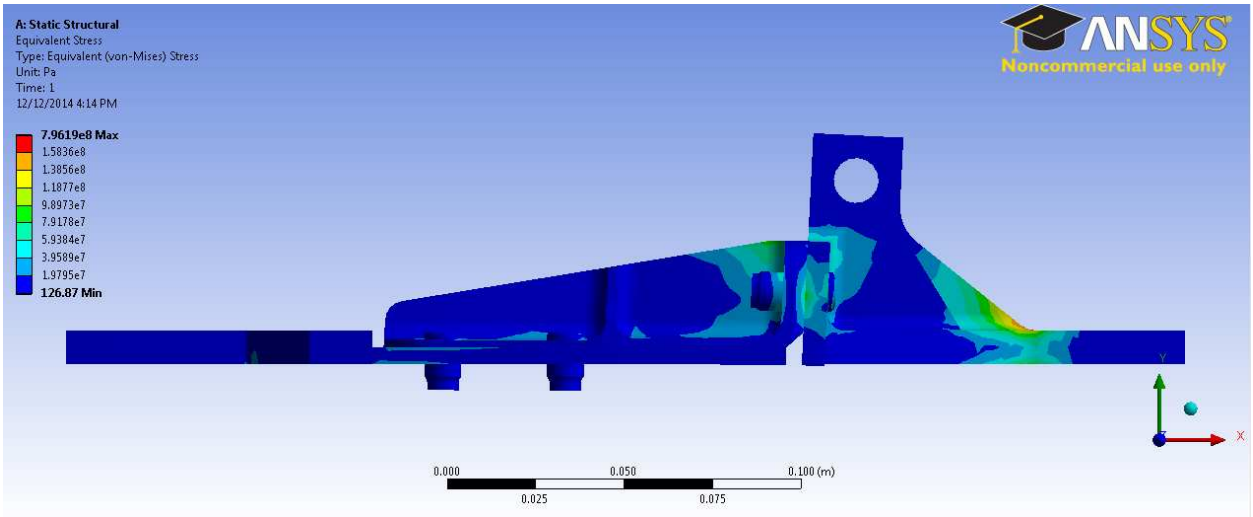

Figure B-1: Assembly side view

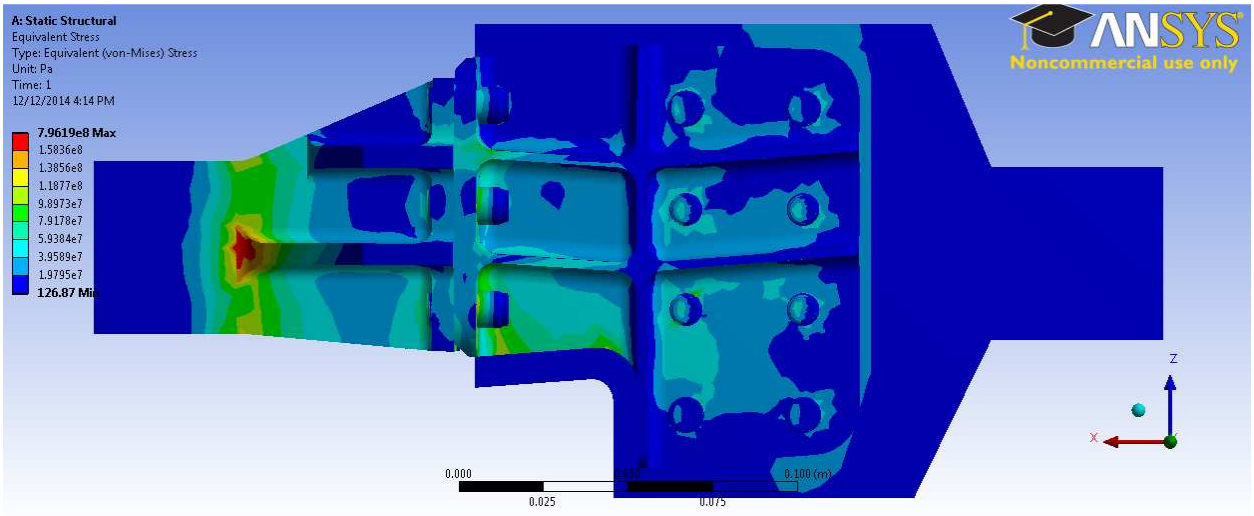

Figure B-2: Assembly top view

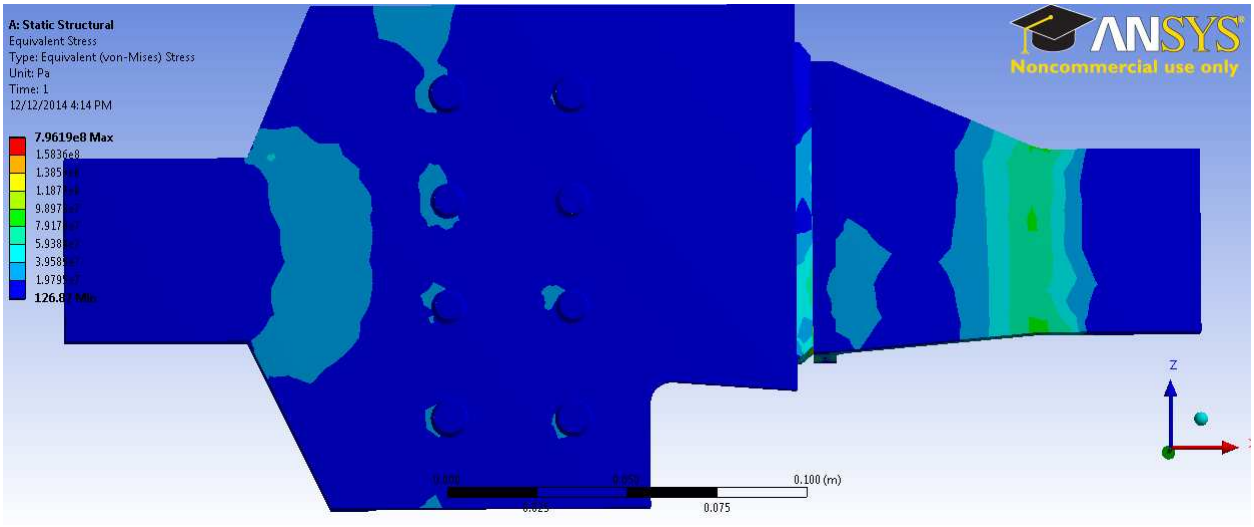

Figure B-3: Assembly bottom view

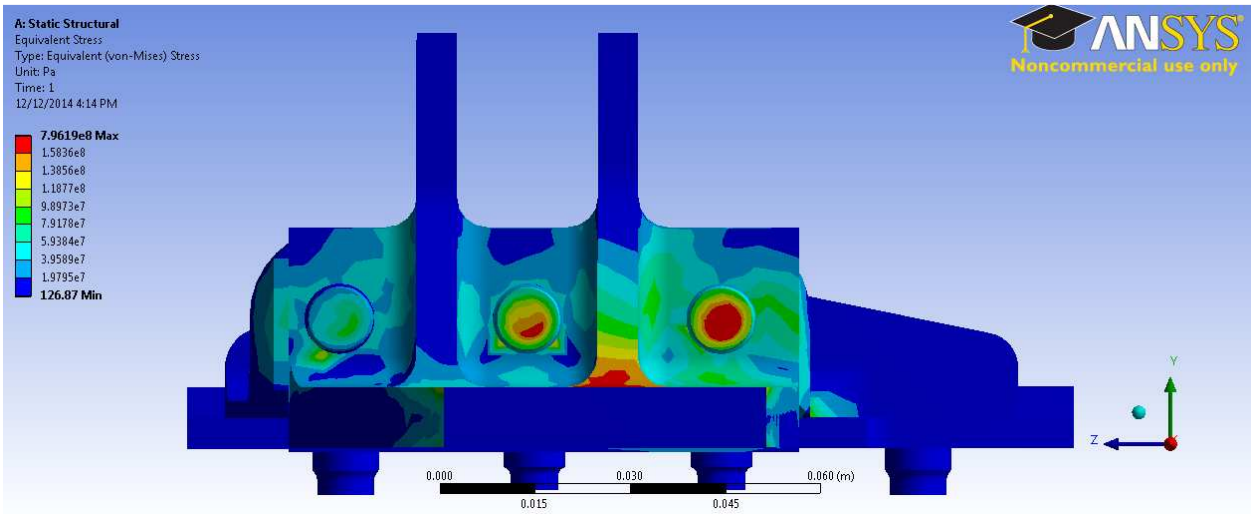

Figure B-4: Assembly at fixture view

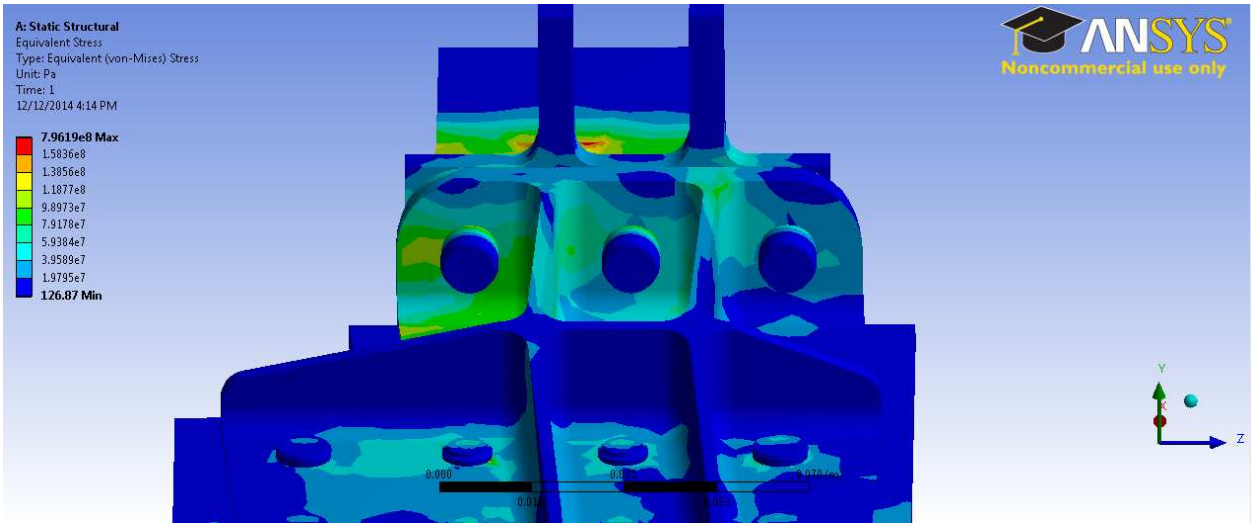

Figure B-5: Assembly view at fasteners 9, 10 and 11

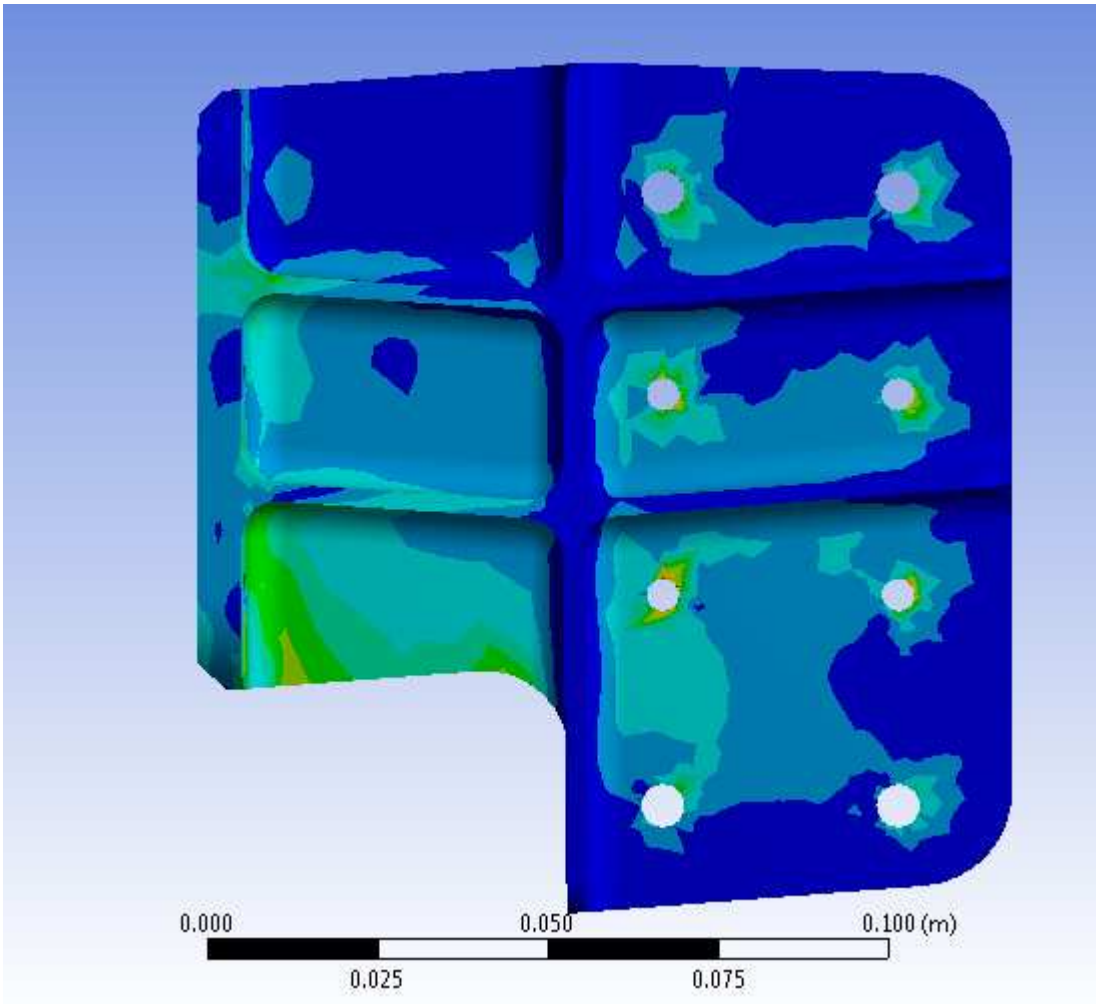

Figure B-6: Top view of EBM component

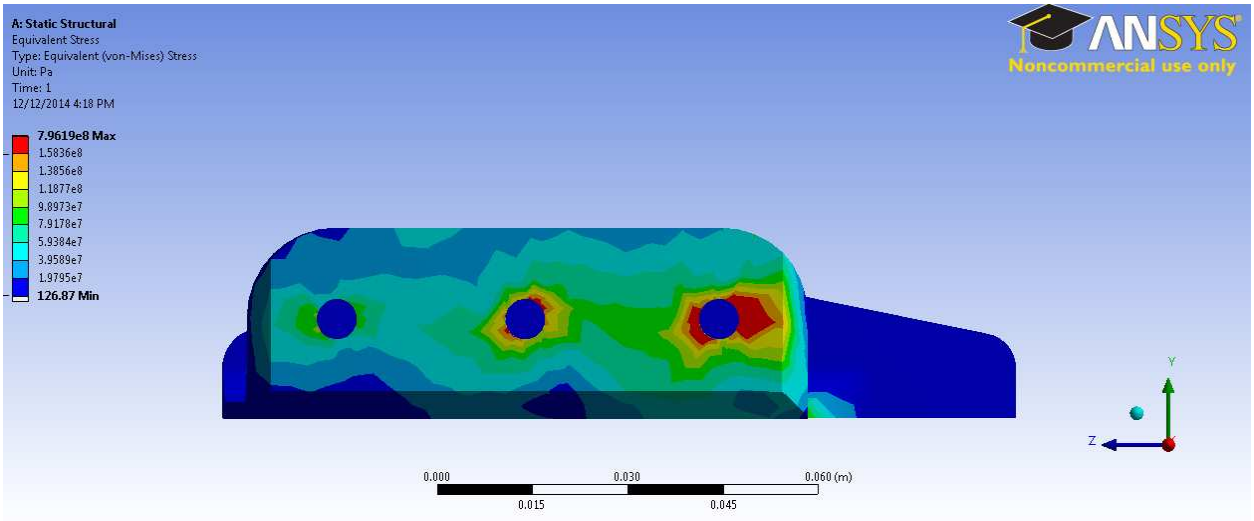

Figure B-7: EBM component fastener locations 9, 10, 11

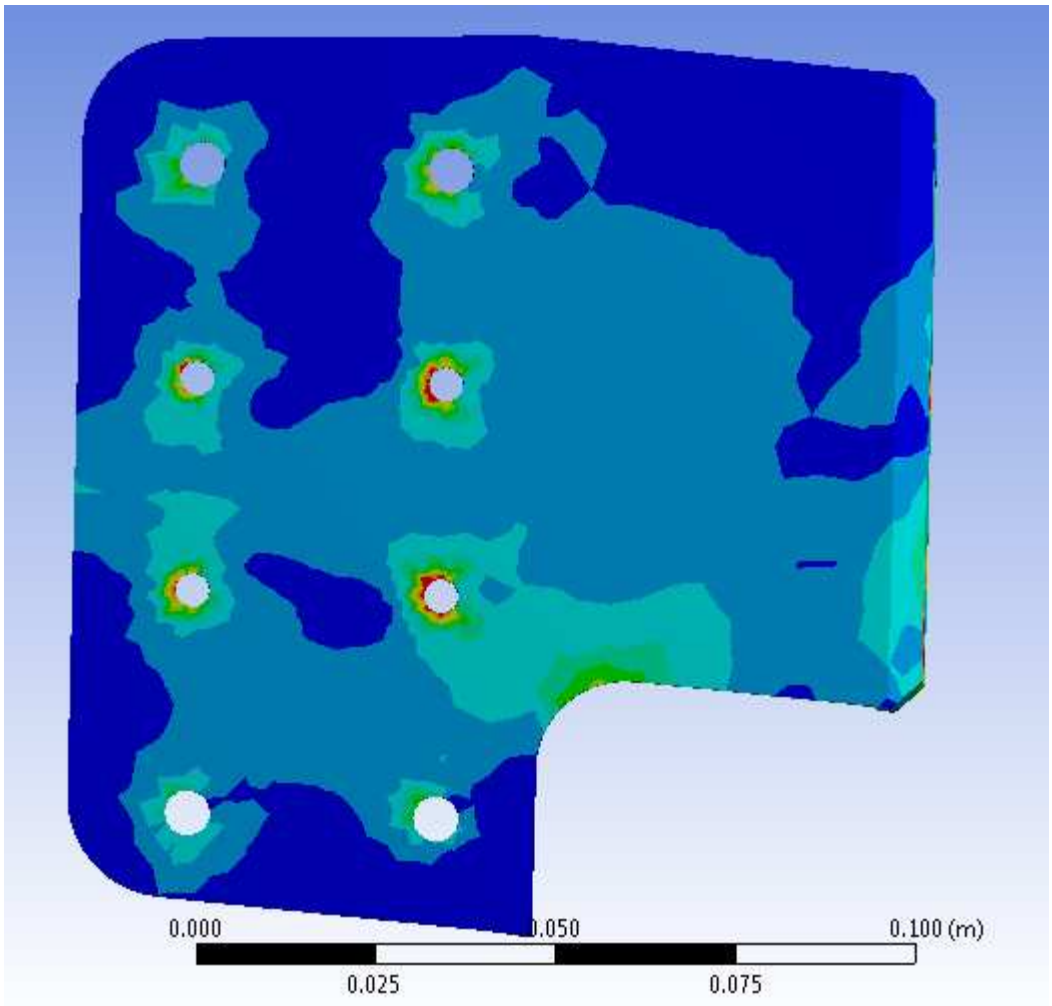

Figure B-8: Bottom view of EBM component

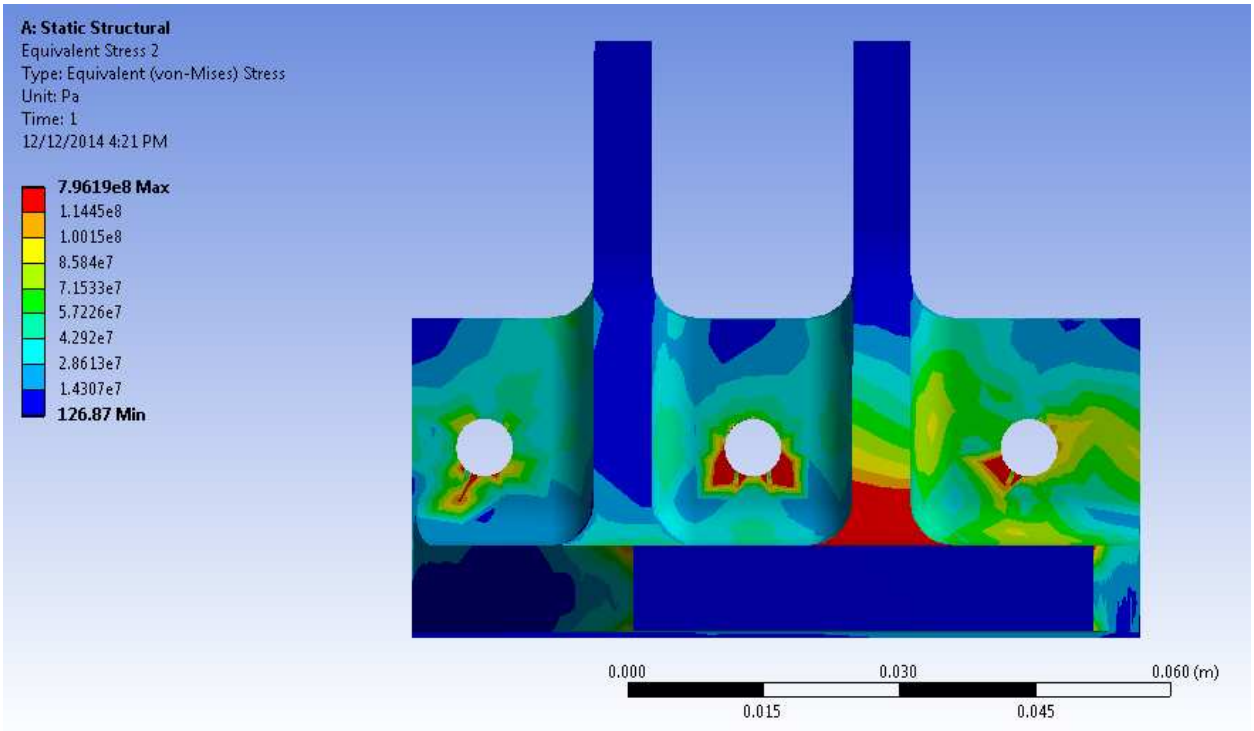

Figure B-9: Fixture for rigid link

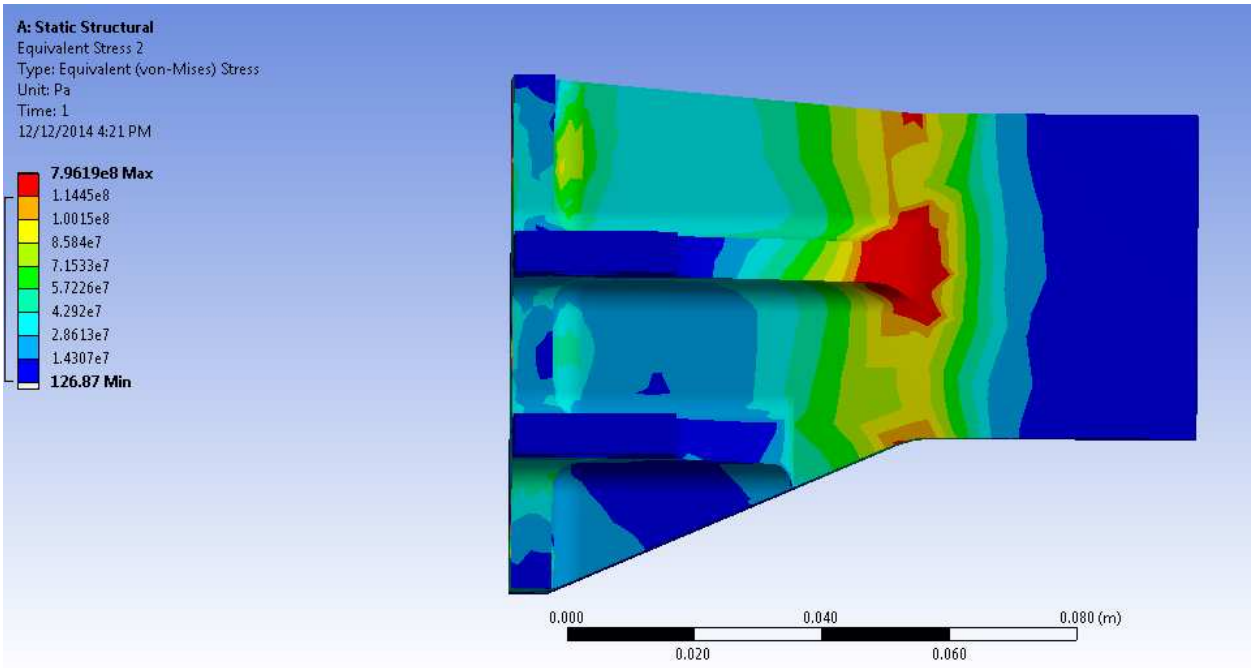

Figure B-10: Fixture for rigid link top view

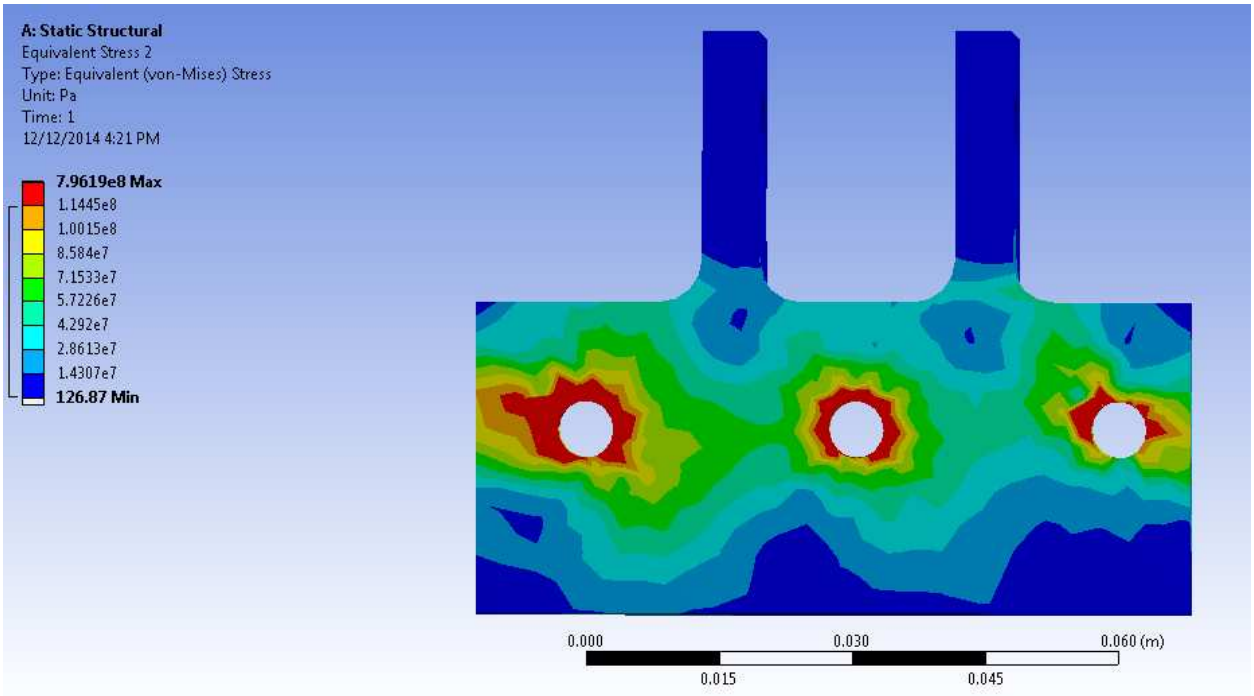

Figure B-11: View of fixture of where it interfaces with the EBM component

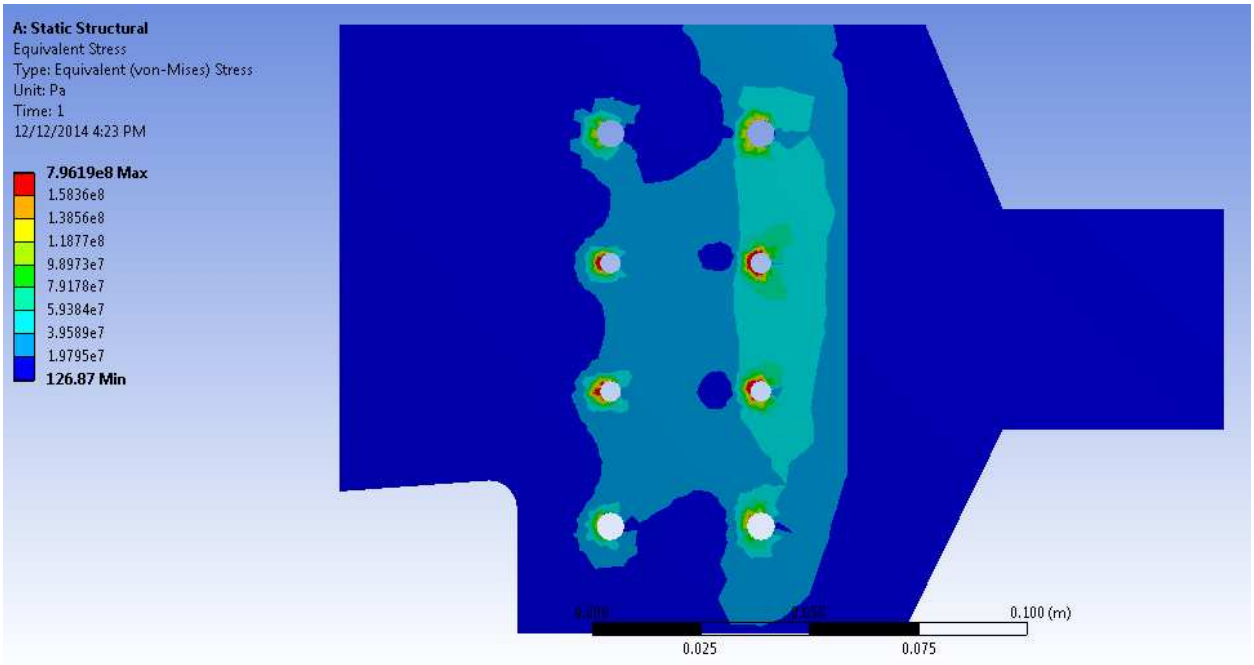

Figure B-12: Top view of base plate

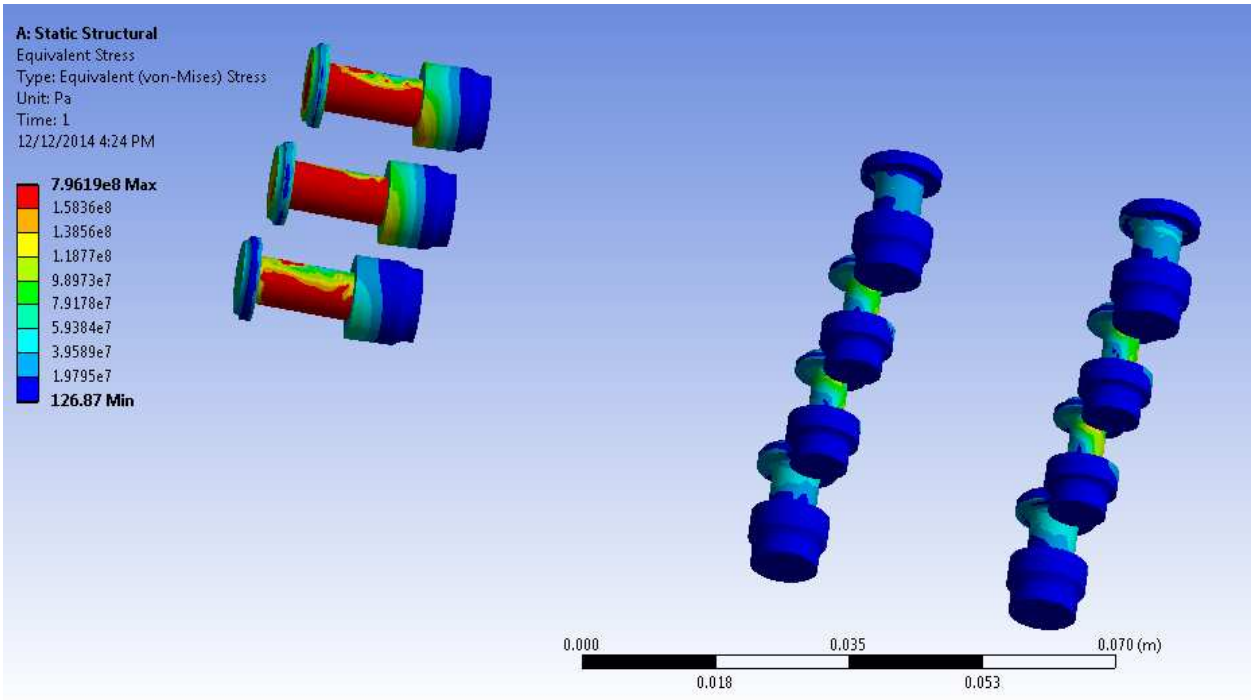

Figure B-13: View of fasteners

Appendix C: Finite Element Stress Distribution for 17.8 kN, 31.1 kN and 35.6 kN Tensile Loads without Rigid link

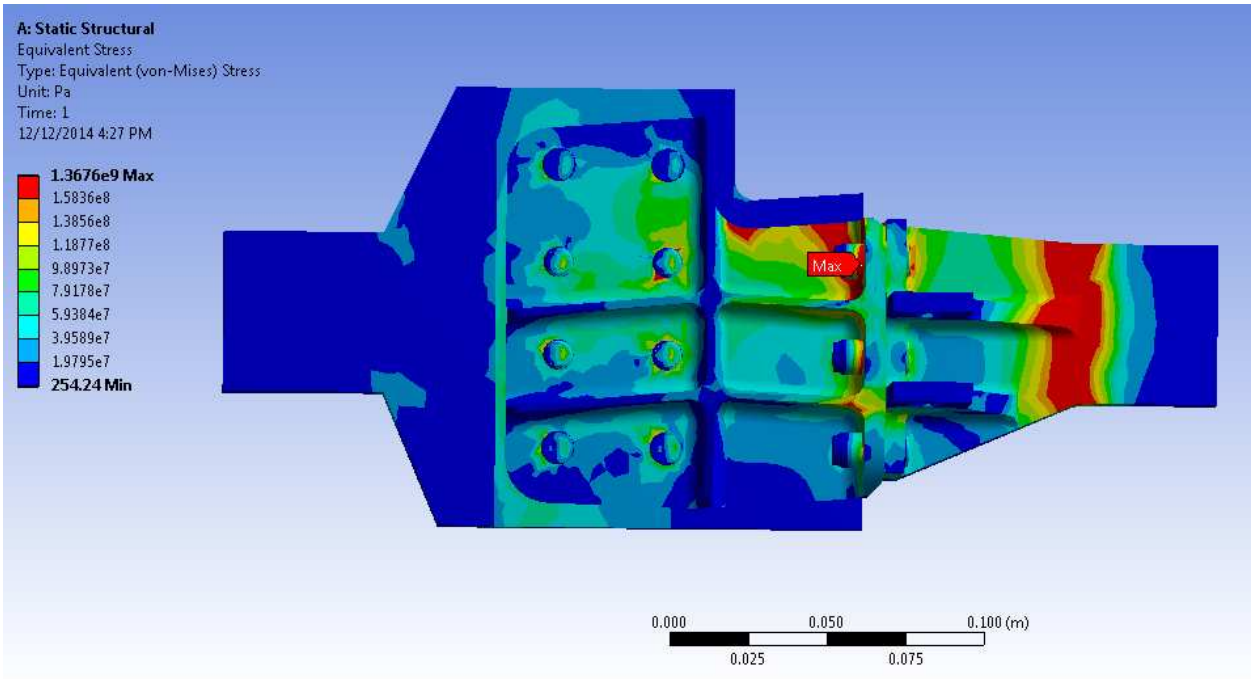

Figure C-1: 17.8 kN tensile load

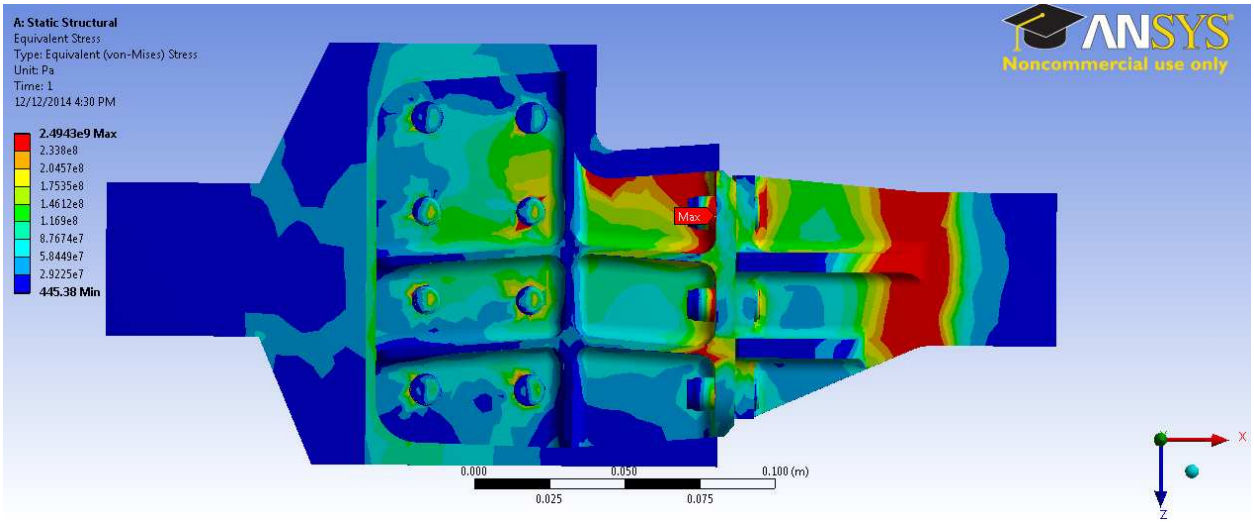

Figure C-2: 31.1 kN tensile load

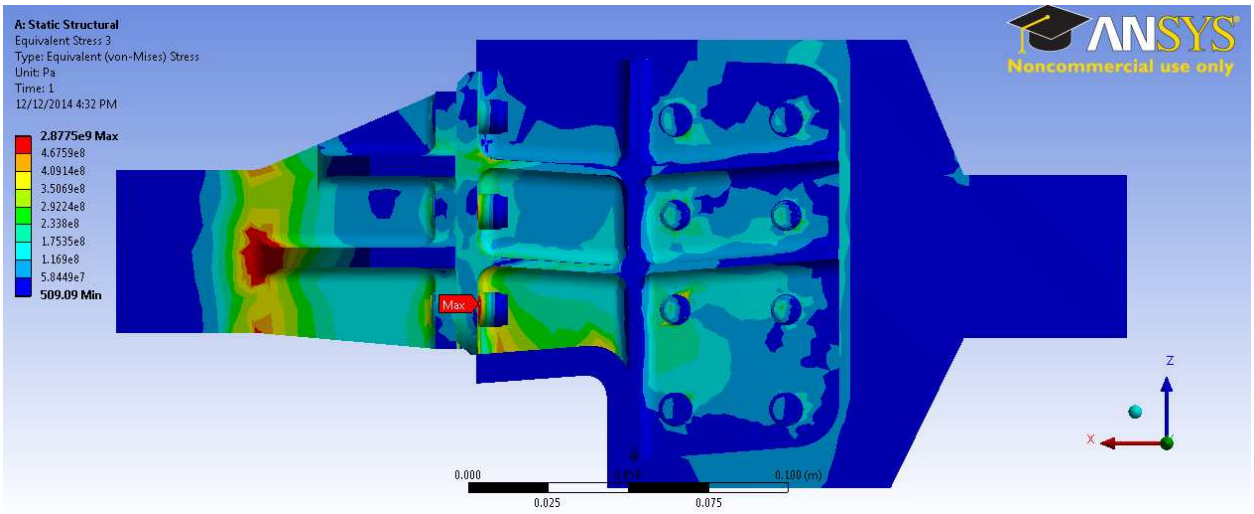

Figure C-3: 35.6 kN tensile load

Appendix D: Stress Distributions for Cyclic Loading (Static Models) with Rigid Link

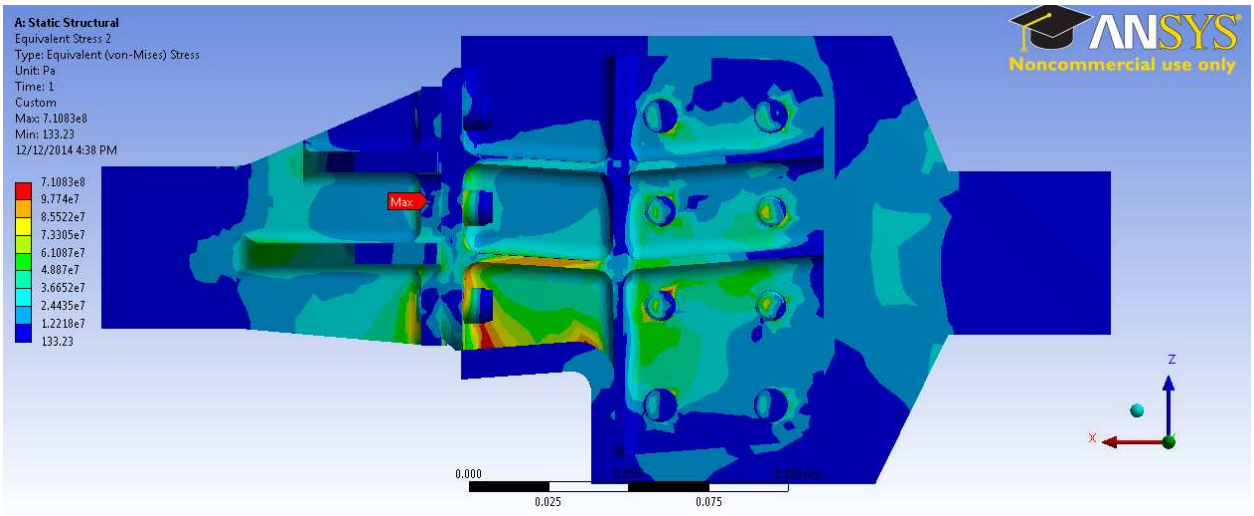

Figure D-1: Design Load Tension

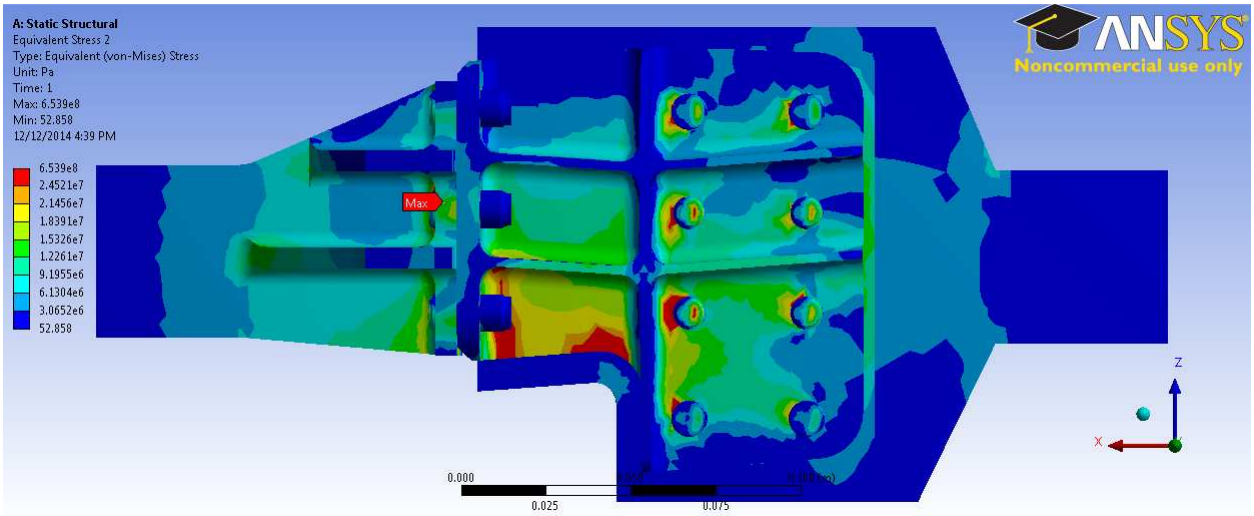

Figure D-2: Design Load Compression

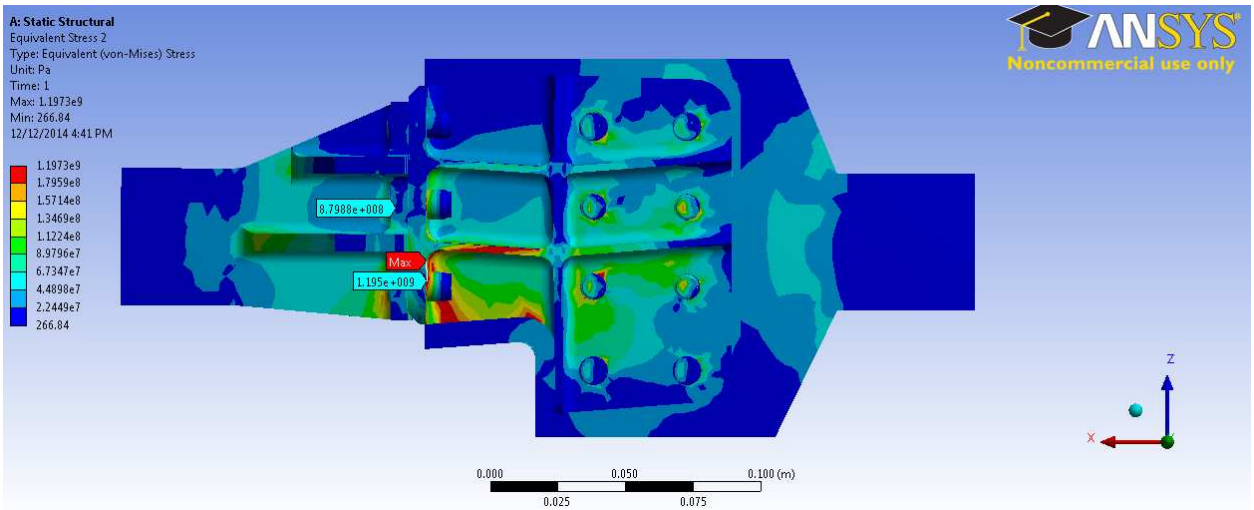

Figure D-3: Double design load (tension)

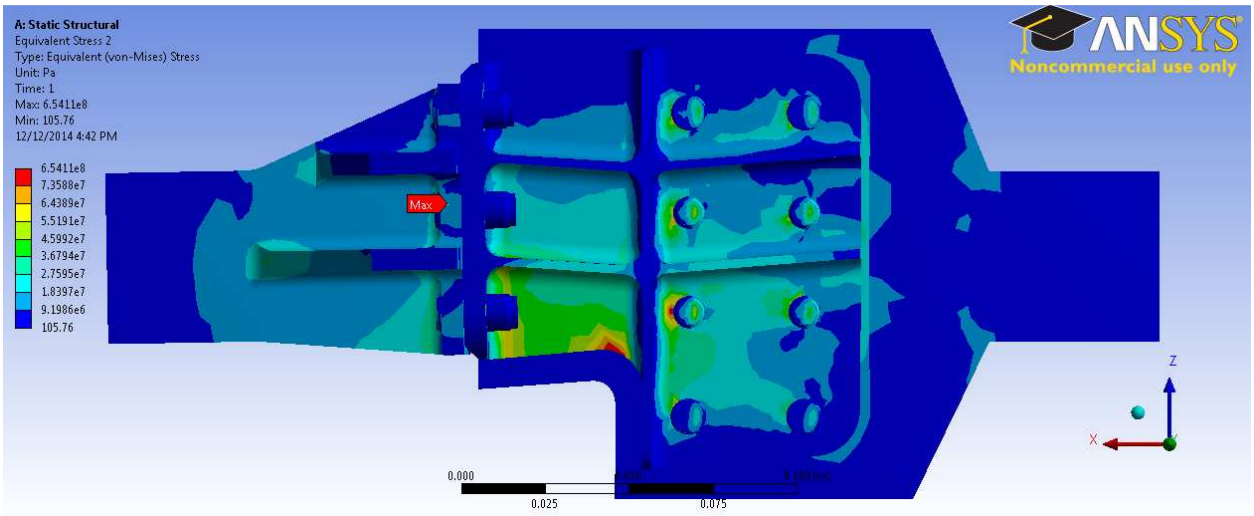

Figure D-4: Double design load (compression)